1968

Evaluation of surface areas from chromatographic and gravimetric adsorption data

Robert Rex Frost
Iowa State University

 69-4236

FROST, Robert Rex, 1940-
EVALUATION OF SURFACE AREAS FROM CHROMATOGRAPHIC AND GRAVIMETRIC ADSORPTION DATA.

Iowa State University, Ph.D., 1968
Chemistry, physical

University Microfilms, Inc., Ann Arbor, Michigan

EVALUATION OF SURFACE AREAS FROM CHROMATOGRAPHIC AND GRAVIMETRIC ADSORPTION DATA

by

Robert Rex Frost

A Dissertation Submitted to the
Graduate Faculty in Partial Fulfillment of
The Requirements for the Degree of
DOCTOR OF PHILOSOPHY

Major Subject: Physical Chemistry

Approved:

Signature was redacted for privacy.

In Charge of Major Work

Signature was redacted for privacy.

Head of Major Department

Signature was redacted for privacy.

Dean of Graduate College

Iowa State University
Ames, Iowa

1968

TABLE OF CONTENTS

		Page
I.	INTRODUCTION	1
II.	MEASUREMENT OF SURFACE AREAS	4
	A. General Background	4
	B. Low Temperature Adsorption	5
	1. Non-porous adsorbents	5
	2. Porous adsorbents of the second structural type	10
	3. Microporous adsorbents	16
	C. High Temperature Physical Adsorption	25
III.	THEORY	28
	A. Simple Theory - Henry's Law	28
	1. Plane surface	28
	2. Capillary surfaces	33
	B. The Two-Dimensional Gas Film Model	35
	C. Statistical Mechanical Theory	38
	D. Evaluation of Second Virial Coefficients	40
	1. Introduction	40
	2. Gas-surface second virial coefficients	40
	a. Plane surface	40
	b. Capillary surface	44
	3. Two-dimensional gas second virial coefficients	48

Page

E. Comparison of Plane and Capillary Surface Models 52

F. Diffusion in Capillaries 54

G. The Evaluation of S_o and/or Z_o 57

IV. APPLICATION OF GAS-SOLID CHROMATOGRAPHY TO STUDY OF PHYSICAL ADSORPTION 60

V. EXPERIMENTAL 69

A. Elution Gas-Solid Chromatography (EGC) 69

B. Frontal Gas Chromatography (FGC) 73

C. Vacuum Microbalance (MB) 77

VI. RESULTS 84

A. Processing of Experimental Data 84

1. Introduction 84

2. Gas chromatographic data 84

3. Microbalance data 85

a. General 85

b. Low temperature nitrogen adsorption data 86

c. High temperature adsorption data 87

B. Low Temperature Nitrogen Adsorption 90

C. Frontal Gas-Solid Chromatography (FGC) 92

D. Elution Gas-Solid Chromatography (EGC) 93

E. Vacuum Microbalance (MB) 96

VII. DISCUSSION 100

A. General 100

		Page
	B. Silica Gel	104
	C. The Activated Charcoals	106
VIII.	SUMMARY	118
IX.	LITERATURE CITED	120
X.	ACKNOWLEDGMENTS	128
XI.	APPENDIX A: FIGURES	129
XII.	APPENDIX B: TABLES	169
XIII.	APPENDIX C: COMPUTER PROGRAMS	198

I. INTRODUCTION

A major problem in the field of surface chemistry has been, and still is, the evaluation of absolute surface areas. It has been appropriately stated by Young and Crowell (1) that

> "The value to scientists and technologists of a universal reliable and relatively simple method for measuring the area of a solid can hardly be over-estimated, for it is a highly significant parameter in nearly all physical and chemical processes involving powdered solids."

In general, the methods for evaluating the surface area of an adsorbent can be classified into two broad groups. First of all are the methods that depend upon the molecular area (σ_m) of the adsorbate molecule which can be calculated assuming that the adsorbed molecules have the same packing as the molecules in a condensed phase have in their plane of closest packing by

$$\sigma_m = 1.091 \left[\frac{M}{N\delta} \right]^{2/3} \tag{1.1}$$

where M is the molecular weight, N is Avogadro's number and δ is the density of the condensed phase (solid or liquid). The monolayer capacity, V_m (volume) or W_m (weight), is defined as the quantity of adsorbate which would be required to cover the adsorbent with a monomolecular layer only. The surface area of the adsorbent is given by

$$A = 0.269\ \sigma_m\ V_m \tag{1.2}$$

where A is in m^2/g, σ_m is in $\mathring{A}^2$ and V_m is in cm^3 at STP/g. The determination of V_m generally depends upon the measurement of the adsorption isotherm of the particular adsorbate being used (usually nitrogen) at or near the boiling point of the adsorbate. The adsorption isotherm is defined as the relationship between the amount adsorbed and the equilibrium pressure above the adsorbent. The various methods by which V_m can be evaluated from the adsorption isotherm will be discussed in the next section.

Secondly, several methods have been developed over the years that lead to the surface area without explicit assumption as to the value of σ_m and the corresponding determination of V_m. This second group of methods can be further divided into two subgroups. The first subgroup contains those methods which are based upon the thermodynamic properties and relationships of the layer or layers of adsorbed molecules. The second subgroup contains the methods based upon high temperature adsorption theories and the methods which do not depend on the adsorption properties of the adsorbent.

The interpretation of adsorption data taken at or near the boiling point is difficult, especially for porous adsorbents, due to multilayer formation, capillary condensation and so on. The interpretation of high temperature adsorption data

cannot be completely unambiguous, but offers a fresh approach to the study of physical adsorption and evaluation of surface areas of solid adsorbents. Hence, a series of adsorption experiments were conducted on three different adsorbents using a number of gases over a range of temperatures to investigate the applicability of high temperaure adsorption data to the evaluation of surface areas. At the same time, different experimental techniques were evaluated as to their applicability in the study of high temperature physical adsorption.

II. MEASUREMENT OF SURFACE AREAS

A. General Background

This review will be limited to various methods that have been developed for the evaluation of surface areas based on physical adsorption measurements, with the theories of physical adsorption and associated phenomena, such as capillary condensation, discussed only to the extent needed to establish a method for the evaluation of the surface area of an adsorbent. The general literature on physical adsorption and the evaluation of surface areas from 1900 to the present has been covered extensively by McBain (2), Brunauer (3), Young and Crowell (1), and by Gregg and Sing (4). Also, Ross and Olivier (5) have written an excellent monograph on physical adsorption concerned primarily with their own work in which they make extensive use of a two-dimensional van der Waals equation of state for the adsorbed phase.

In general, solid adsorbents can be either porous or non-porous. It shall be convenient to follow Dubinin (6) and classify the pores of a porous adsorbent according to the average width of the pore, i.e., the diameter of a cylindrical pore or the distance between the walls of a slit-shaped pore. Pores with average widths below ~20 Å are described as micropores, those with widths between ~20 Å and

~200 Å as transitional pores and those with widths above 200 Å as macropores. Dubinin (7) also classifies adsorbents in which the pores are primarily micro as the first structural type and adsorbents in which the pores fall in the transitional and macro range as the second structural type. It is also convenient to use the classification of Brunauer, Deming, Deming and Teller (BDDT) (8) shown in Figure 1 when referring to the various types of adsorption isotherms. Type I isotherms are associated with monolayer adsorption and are usually obtained with adsorbents of the first structural type. Type II-V isotherms are associated with multilayer adsorption. Type IV and V isotherms are associated with capillary condensation effects and generally occur when the adsorbent is of the second structural type.

In the following discussion, the methods for the measurement of surface areas will be divided into those involving low temperature adsorption at or near the boiling point of the adsorbate and those involving high temperature adsorption, usually above the adsorbate's critical temperature.

B. Low Temperature Adsorption

1. Non-porous adsorbents

It is generally accepted now that multilayer adsorption on non-porous adsorbents leads to Type II and III isotherms of the BDDT classification (Figure 1). In 1935, Brunauer and

Emmett (9), in an attempt to estimate the surface area of iron synthetic ammonia catalysts, measured the isotherms for a number of gases near their boiling points. These were Type II isotherms. Brunauer and Emmett considered that the linear part (B-D in Figure 1) indicated the build up of the second layer of adsorbate on the surface, and that the extrapolation of this line to zero pressure (Point A in Figure 1) should represent the volume of gas required to fill the monolayer (V_m). Later, Emmett and Brunauer (10) expanded their adsorption studies to include additional iron-synthetic ammonia catalysis and considered all points A-E (Figure 1) as possibly representing the completion of the monolayer. The minimum deviation in the calculated surface area for a given adsorbent for the series of adsorbates was given by Point B. Additional evidence for the use of Point B to determine the monolayer capacity was provided by the heats of adsorption and has been supported by various other studies (4). Although the determination of the actual point is rather arbitrary, the Point B method for estimating the monolayer capacity has found considerable use, especially on adsorbents whose isotherms exhibit well-defined 'knee-bends', which quite often are Type I rather than Type II.

The evaluation of the monolayer capacity (V_m) quantitatively rather than qualitatively (i.e. Point B) requires an analytical expression for the adsorption isotherm and hence the

development of an adsorption theory. Prior to the development of the now famous BET theory in 1938, only the Langmuir equation (11) provided a means of evaluating V_m. Discussion of the Langmuir equation will be reserved for the section on microporous adsorbents, since, although based upon a monomolecular model and analytically describing Type I isotherms, it gives reliable V_m values only for adsorbents, known to contain micropores, which usually exhibit Type I isotherms.

In 1938, Brunauer, Emmett and Teller (12), henceforth referred to as the BET theory, extending the kinetic approach of Langmuir to the case of multilayer adsorption, obtained

$$V = \frac{V_m \, CP}{(P_o - P)\,[1 + (C - 1)\,P/P_o]} \tag{2.1}$$

which is known as the 'simple' or '∞-form' of the BET equation, where P_o is the saturation vapor pressure and C is a constant defined by

$$C = e^{(E_1 - E_L)/RT} \tag{2.2}$$

The difference $E_1 - E_L$ represents the net heat of adsorption, i.e., the heat of adsorption in the first layer minus the heat of liquefaction. Equation 2.1 can be rewritten in a more useful form as

$$\frac{P}{V(P_o - P)} = \frac{1}{V_m C} + \frac{C-1}{V_m C} \cdot \frac{P}{P_o} \tag{2.3}$$

Hence, a plot of $P/\,V(P_o - P)$ versus P/P_o should give a straight

line with V_m equal to 1/(slope + intercept). Therefore, the BET equation (2.3) can be regarded (13) as an analytical means of locating Point B. Applicability of Equation 2.3 is generally restricted to relative pressures between 0.05 and 0.35. Unless stated otherwise, any reference to the BET equation will mean Equation 2.3.

If the adsorption is restricted to a finite number of layers (n) such as on the walls of a capillary, then the BET treatment leads to the equation

$$V = \frac{V_m Cx}{(1-x)} \frac{(1 - (n + 1)x^n + nx^{n+1})}{(1 + (C - 1)x - Cx^{n+1})} \tag{2.4}$$

where $x = P/P_o$. Equation 2.4 is generally referred to as the 'n-layer' BET equation which reduces to Equation 2.1 for $n = \infty$ and the Langmuir equation (2.15) for $n = 1$.

The numerous criticisms as well as modifications of the BET theory have been discussed in detail (3) and will not be repeated here. The correctness of the monolayer capacity (BET as well as Point B) has also been discussed in detail (4). Both the ∞-form and the n-layer BET equations have been derived by Hill (14) and others using statistical mechanics.

A rather extensive comparison of nitrogen BET surface areas with "geometric areas" as determined by electron microscopy based on a particle size analysis of carefully prepared adsorbents and with BET areas determined using other

vapors has been given by Gregg and Sing (4). The agreement between nitrogen BET areas and the other areas is generally within 10 percent.

At this point a few general observations with regard to the measurement of surface areas can and should be made. For non-porous adsorbents as well as porous adsorbents of the second structural type, the value of the surface area obtained is relatively independent of the physical model and method of calculation. This has led in many instances to the unfortunate use of the BET surface area in determining whether the surface area thus obtained is correct or incorrect. BET surface areas have also been reported for microporous adsorbents with little justification as to the applicability of the BET model to these adsorbents. Areas as high as 3000 m^2/g have been reported for some charcoals, which requires that approximately nine-tenths of the carbon atoms of the sample be available to the gas.

An entirely different approach to the problem of low temperature physical adsorption is that of Ross and Olivier (5). Their approach makes use of the Gibbs adsorption equation (15) and various two-dimensional analogs of the van der Waals equation of state to obtain the adsorption isotherm indirectly. The two-dimensional van der Waals equation of state for the adsorbed phase accounts for intermolecular attraction and the concept of surface heterogeneity is introduced by dividing

the surface into a number of homogeneous patches with a Gaussian distribution of adsorptive potential energies among the patches. After a rather complicated process which leads to the matching of model isotherms with the experimental isotherms, the monolayer capacity can be obtained.

2. Porous adsorbents of the second structural type

Adsorbents with transitional pores give rise to Type IV or V, rather than Type II or III, isotherms (Figure 1). Discussion in this section will be confined to Type IV isotherms.

The analysis of the Type IV isotherms is generally as follows. Along the branch AB, monolayer and multilayer adsorption occurs on the walls of the transitional pores and on the free surface or macropores. The adsorption branch BCD and the corresponding desorption branch or hysteresis loop DFB is associated with "capillary condensation" in the transitional pores. At point D, the transitional pores have been completely filled with liquid-like material after which adsorption increases very slowly on the outside of the particles along DE. Instead of the horizontal branch DC, the isotherm can approach the saturation axis along DG which is attributed to condensation in the macropores or in the interstices between particles.

The capillary condensation hypothesis that the pores have all been filled with liquid adsorbate in the region DE implies that the liquid volume adsorbed should be the same for

all adsorbates. If the region DE is truly horizontal, the hypothesis is contained in a generalization given by Gurvitsch (16) for the uptake of vapor by adsorbents under condition of saturation vapor pressure, and it will be known as Gurvitsch's rule. Confirmation of Gurvitsch's rule for adsorbents with a highly developed transitional porous structure has been given in many cases (e.g. silica gels (17)).

The evaluation of surface areas for adsorbents exhibiting Type IV isotherms has followed two different approaches utilizing either the low pressure monolayer/multilayer region or the high pressure region where all of the transitional pores have been filled either through the process of multilayer formation or capillary condensation.

In the low pressure region either Point B or BET equation (2.3) can be used to evaluate the surface area. If adsorption is restricted to n-layers due to the presence of the transitional pores, it may be necessary to use the n-layer BET equation (2.4). Joyner et al. (18) have described a method by which the n-layer BET equation can be put into linear form such that the parameters n, C and V_m can be evaluated in a reasonably straightforward manner.

Recently, de Boer and co-workers (19,20) have developed what is referred to as the "t-method" for analyzing nitrogen adsorption data to evaluate the surface area and to indicate

the start of capillary condensation. First of all, adsorption isotherms were obtained on a number of 'non-porous' adsorbents. A nearly universal curve was obtained when the statistical thickness of the adsorbed layer defined by

$$t = 3.54\ V_a/V_m \quad ^* \tag{2.5}$$

where V_a is the volume of nitrogen adsorbed in cm^3 STP/g and V_m is the BET monolayer capacity (Equation 2.3) in cm^3 STP/g is plotted against the reduced pressure (P/P_o). Application of the 't-method' to a porous adsorbent consists of plotting V_a (cm^3 STP/g) versus t at the corresponding P/P_o. A t-plot for an adsorbent containing transitional pores sufficiently large that adsorption can occur unhindered is shown in Figure 2 (b). From the slope of the linear portion, the surface area can be calculated by

$$A = 15.47\ V_a/t \tag{2.6}$$

where A is in m^2/g adsorbent. The onset of capillary condensation is indicated by the upward turn of the plot at point F.

The use of the high pressure region for evaluation of surface areas has followed two different approaches depending on whether or not an evaluation of the pore size distribution is also desired. From discussion originally presented by Thomson (21) for the equilibrium of a vapor at the curved surface of a liquid in a capillary and simple thermodynamic

*When referring to the t-method, t is in Å.

considerations, the following relationships can be derived. The surface area of an adsorbent containing transitional pores is given by

$$A = \frac{RT}{\gamma\bar{V}} \int_{V_o}^{V_s} \ln P_o/P \, dV \tag{2.7}$$

where V_o is the volume of liquid adsorbate corresponding to the beginning of capillary condensation, V_s is the volume of liquid adsorbate at saturation, γ is the surface tension of the liquid adsorbate and $\bar{V}$ is the molar volume of the adsorbate in liquid state. The application of Equation 2.7 to the evaluation of surface area is restricted to adsorbents that contain pores large enough such that they cannot be filled from multilayer formation alone. The derivation of Equation 2.7 is independent of the size or shape of the capillaries. The relationship between the size and shape of capillaries is given by

$$\ln P/P_o = -\frac{\gamma\bar{V}}{RT} \cdot \left(\frac{1}{r_1} + \frac{1}{r_2}\right) \tag{2.8}$$

where $\bar{V}$ is the molar volume of the liquid adsorbate and r_1, r_2 are the radii of curvature of the liquid surfaces. For a cylindrical capillary, Equation 2.8 reduces to

$$\ln P/P_o = -\frac{2\gamma\bar{V}}{r_k RT} \tag{2.9}$$

which is generally referred to as the 'Kelvin' equation where r_k is the 'Kelvin' radius and it has been assumed that the liquid wets the walls of the pores. The 'Kelvin' radius in Equation 2.9 is related to the actual radius of the pore by

$$r_p = r_k + t \tag{2.10}$$

where t is the thickness of the adsorbed layer defined by Equation 2.5. If the pores are slit-shaped instead of cylindrical, the 'Kelvin' radius is defined in terms of the diameter (i.e. width) of the pore by

$$d = r_k + 2t \tag{2.11}$$

The interconversion of Equations 2.7 and 2.8 can be readily performed using the proper relationship between the 'Kelvin' radius, volume and surface area of the pore.

Kistler, Fischer, and Freeman (22) developed an equivalent of Equation 2.7 where V_o was determined by use of the Langmuir adsorption equation (11). Their procedure has found very limited application. Derjaguin (23) has derived a corrected form of Equation 2.7 that takes into account the adsorbed layer. The most extensive use of Equation 2.7 for the evaluation of the surface area of transitional pores has been by Dubinin and co-workers (6,24).

Equation 2.9 has been used very extensively in discussions of capillary condensation and associated hysteresis phenomena.

It has also been used to determine what are termed cumulative surface areas and pore volumes. Surface areas are given by

$$S_{cum} = \Sigma\Delta S_k = \Sigma \frac{2\Delta V_k}{r_k} \tag{2.12}$$

for cylindrical pores and

$$S_{cum} = \Sigma\Delta S_k = \Sigma \frac{2\Delta V_k}{d_k} \tag{2.13}$$

for slit-shaped pores. Pore volumes are given by

$$V_{cum} = \Sigma\Delta V_k \tag{2.14}$$

Above, r_k and d_k are the corresponding 'Kelvin' radii and the summations are performed over a distribution of radii calculated from the 'Kelvin' equation. Several treatments for the evaluation of S_{cum} and V_{cum} for cylindrical pores (25-29) and for slit-shaped pores (30-33) have been given which generally differ only slightly in mathematical analysis and computational procedure.

Comparison of surface areas calculated from the low and high pressure regions of adsorption isotherms can only be made with reservations assuming that the adsorbent does not contain micropores. In cases where the proper branch of the adsorption isotherm (i.e. the equilibrium branch (34) which is the adsorption branch for ink-bottle pores and the desorption branch for slit-shaped pores) is used and where the thickness of the adsorbed layer t in Equations 2.10 and 2.11

is the same defined by Equation 2.5, the surface areas determined using the BET equation, Equations 2.6 or 2.7 and S_{cum} are in near-perfect agreement. This is exactly what should be expected from the calculations which are nearly circular in nature. Considerable deviations do occur when different methods are employed to correct for the adsorbed layer, when the shapes of the actual pores deviate widely from the idealized shapes and when micropores are actually present. Therefore, although a given surface area may agree with the BET surface area, it does not necessarily follow that either one or both of the surface areas represents the true area of the adsorbent.

The list of methods by which the surface area of the adsorbent containing transitional pores can be evaluated has by no means been exhausted. The methods employing low temperature adsorption data are generally based on empirical adsorption equations.

3. Microporous adsorbents

The classification of an adsorbent as microporous or as being of the first structural type does not preclude the existence of both transitional and macro pores. Generally, an adsorbent will have a polydisperse pore system with all types existing in various portions with a distribution of sizes. Active charcoals usually have a polydisperse pore system while oxide gels usually do not contain micropores.

Hence, the existence of micropores creates numerous problems in the interpretation of adsorption data and in ascertaining the true surface area of the adsorbent.

In many instances the surface area of a microporous adsorbent quoted is that determined by use of the BET equation or Point B without any justification as to the applicability of these methods to microporous adsorbents. The values of the surface areas determined by these methods are also used in comparing values determined by other methods and as justification for the correctness of the values. The adsorption isotherm would be of Type I (Figure 1) if only micropores were present, but the presence of transitional and/or macro pores will give an adsorption isotherm mixture of Types I, II and IV. The Type I isotherm has been interpreted classically as representing monomolecular adsorption on pores so narrow that adsorption is limited to a monolayer with the isotherm plateau representing the completion of the monolayer. The Type I isotherm can be represented analytically by the Langmuir equation

$$V = \frac{V_m BP}{1 + BP} \tag{2.15}$$

which can be rewritten in the linear form

$$\frac{P}{V} = \frac{1}{BV_m} + \frac{P}{V_m} \tag{2.16}$$

where B is a constant at any given temperature. Therefore, Equation 2.16 can be used to evaluate the surface area of an adsorbent exhibiting a Type I isotherm. In many cases where the adsorption isotherm is a mixture of Types I and II, the Langmuir equation will represent the data much better than the BET equation. Obviously, the Langmuir equation will give a larger surface area than either the BET equation or the Point B method.

There is considerable evidence available that the classical interpretation for the Type I isotherm is incorrect. The evidence includes surface areas as high as 3000 m^2/g for adsorbents giving Type I isotherms; the observations of Pierce, Wiley and Smith (35) for a particular charcoal that further activation increased the amount adsorbed by a factor of three but the isotherm was still Type I; and that in many instances, Gurvitsch's rule is obeyed for adsorbents exhibiting Type I isotherms.

A discussion of microporous adsorbents would not be complete unless the work of Dubinin and co-workers was covered. Polanyi (36) formulated the potential theory of adsorption where the adsorption potential is given by

$$\varepsilon = RT \ln \frac{P_o}{P} \qquad (2.17)$$

but did not attempt to derive an expression for the adsorption isotherm. It is therefore necessary to find the distribution

of filled adsorption space (W) as a function of the adsorption potential. Dubinin and co-workers (37,7,24,38) have derived expressions for the adsorption isotherm through the following very simplified procedure. For a microporous adsorbent the distribution function is given by

$$W = W_o \exp\ (-K'\varepsilon'^2) \tag{2.18}$$

where W_o is the limiting volume of adsorption space, which, if only micropores are present, is equal to the volume of the micropores, and K' is a constant for a particular vapor. Equation 2.18 represents the characteristic curve of the potential theory of adsorption and is independent of temperature. If the adsorption space is filled to the same extent by two different vapors, Equation 2.18 implies

$$\frac{\varepsilon}{\varepsilon_o} = \left(\frac{K_o}{K}\right)^{1/2} = \beta \tag{2.19}$$

where β is called affinity coefficient and to a first approximation is given by the ratio of the molar volumes of the vapors. Replacing K' and ε' in Equation 2.18 with K_o and ε_o corresponding to a standard vapor (such as benzene at 20°C) and using Equation 2.19 the following is obtained for any vapor.

$$W = W_o \exp\left(-K_o \frac{\varepsilon^2}{\beta^2}\right) \tag{2.20}$$

The filled volume W of adsorption space in terms of the amount of vapor adsorbed (a) is given by

$$W = aV \tag{2.21}$$

where V is molar volume of the liquified vapor. Substituting Equations 2.17 and 2.21 into Equation 2.20 yields as the equation for the adsorption isotherm

$$a = \frac{W_o}{V} \exp \left[-B \frac{T^2}{\beta^2} \left(\log \frac{P_o}{P}\right)^2\right] \tag{2.22}$$

which can be put into the convenient linear form

$$\log a = C - D \left(\log \frac{P_o}{P}\right)^2 \tag{2.23}$$

where $$C = \log \frac{W_o}{V} \tag{2.24}$$

and $$D = 0.434\ B \frac{T^2}{\beta^2} \tag{2.25}$$

The important parameter in the preceding analysis is W_o, obtained by extrapolation of the plot log a versus $[\log (P_o/P)]^2$ to $P_o/P = 1$. For an adsorbent that contained only micropores, the plot would be linear up to $P_o/P = 1$ and hence, W_o would equal the volume of the micropores (V_{mi}). But for most adsorbents, Equation 2.23 holds only for relative pressures below ~0.2 indicating the presence of transitional and/or macro pores requiring correction of W_o values for adsorption in these pores to obtain V_{mi}. The use

of Equation 2.23 also provides a means by which more detailed information on the microporous structure could be obtained through the use of different adsorbates as "molecular probes". The use of Equation 2.23 actually requires that the molar volume (V) be known as a function of temperature and this is of critical importance at temperatures above the boiling point of the adsorbate.

For adsorbents of the second structural type containing transitional and macro pores Dubinin and co-workers have assumed that the distribution of adsorption space is given by

$$W = W_o' \exp(-m\varepsilon) \tag{2.26}$$

From an analysis similar to the previous case, the adsorption equation is found to be

$$a' = \frac{W_o'}{V} \exp\left[- A \frac{T}{\beta} \log \frac{P_o}{P} \right] \tag{2.27}$$

The linear form is

$$\log a' = M - N \log \frac{P_o}{P} \tag{2.28}$$

where $$M = \log \frac{W_o'}{V} \tag{2.29}$$

and $$N = 0.434\ A \frac{T}{\beta} \tag{2.30}$$

The range of applicability of Equation 2.28 is for relative pressures below 0.2; while Equation 2.27 indicates formally that W_o' is the liquid volume adsorbed when $P = P_o$, since the equation does not apply for this range interpretation of W_o' as total pore volume is incorrect.

For an adsorbent of the mixed structural type containing the whole distribution of pore sizes, Equations 2.27 and 2.22 can be combined to give the adsorption equation

$$a'' = \alpha \cdot a + (1 - \alpha) \cdot a' \qquad (2.31)$$

where α is simply the fraction of adsorption space contained in the micropores.

Through the use of Equations 2.22 and 2.27 Dubinin and co-workers have extensively studied the pore system in numerous active carbons and oxide gels.

Kaganer (39-41) has endeavored to apply Dubinin's treatment to the evaluation of surface areas of microporous adsorbents. He assumes that in the region of monomolecular adsorption Equation 2.18 represents the distribution of adsorption energy over the adsorption surface instead of the adsorption volume. This leads to the writing of Equation 2.24 as

$$C = \log a_m \qquad (2.32)$$

where a_m is the monolayer capacity which can be obtained from the intercept of a plot of log a versus $[\log P_o/P]^2$.

Since the applicability of Equation 2.23 is generally restricted to relative pressures below 0.2, the extrapolation must be made over the most ill-defined region of the adsorption isotherm. Kaganer has compared the surface areas obtained by using Equation 2.32 in Equation 2.23 with surface areas obtained by use of the BET equation and the method of Harkins and Jura (42) for a wide variety of adsorbents and several adsorbates. General agreement within 2 percent is observed for high area adsorbents and within 5 percent for low area adsorbents. As a check on the assumption embodied in Equation 2.32, Kaganer measured the nitrogen adsorption isotherm on dehydrated chabazite at 90°K and all data points fell on a straight line when plotted according to Equation 2.23.

A few general comments on the work of Dubinin and co-workers are in order. A considerable amount of the data obtained by them is in the pressure range 10^{-5} to 1 mm which is neglected in the adsorption studies of many workers, but, on the other hand, extrapolation is required to saturation vapor pressure to obtain the desired parameters. Application of the theory is usually limited to adsorbates at or below their normal boiling points and the presence of a distribution of pore sizes necessitates the use of appropriate correction factors in the evaluation of the various parameters. Although the theory can be considered as rather empirical, it has

provided the basis for the study of the porous structure of adsorbents.

Kaganer's use of Equation 2.23 to represent monomolecular adsorption appears to be unjustified. The excellent agreement observed when values of surface areas are compared does not necessarily validate any of the methods compared. There are reasons to suspect that one is measuring a 'pore volume' instead of determining the monolayer capacity. The adsorption of nitrogen by chabazite would appear to provide more evidence that Equation 2.23 should be used to represent volume filling of pores than monomolecular adsorption on the walls of the pores. The structure of chabazite has been discussed by Barrer and Kerr (43). The cavities in chabazite are approximately 11 Å long with an average diameter of 6.6 Å. Each cavity has six windows with an average free diameter of 3.9 Å. Therefore, monomolecular adsorption in the usual sense cannot occur, but a 'volume filling' can occur.

In the section on adsorbents of the second structural type, the t-method for evaluating surface areas was covered. If the distribution of pores sizes moves from the transitional to the micro region, a t-plot of the type shown in Figure 2 (a) is obtained. The original interpretation (19) of this type of t-plot concluded that multilayer adsorption occurred on all the surface until the break at BC where some of the pores have been filled by the process of multilayer adsorption and,

hence, the region CD represents additional adsorption on the remaining available surface. This interpretation assumes that the pores are slit-shaped. Recently, Sing (44) has proposed a more general interpretation for t-plots of the type shown in Figure 2 (a). He proposes that the region AB represents both micropore filling and multilayer adsorption on walls of the larger pores and that the region CD can then be extrapolated to the volume axis to give an effective origin at O'. The micropore volume can be calculated from V_o' and the surface area of the adsorbent (excluding the micropore area) can be calculated from the slope of O'CD. A similar analysis has been implied by de Boer and co-workers in discussing their results on carbon blacks (45). The approach of Sing appears to have an important advantage over that of Dubinin and co-workers in that no assumption as to the distribution of adsorption energy is required to obtain essentially the same information.

C. High Temperature Physical Adsorption

The transition from low temperature to high temperature adsorption is rather vaguely defined. The high temperature physical adsorption region shall be specified as occurring at sufficiently high temperatures that adsorption does not exceed one or two per cent of a monolayer. Hence, the temperature is sufficiently high that effects due to two-dimensional

condenstaion, capillary condensation, and multilayer formation can be ignored.

There have been two different approaches taken in the development of high temperature adsorption theory. Halsey and co-workers (46) have treated the interaction of gases with solid surfaces in a manner analogous to imperfect gas theory. Barker and Everett (47) have used more conventional adsorption theory to obtain the same results. In the second-order or Henry's Law region of the adsorption isotherm, both approaches give

$$n_a = K_H AP \tag{2.33}$$

where n_a is the number of moles adsorbed, K_H the 'Henry's Law' constant per unit area and A the surface area. Hence, if K_H can be evaluated either experimentally or theoretically, then the surface area of the adsorbent can be calculated.

If small deviations from Henry's Law are taken into consideration, then, instead of Equation 2.33, the following is obtained

$$n_a = K_1(T)P + K_2(T)P^2 \tag{2.34}$$

where $K_1 = K_H A$ and K_2 is a third-order interaction constant. The treatments of either Barker and Everett (47) or Sams *et al*. (48) give for the surface area (A)

$$\frac{A}{B_2} = -\frac{2K_1^2}{K_2} \tag{2.35}$$

where B_2 is the second virial coefficient for a two-dimensional gas film. Hence, if B_2 is known or can be calculated, A can be calculated.

A more extensive development of the high temperature adsorption theory and application to the evaluation of surface areas will be given in subsequent sections.

Bond and Spencer (49) have proposed a method based on Henry's Law for evaluating the surface areas of coals. They determined the amount of neon adsorbed by a coal of "known" surface area at 0°C and 1 atm pressure. A value for K_H per unit area could then be calculated and subsequently used to calculate surface areas of other coals. Although there is a certain amount of merit to this proposal, the problem of recognizing the "known" surface area remains unsolved.

III. THEORY

A. Simple Theory - Henry's Law

1. Plane surface

The simple theory will be derived in terms of a dilute gas interacting with a plane adsorbing surface where the nuclei of the surface atoms define the xy-plane. An extension of the simple theory will then be made for a capillary surface. As a molecule moves along a normal path towards the surface, its potential energy varies as the distance Z from the surface as shown in Figure 3(a). If it is assumed that the gas is so dilute that the potential energy of a gas is dependent only on its coordinates and that gas-gas interactions can be neglected, then the average concentration of gas molecules at any point in the adsorption field can be calculated from the Boltzmann distribution law:

$$C = C_o \exp\ (-E(Z)/kT) \tag{3.1}$$

By choice of energy reference, $E \rightarrow o$ as $Z \rightarrow \infty$, and so also $C \rightarrow C_o$ as $Z \rightarrow \infty$ (Figure 3(b)).

Use shall be made of the Gibbs definition of adsorption: the number of molecules adsorbed by an element of surface is the excess of the number present, over and above the number which would be present if the bulk gas concentration were maintained up to a chosen surface separating the solid and

gas phases. Let $Z = o$ be a plane passing through the nuclei of the surface atoms, the half space $Z < o$ be the solid, the half space $Z > o$ be the gas, and $C(Z)$ be the gas concentration, moles/cc, at Z. Suppose $C = o$ for $Z < o$, $\lim_{Z \to \infty} C(Z) = C_o$, and let $Z = \ell$ be the Gibbs dividing surface. The surface excess referred to the plane $Z = \ell$ is then

$$\Gamma_\ell = \int_o^\ell C(Z)dZ + \int_\ell^\infty (C(Z) - C_o)\, dZ \qquad (3.2)$$

or

$$\Gamma_\ell = C_o \ell + \int_o^\infty (C(Z) - C_o)dZ \qquad (3.3)$$

Evidently Γ_ℓ varies linearly with ℓ; so far as the Gibbs convention is concerned choice of ℓ is arbitrary. Barker and Everett (47) have substantially chosen $\ell = S_o$, the position at which $E(Z) = o$ (i.e. the distance from the surface at which the potential changes from attractive to repulsive), whereas Halsey and co-worker's statistical mechanical treatment functionally chooses $\ell = o$. The surface excess is represented by the shaded areas in Figure 3(b).

Substituting Equation 3.1 into Equation 3.3 with $\ell = o$ gives

$$\Gamma = C_o \int_o^\infty (\exp\,(-E(Z)/kT)-1)dZ \qquad (3.4)$$

or exactly

$$\lim_{C_o \to o} \frac{\Gamma}{C_o} = \int_o^\infty (\exp(-E(Z)/kT)-1)dZ \tag{3.5}$$

Assuming an ideal bulk gas so that $C_o = P/RT$ and substituting n_a/A for Γ, Equation 3.4 becomes

$$n_a = AP \frac{1}{RT}\int_o^\infty (\exp(-E(Z)/kT)-1)dZ \tag{3.6}$$

or $$\lim_{P \to o} \frac{n_a}{P} = K_H A \tag{3.7}$$

where

$$K_H = \frac{1}{RT}\int_o^\infty (\exp(-E(Z)/kT)-1)dZ \tag{3.8}$$

Equation 3.7 is identical to Equation 2.33 and hence, represents Henry's Law for the system. If K_H can be evaluated experimentally (e.g. Bond and Spencer (49)) or calculated theoretically by use of Equation 3.8, then the surface area A can be calculated from experimental limiting values of n_a/P. The use of Equation 3.8 to calculate K_H requires that E(Z) be known. The evaluation of K_H theoretically will be covered in a later section.

It is usual to define an "excess volume" (V_{ex}) as the volume that n_a moles of adsorbed gas would occupy if present at a pressure P, or

$$V_{ex} = \frac{n_a RT}{P} \tag{3.9}$$

also,

$$V^o_{ex} = \lim_{P \to o} V_{ex} = K_H A \cdot RT \tag{3.10}$$

Hence,

$$V^o_{ex} = A \int_o^\infty (\exp(-E(Z)/kT)-1)dZ \tag{3.11}$$

Hitherto it has been assumed that the system under consideration consists of a solid adsorbent in the presence of n moles of gas and hence an excess volume is defined. If the number of moles of gas adsorbed is directly measured by an experimental technique (gravimetrically with a vacuum microbalance) Hansen (50) has shown that if the solid structure is undistorted near the surface the measurement yields an unambiguous volume excess referred to the plane $\ell = o$. But, most experimental techniques used in adsorption studies determine the volume of gas adsorbed and hence the excess volume by an indirect measurement. Defining nRT/P as V_a (the apparent volume of the vessel containing the adsorbent when n moles of gas are introduced), the excess volume is given by

$$V_{ex} = V_a - V \tag{3.12}$$

The use of Equation 3.12 to calculate V_{ex} requires that V, the volume of the vessel minus the volume of the solid or

the "dead-space" volume, be known. The previous discussion has implied that for large T, $V_{ex} = o$; hence, $V = V_a$. In general, it is either impractical or undesirable to determine V in this fashion. Hence, the usual procedure is to use a "non-adsorbed" gas such as helium, hydrogen, or neon to obtain V. Making use of the Boltzmann distribution function, the apparent volume (V_a) of an adsorbed gas is given by

$$\lim_{P \to o} V_a = \lim_{P \to o} \frac{n}{C_o} = \frac{A}{C_o}\int_o^\infty C(Z)dZ = A\int_o^\infty \exp(-E(Z)/kT)dZ \quad (3.13)$$

and for a non-adsorbed gas the apparent volume (V_a') is given by

$$\lim_{P \to o} V_a' = \lim_{C_o' \to o} \frac{n'}{C_o'} = A\int_o^\infty \exp(-E'(Z)/kT)dZ \quad (3.14)$$

whence, the excess volume (V_{ex}^o) is obtained as

$$V_{ex}^o = \lim_{P \to o} V_a - V_a' = A\int_o^\infty [\exp(-E(Z)/kT) - \exp(-E'(Z)/kT)]dZ \quad (3.15)$$

In order to reduce Equation 3.15 to 3.11 it is necessary to assume that E'(Z)/kT is zero for all Z. For practical purposes, the assumption can be safely made for helium at ice temperature and for hydrogen and neon above room temperature for values of Z greater than the S_o value for the adsorbed gas.

The previous discussion has been an attempt to examine more closely the assumptions and approximations inherent in the theoretical as well as experimental evaluation of Henry's law constant and hence, the surface area of a solid from high temperature adsorption data. From a practical point of view, it is impossible to obtain the experimental accuracy necessary to distinguish between approximate and exact theoretical treatments.

Up to this point it has been presumed that the potential energy function $E(Z)/k$ is known, but in practice it is necessary to assume an analytical form for $E(Z)/k$, which is impossible to verify exactly through adsorption studies. The representation $E(Z)/k$ implies that the potential energy function is only dependent upon the distance from the surface and not upon the position on the surface. In more usual terms, the surface is treated as being homogeneous rather than heterogeneous. The treatments could be generalized simply by replacing the surface area A by a double integration over the surface.

2. Capillary surfaces

The treatment of high temperature adsorption on a capillary surface is exactly the same as that for a plane surface except for a change in coordinate system. If it is assumed that surface exists as cylindrical capillary holes, and if the coordinate axis lies on the axis of the cylinder,

then the surface excess per unit area of capillary is given by

$$\Gamma = \frac{1}{2\pi R}\int_{o}^{R}\int_{o}^{2\pi}[C(\theta,r) - C_o(\theta,r)]r d\theta dr \qquad (3.16)$$

where R is the radius of the cylindrical capillary surface passing through the surface atoms. Since the potential energy field of the solid is cylindrically symmetrical, the usual Boltzmann distribution function can be used; hence the equivalent of Equation 3.5 for a cylindrical capillary is given by

$$\lim_{C_o \to o} \frac{\Gamma}{C_o} = \frac{1}{R}\int_{o}^{R}[\exp(-E(r)/kT)-1]r dr \qquad (3.17)$$

which can be written in the form of Equation 3.11 as

$$V_{ex}^{o} = \frac{A}{R}\int_{o}^{R}[\exp(-E(r)/kT)-1]r dr \qquad (3.18)$$

or in dimensionless form

$$\frac{V_{ex}^{o}}{AS_o} = \int_{o}^{R/S_o}[\exp(-E(r/S_o)/kT)-1](r/R)d(r/S_o) \qquad (3.19)$$

A brief comment on the concept of a bulk gas concentration in a capillary is in order. For reasonably large capillaries the distinction between a curved surface and a plane surface ceases to exist, but for capillaries with diameters on the

order of molecular dimensions the overlap of potential energy fields becomes appreciable resulting in an increase in the concentration above that for a plane surface with the same free volume/surface area ratio.

B. The Two-Dimensional Gas Film Model

If only small deviations from Henry's Law behavior are assumed, and if $-E^{*}_{AS}/kT$ [*] is sufficiently large, then the "adsorbed gas" can be treated as a "two-dimensional gas" moving in a plane parallel to the solid surface, but at a mean distance Z_o from the surface. The extent of the adsorbed gas is given by the shaded areas under the curve in Figure 3(b) which was calculated for $-E^{*}_{AS}/kT = 3$ for convenience in plotting. Most systems of experimental interest have values of $-E^{*}_{AS}/kT > 5$ which confines the adsorbed gas to an even smaller region about Z_o. In addition to the two-dimensional motion, there is a vibrational motion of the molecules perpendicular to the surface which is governed by the curvature of the potential energy curve at its minimum. It can be easily shown that for a 3-9 potential function (Equation 3.34) the mean square displacement is given classically by

$$<(q^2/Z_o^2)> = [kT/27(-E^{*}_{AS})] \qquad (3.20)$$

---

[*] E^{*}_{AS} is the minimum potential energy for gas-solid interactions.

where $q = Z - Z_o$ and the (3-9) potential energy function has been treated as a simple harmonic function near the minimum. For $-E^*_{AS}/kT > 5$, the root mean square displacement $\langle q^2 \rangle^{1/2}$ is always less than 0.086 Z. Therefore, the initial assumption of the two-dimensional gas model is reasonable.

Statistical mechanical treatments of the two-dimensional gas model have been given by Sams et al. (48) and Barker and Everett (47). Barker and Everett have also given a simplified treatment which shall be followed here. The virial equation of state for an imperfect two-dimensional gas is

$$\Phi A = n_a RT \left(1 + B_2 n_a/A + \ldots \right) \tag{3.21}$$

where Φ is the spreading pressure and B_2 is the two-dimensional second viral coefficient. The Gibbs adsorption equation (15) is

$$A d\Phi = n_a RT \, d \ln P + B dP \tag{3.22}$$

where B is the second virial coefficient of the bulk gas. Differentiating Equation 3.21 and substituting Equation 3.22 in the result gives upon rearrangement

$$d \ln \frac{n_a}{P} = \frac{B}{RT} dP - 2 \frac{B_2}{A} dn_a \tag{3.23}$$

Integration of Equation 3.23 making use of $\lim_{P \to o} n_a/P = K_H A = K_1$ gives

$$\ln \frac{n_a}{P} \cdot \frac{1}{K_1} = \frac{BP}{RT} - \frac{2B_2 n_a}{A} \tag{3.24}$$

For small adsorptions, Equation 3.24 can be rewritten in exponential form, and the exponential expanded to first order terms. This gives

$$\frac{n_a}{P} = K_1 \left[1 - \frac{2B_2 n_a}{A} + \frac{BP}{RT} \right] \tag{3.25}$$

Experimentally and theoretically (47,48) it has been shown that n_a can be written as a power series in the pressure

$$n_a = K_1(T)P + K_2(T)P^2 + \ldots \tag{2.34}$$

Substituting Equation 2.34 into 3.25 and ignoring the term containing the product K_1K_2 yields

$$\frac{A}{B_2} = - \frac{2K_1^{\ 2}}{K_2 - K_1 \frac{B}{RT}} \tag{3.26}$$

Theoretically $B_2(T)$ is given by

$$B_2(T) = - N\pi \int_0^\infty [\exp(-E^*(r)/kT)-1]rdr \tag{3.27}$$

where N is Avogadro's number and $E^*(r)$ is the potential energy function between two adsorbed molecules. Hence, if $E^*(r)$ is known, then $B_2(T)$ can be calculated and if experimental values of $A/B_2(T)$ are evaluated using Equation 3.26, then the surface area A of the adsorbent can be calculated.

C. Statistical Mechanical Theory

As stated in the last two sections, the application of the principles of statistical mechanics to a system of N molecules in the presence of a solid surface give essentially the same results as the simple approaches which is, of course, fully expected. The differences lie not in the basic equations but in the small "correction" term or terms. Only a very brief outline of the statistical mechanical theory will be given.

The total potential energy U of N gas molecules in the potential field of a solid adsorbent can be written as the sum of separate gas-solid interaction potentials, $E(R_i)$, and the gas-gas interaction potentials $u(R_{jk})$. U is given by

$$U = \sum_{i=1}^{N} E(R_i) + \sum_{j>k}^{N} \sum_{k=1}^{N-1} u(R_{jk}) \tag{3.28}$$

The partition function Z is then

$$Z = \left(\frac{2\pi mkT}{h^2}\right)^{3N/2} \frac{1}{N!} \int \cdots \int \exp - \frac{U}{kT} \, dR_1 \ldots dR_N \tag{3.29}$$

This is developed by the standard methods of the theory of imperfect gas with the exact procedure dependent upon the desired end result.

Halsey and co-workers (46,51) have preferred to treat the interaction of gases with a solid surface by a virial

coefficient treatment that can be written as

$$n_a = \frac{B_{AS}}{RT} P + \frac{C_{AAS}}{(RT)^2} P^2 + \ldots \tag{3.30}$$

where B_{AS} and C_{AAS} are the second and third-gas surface virial coefficients respectively. Comparison of Equations 3.30 and 2.34 shows that $K_1(T) = B_{AS}/RT$ and $K_2(T) = C_{AAS}/(RT)^2$. Therefore, B_{AS} is effectively the Henry's Law constant and theoretically is given by

$$B_{AS} = A \int_0^\infty [\exp(-E(Z)/kT)-1]dZ \tag{3.31}$$

which is equivalent to Equation 3.11.

The extension of the statistical mechanical treatment to the two-dimensional gas model by Sams _et al_. (48) is along the same lines as the simple treatment given in the last section. Barker and Everett (47) have given a more formal statistical mechanical treatment which gives the Henry's Law model in the limit of zero pressure and the two-dimensional gas model when third-order interactions are included. The formal theory for the two-dimensional model gives

$$\frac{A}{(B_2-\alpha)} = - \frac{2K_1^{\,2}}{K_2 + \frac{3K_1B}{RT}} \tag{3.32}$$

which differs from Equation 3.26 only in the correction term involving the bulk gas second virial coefficient and the

inclusion of α which corrects for nonplanarity of the adsorbed phase.

D. Evaluation of Second Virial Coefficients

1. Introduction

The evaluation of second virial coefficients for gas-surface interactions or Henry's Law constants and the second virial coefficient for a two-dimensional gas as defined by Equations 3.11, 3.19 and 3.27 depends upon knowing the interaction potential as a function of distance. Initially, Steele and Halsey (46,52) assummed that the potential consisted of a London inverse sixth power attractive potential coupled with a hard sphere repulsive potential for molecular-molecular interactions. Since then, numerous authors (53 -56) have used a Lennard-Jones type potential function which in a generalized form is given by

$$E(r) = - \alpha r^{-p} + \beta r^{-q} \tag{3.33}$$

The special problem of the effect of a solid surface on the interaction potential between adsorbed molecules has been attacked by Barker and Everett (47) and by Sinanoglu and Pitzer (57).

2. Gas-surface second virial coefficients

a. Plane surface In general, Equation 3.33 should be summed over all the atoms of the solid, but is usual practice to replace the summation by integration over all

the atoms of a semi-infinite solid to yield for p = 6, q = 12

$$E(X) = E^{*}_{AS}\left[\frac{3}{2}X^{-3} - \frac{1}{2}X^{-9}\right] \tag{3.34}$$

where $X = Z/Z_o$ and E^{*}_{AS} is the minimum potential energy of gas surface interaction at $Z = Z_o$. The convention used throughout this dissertation is that all attractive energies are negative. Many of the previous equations contained the parameter S_o, the value of Z at which E(X) = 0. By use of Equation 3.34 it can be easily shown that

$$S_o = 3^{-1/6} Z_o \tag{3.35}$$

It shall be convenient to rewrite Equation 3.31 in dimensionless form as

$$\frac{B_{AS}}{AZ_o} = \int_o^{\infty} [\exp(-E(X)/kT)-1]dX \tag{3.36}$$

The integral can be evaluated for E(X) given by Equation 3.34 with the result

$$B_{AS} = AZ_o \left(\frac{t}{2}\right)^{1/9} \sum_{n=o}^{\infty} \frac{\left[3^{1/3}\left(\frac{3t}{2}\right)^{3/2}\right]^n}{n!(3n-1)} \Gamma\left(\frac{3n+8}{9}\right) \tag{3.37}$$

where $t = -E^{*}_{AS}/kT$. Therefore, it is readily seen that evaluation of B_{AS} depends upon knowing both t and the product AZ_o which is usually referred to as the capacity factor.

The preceding discussion suggests the following comments on notation. In general, the notation used depends upon the basic theoretical approach, i.e., from the surface excess and volume excess approach or by the statistical mechanical imperfect gas approach. The definition of the excess volume by Equation 3.12 is valid for any concentration of gas above the adsorbate. The expressions given by Equations 3.11 and 3.18 for the excess volume, for plane and capillary surfaces respectively, are only exact in the limit of zero pressure as implied by Equations 3.5 and 3.17 respectively. Likewise, Equation 3.31 for B_{AS} is only exact in the limit of zero pressure. To summarize,

$$\lim_{P \to o} V_{ex} = V_{ex}^{o} = B_{AS} = K_H A \cdot (RT) = K_1(T) \cdot (RT) \qquad (3.38)$$

Also, in the region of small deviations from Henry's Law behavior

$$\lim_{P \to o} \frac{dV_{ex}}{dP} = \frac{C_{AAS}}{RT} = K_2(T) \cdot (RT)^2 \qquad (3.39)$$

Henceforth, V_{ex}^{o} shall be used to represent experimental values of Henry's Law constant $K_H A$ or $K_1(T)$ and B_{AS} as the theoretical values of the same constants. Inasmuch as the theoretical value of dV_{ex}/dP is of no interest in the present work, C_{AAS}/RT will be used to represent its experimental value.

The evaluation of the gas-solid interaction potential $-E^{*}_{AS}/k$ and the capacity factor AZ_o requires that V^o_{ex} be determined as a function of temperature and the use of a procedure such as

$$\sum_T \ln V^o_{ex} - \sum_T \ln B_{AS}/AZ_o = \ln AZ_o \sum_T 1 \qquad (3.40)$$

where the summation is performed over all experimental points. In effect $-E^{*}_{AS}/k$ has become an adjustable parameter which can be used to minimize the sum $(V^o_{ex} - B_{AS})^2$. The slope of the plot $\ln V^o_{ex}$ versus $1/T$ can be used as an approximate value of $-E^{*}_{AS}/k$. If the value of Z_o is known or can be calculated, then the surface area A of the solid can be evaluated.

The above evaluation of the capacity factor AZ_o is rather complicated and generally obscures the relationship between the parameters. To increase the ease of parameter evaluation and to clarify the relationship between the parameters, an asymptotic expansion valid for large t has been developed by Hansen and Murphy (58) for the evaluation of the right hand side of Equation 3.36 and is given by

$$B_{AS} = AZ_o \, t^{-1/2} \, e^t \left(\frac{2\pi}{27}\right)^{1/2} \left[1 + \frac{175}{216t} + \frac{140105}{93312t^2}\right] \qquad (3.41)$$

or to about the same approximation

$$\ln B_{AS} \, T^{-1/2} = \frac{T_o}{T} + \ln \left(\frac{2\pi}{27 \, T_o}\right)^{1/2} AZ_o$$

$$+ \frac{175}{216} \frac{T}{T_o} + \frac{109480}{93312} \left(\frac{T}{T_o} \right)^2 \tag{3.42}$$

where $T_o = -E^*_{AS}/k$. Murphy (59) has shown that Equation 3.41 and 3.37 are equivalent for $t > 4$.

It can be seen from Equation 3.42 that if the left side is plotted against $1/T$, then, in the zeroth approximation, the limiting slope equals $-E^*_{AS}/k$ and the capacity factor AZ_o can be calculated from the intercept. The third and fourth terms on the right side of Equation 3.42 are correction terms to be used in successive approximations. They are calculated and then subtracted from the left hand side of the equation after which the limiting slope and intercept are once again determined. Three cycles are sufficient for convergence. Although it is not obvious from Equations 3.42, the intercept

$$\ln \left[\left(\frac{2\pi}{27T_o} \right)^{1/2} AZ_o \right]$$

is dependent upon the curvature of the potential minimum as well as the depth of the potential well. (See Hansen and Murphy (58) for more details.)

b. <u>Capillary surface</u> The evaluation of the second gas-surface virial coefficient for a capillary surface by Equation 3.19 necessitates the evaluation of $E(r/S_o)$ for various values of the capillary radius R. The capillary model of Steele and Halsey (52) shall be extended to replace their hard sphere repulsive potential with an r^{-12} repulsive

potential. It is convenient to identify the attractive part of Equation 3.33 with London forces for two isolated molecules as

$$E(r) = - C/r^6 \tag{3.43}$$

and the entire potential as the Lennard-Jones function

$$E(r) = 4\ E_o \left[\left(\frac{r_o}{r}\right)^6 - \left(\frac{r_o}{r}\right)^{12} \right] \tag{3.44}$$

To make Equation 3.43 and 3.44 consistant at large separations, it follows that

$$C = 4\ E_o\ (r_o)^6 \tag{3.45}$$

hence

$$E(r) = - C \left[\frac{1}{r^6} - \frac{r_o^6}{r^{12}} \right] \tag{3.46}$$

To obtain the gas-solid interaction potential it is necessary to sum the interaction between a gas molecule in the pore and all atoms in the solid; for this purpose Equation 3.46 must be integrated with appropriate boundary conditions over all the solid. A cylindrical coordinate system (ρ, Θ, Z) shall be used. The coordinate origin is the gas molecule and the Z axis is parallel to the axis of the cylindrical capillary. If the distance between interacting particles in a plane perpendicular to the Z axis is given by ρ, then the distance between a gas molecule and any point in the solid is

$(\rho^2 + Z^2)^{1/2}$. The interaction potential of a gas molecule at a distance r' from the axis of the capillary is given by

$$E(r') = -2N_oC \int_o^{\pi} \int_S^{\infty} \int_{-\infty}^{\infty} \left[\frac{1}{(\rho^2+Z^2)^3} - \frac{r_o^6}{(\rho^2+Z^2)^6} \right] \rho\, dZ d\rho\, d\Theta$$

$$o \leq r' < R \tag{3.47}$$

where S is the distance in ρ plane between the gas molecule and the wall of the capillary and N_o is the number of atoms per cm^3 in the solid. Performing the first and second integrations gives

$$E(r') = -\frac{\pi N_o C}{4} \int_o^{\pi} \left[\frac{1}{S^3} - \frac{7}{32} r_o^6 \frac{1}{S^9} \right] d\Theta \tag{3.48}$$

Applying the law of cosines to the triangle formed by S, r', and R gives

$$S = r' \cos \Theta + [R^2 - r'^2 \sin^2 \Theta]^{1/2} \tag{3.49}$$

Rewriting Equations 3.48 and 3.49 in terms of reduced variables gives

$$E(r'/S_o) = -\frac{\pi N_o C}{4S_o^3} \int_o^{\pi} \left[\frac{1}{(S/S_o)^3} - \frac{7}{32} \frac{r_o^6}{S_o^6} \frac{1}{(S/S_o)^9} \right] d\Theta \tag{3.50}$$

and

$$S/S_o = (r'/S_o) \cos \Theta + [(R/S_o)^2 - (r'/S_o)^2 \sin^2 \Theta]^{1/2} \tag{3.51}$$

If the potential function given by Equation 3.46 had been integrated over a semi-infinite solid instead of the capillary solid, then it can be easily shown that

$$r_o = \left(\frac{15}{2}\right)^{1/6} S_o \tag{3.52}$$

and

$$E^*_{AS} = -\frac{1}{9(3)^{1/2}} \frac{\pi N_o C}{S_o^{\,3}} \tag{3.53}$$

Substitution of the last two equations into Equation 3.50 results in

$$E(r'/S_o) = \frac{9(3)^{1/2}}{4} E^*_{AS} \int_o^{\pi} \left[\frac{1}{(S/S_o)^3} - \frac{105}{64} \frac{1}{(S/S_o)^9}\right] d\theta \tag{3.54}$$

It has been necessary to assume that the distance from the surface where $E(r'/S_o) = 0$ is the same as that for a plane surface. The integration in Equation 3.54 was performed numerically by computer for various values of R/S_o. Relative potential energy curves for some values of R/S_o are shown in Figure 4. As can be seen, the curved surface only affects the potential appreciably for small values of R/S_o.

The second gas-surface virial coefficient for a capillary solid surface is given by Equation 3.19 or

$$\frac{B'_{AS}}{A'S_o} = \int_o^{R/S_o} [\exp(-E(r'/S_o)/kT) - 1](r'/R)\,d(r'/S_o) \tag{3.55}$$

The integration of Equation 3.55 was performed numerically by computer to obtain $B'_{AS}/A'S_o$ as a function of $-E^*_{AS}/kT$ for various values of R/S_o. A comparison of the surface areas and interaction potentials evaluated for the plane and capillary surface models will be made in a later section.

3. Two-dimensional gas second virial coefficients

In principle, the two-dimensional gas second virial coefficient $B_2(T)$ is experimentally measurable for a given adsorbate-adsorbent system if the surface area of the adsorbent is known. But, since the surface area of the adsorbent is the parameter of interest, it is necessary to calculate $B_2(T)$ theoretically so that the surface area can be calculated from Equation 3.26 or 3.37.

Initially, Sams et al. (48) and Barker and Everett (47) used the Lennard-Jones (6-12) potential function in the form suggested by Hirschfelder, Curtiss and Bird (60) to facilitate use of their tabulated parameters and written as

$$E^*(r) = 4E_o \left[\xi \left(\frac{\sigma}{r}\right)^6 - \left(\frac{\sigma}{r}\right)^{12} \right] \qquad (3.56)$$

where $\xi = 1$ for the time being and E_o, σ are the bulk gas parameters. The assumption that $\xi = 1$ for molecular interactions in the presence of a solid surface presumes that gas-gas and gas-surface interactions are additive. Freeman (61) has experimentally shown that this is not a good approximation. Barker and Everett (47) assumed that the attractive potential

was modified but the repulsive potential remained unchanged, i.e., $\xi \neq 1$ in Equation 3.56 which can be rewritten in the form

$$E^*(r) = 4E_o^* \left[\left(\frac{\sigma^*}{r}\right)^6 - \left(\frac{\sigma^*}{r}\right)^{12} \right] \tag{3.57}$$

where $E_o^* = \xi^2 E_o$ and $\sigma^* = (\xi)^{-1/6}\,\sigma$. Sinanoglu and Pitzer (57), using third-order perturbation theory, have shown that an additional r^{-3} term should be included in the interaction potential function to give

$$E^*(r) = 4E_o^* \left[\left(\frac{\sigma}{r}\right)^6 - \left(\frac{\sigma}{r}\right)^{12} - \eta \left(\frac{\sigma}{r}\right)^3 \right] \tag{3.58}$$

where $\eta = CS/4E_o\sigma^3R_m^3$. The effects of ξ and η upon the bulk gas potential are shown in Figure 5.

Substituting the potential functions given by Equations 3.57 and 3.58 into Equation 3.27 for the two-dimensional second virial coefficient and performing the integrations gives

$$\frac{B_2^{BE}}{N\pi\sigma^{*2}} = \xi^{1/3}\,\frac{B_2}{N\pi\sigma^2} = \xi^{1/3}\,\psi(T^*) \tag{3.59}$$

and

$$\frac{B_2^{SP}}{N\pi\sigma^2} = \psi(T^*) + \psi'(T^*) \tag{3.60}$$

with the functions ψ and ψ' defined as

$$\psi(T^*) = \frac{T^{*1/6}}{12}\,\Gamma(5/6) - \sum_{n=1}^{\infty} \frac{(T^*)^{n/2}}{n!}\,\Gamma\left(\frac{3n-1}{6}\right) \tag{3.61}$$

and

$$\psi(T^*) = \frac{T^{*\,1/6}}{12} \sum_{m=o}^{\infty} \sum_{n=o}^{\infty} \frac{(T^*)^{1/4(2n+3m+3)}}{!(m+1)!} \times$$

$$\Gamma\left(\frac{3m+6\ +1}{12}\right)\rho^{m+1} \qquad (3.62)$$

where $T^* = (4E_o/kT)$ and $\rho = -\eta$.

The function ψ and ψ' have been evaluated for various values of T^* and η and some values of $B_2^{SP}/N\pi\sigma^2$ are given in Table 1. The values in Table 1 agree with those of Johnson and Klein (62).

Johnson and Klein (62) have analyzed the data of Sams et al. (48) using the potential function of Sinanoglu and Pitzer as well as the potential function of Barker and Everett. Krizan and Crowell (63) have analyzed the data of Freeman (61) using the Sinanoglu and Pitzer potential function. Generally, the successful application of the Sinanoglu and Pitzer potential requires more accurate data and data obtained at temperatures near the two-dimensional Boyle point.

If the data are sufficiently accurate, the complete Equation 3.32 should be used where the two-dimensional second virial coefficient is corrected for nonplanarity of the adsorbed phase. An analytical expression for α has been given by Barker and Everett (47) and its use involves an iteration procedure which has been described in detail by Wolf and Sams (64).

The calculation and use of the two-dimensional second virial coefficients was performed by computer Program 5 (Appendix C). The calculations of $\psi(T^*)$ and $\psi'(T^*)$ involve summations requiring the use of recursion formulas. Since the recursion formulas are omitted in most treatments, they shall be included here.

Evaluation of $\psi(T^*)$ by computer requires a recurrence relation involving the function

$$F(n) = \frac{1}{n!}\,\Gamma\left(\frac{3n-1}{6}\right) \tag{3.63}$$

$$n = 0,\ 1,\ 2,\ \ldots$$

Using the property $\Gamma(n+1) = n\Gamma(n)$, it is readily shown that

$$F(n) = \frac{3(n-2)-1}{6(n-1)(n-2)}\,F(n-2) \tag{3.64}$$

$$n = 2,\ 3,\ 4,\ \ldots$$

with $F(0) = -\ 6.77274$ and $F(1) = 2.67888$.

Evaluation of $\psi'(T^*)$ by computer requires recurrence relations involving the function

$$G(m,n) = \frac{1}{n!\,(m+1)!}\,\Gamma\left(\frac{3m+6n+1}{12}\right) \tag{3.65}$$

$$m = 0,\ 1,\ 2,\ \ldots\ ;\ n = 0,\ 1,\ 2,\ \ldots$$

Using the property $\Gamma(n+1) = n\Gamma(n)$, it is readily shown that

$$G(m,n) = \frac{3(m-4)\ +\ 6n+1}{12(m)(m-1)(m-2)(m-3)}\,G(m-4,n) \tag{3.66}$$

$$m = 4,\ 5,\ 6,\ \ldots\ ;\ n = 0,\ 1$$

and

$$G(m,n) = \frac{3m + 6\ (n-2)+1}{12(m+1)(n)(n-1)}\ G(m,n-2) \tag{3.67}$$

$$m = 0,\ 1,\ 2,\ \ldots\ ;\ n = 2,\ 3,\ 4,\ \ldots$$

with $G(0,0) = 11.4984$, $G(1,0) = 1.33944$, $G(2,0) = 0.25364$, $G(3,0) = 0.06271$, $G(0,1) = 1.52187$, $G(1,1) = 0.564395$, $G(2,1) = 0.15970$ and $G(3,1) = 0.04961$.

E. Comparison of Plane and Capillary Surface Models

The potential energy for the interaction of a given gas molecule with a given solid having a plane surface has a minimum E^{*}_{AS} at a distance Z_o from the surface. The same gas molecule interacting with the same solid but within a cylindrical capillary of radius R will also give rise to a potential energy minimum $E^{*\prime}_{AS}$, but it will differ from E^{*}_{AS}, and its position and magnitude will vary with the ratio R/S_o. The ratio $E^{*\prime}_{AS}/E^{*}_{AS}$ was evaluated numerically and is presented as a function of R/S_o in Figure 7. The discontinuity appearing in the curve at $R/S_o \simeq 1.4$ reflects the value of R/S_o at which the position of the potential minimum coincides with the axis of the capillary. For values of $R/S_o < 1.4$ the overlap of potential fields decreases the interaction energy ratio until it becomes zero for $R/S_o = 1$ and repulsive in nature for $R/S_o < 1$ (i.e. the gas molecule cannot enter the capillary).

Whether adsorption occurs on a plane surface or in capillaries, a plot of $\ln V^{o}_{ex}$ versus $1/T$ will be nearly linear for T sufficiently small, i.e.,

$$\ln V^{o}_{ex} = \frac{S}{T} + I \tag{3.68}$$

Theoretically (see Equation 3.42), a plot of $\ln (B_{AS}/AS_{o})$ against $-E^{*}_{AS}/kT$ for the interaction of a gas with a plane surface will be nearly linear for $-E^{*}_{AS}/kT > 5$, i.e., it will very nearly coincide with its tangent whose equation is

$$\ln \frac{B_{AS}}{AS_{o}} = Q_1 \frac{-E^{*}_{AS}}{kT} + Q_2 \tag{3.69}$$

with Q_1 very nearly unity for $-E^{*}_{AS}/kT > 5$. A similar plot for the interaction of a gas with a capillary system will also be nearly linear, as can be shown by numerical integration of Equation 3.56. For the capillary system, therefore,

$$\ln \frac{B'_{AS}}{A'S_{o}} = Q'_1 \frac{-E^{*}_{AS}}{kT} + Q'_2 \tag{3.70}$$

The coefficient of $1/T$ could be treated so that the ratio $E^{*\prime}_{AS}/E^{*}_{AS}$ discussed above is included explicitly, but it is not pertinent to the present discussion to do so.

The surface areas are calculated from the intercepts of $\ln V^{o}_{ex}$ versus $1/T$ plots; from Equations 3.69 and 3.70 it follows that (since comparison will be based on the identification $V^{o}_{ex} = B_{AS} = B'_{AS}$)

$$\ln \frac{A}{A'} = \ln A_{app} = Q_2' - Q_2 \tag{3.71}$$

where A_{app} is the plane surface area equivalent to 1 cm^2 of capillary surface area. The dependence of A_{app} on R/S_o is shown in Figure 6. The identification $V_{ex}^o = B_{AS} = B_{AS}'$ implies that the coefficients of $1/T$ in Equations 3.68, 3.69 and 3.70 are also equivalent.

F. Diffusion in Capillaries

The different methods used to study high temperature adsorption in this work have different time parameters. In elution gas-solid chromatography, for example, this is the time required for an elution peak to pass a point in the column (about 1 sec). In the gravimetric adsorption system it is the time allowed for equilibration. In the interpretation of experiments with porous adsorbents, it is important to realize that there is also a characteristic time for penetration of the capillary and the capillary surface will or will not reach substantial adsorption equilibrium depending on whether this latter time is short or long compared to the characteristic experimental time.

Clausing (65), from an interest in measuring the time of adsorption (τ), calculated the average time required for a molecule to pass through a capillary of length ℓ and diameter d as

$$\bar{t} = \frac{\ell^2}{2d\bar{u}} + \frac{\ell^2\tau}{2d^2} \tag{3.72}$$

where $\bar{u}$ is the mean velocity of the molecules. The first term arises from Knudsen diffusion while the second reflects the existance of τ. The time of adsorption τ is given by

$$\tau = \tau_o \exp\,(q_{diff}/RT) \tag{3.73}$$

where τ_o is the time of vibration of the adsorbed molecule and q_{diff} is the differential heat of adsorption.

It may be necessary to correct Equation 3.72 for surface migration. Clausing (66) approached the surface migration as being a two-dimensional diffusion problem and obtained $\bar{t}_1' = \alpha\bar{t}$ where

$$\alpha = 1 + \frac{3\tau\bar{L}_m\bar{u}}{2d^2} \tag{3.74}$$

and where $\bar{L}_m$ is the mean free path on the surface.

Kruyer (67) has considered a hopping molecule as the mechanism for surface migration which gives $\bar{t}_2' = \beta\bar{t}$ where

$$\beta = 1 + \frac{3}{4}\frac{\tau}{\tau'}\frac{a^2}{d^2} \tag{3.75}$$

and where (a) is the hopping distance and τ' is the lingering time after each hop.

For small values of ℓ and d, a simplified equation can be written for the two-dimensional diffusion model for surface migration as

$$\bar{t}_1' = \frac{\ell^2}{3\bar{L}_m\bar{u}} \tag{3.76}$$

which indicates that the diffusion is independent of the capillary diameter. If (a) is taken as approximately equal to interatomic distances of the surface atoms and if d approaches (a), then a simplified equation is obtained for the case of hopping molecules as

$$\bar{t}_2' = \frac{2\ell^2\tau'}{3a^2} \tag{3.77}$$

Everett (68) has shown that for nonlocalized van der Waals monolayer the isosteric heat of adsorption is given by

$$q_{st} = - E_{AS}^{*} + 1/2\ RT \tag{3.78}$$

Also, it can be shown that

$$q_{diff} = q_{st} - RT \tag{3.79}$$

hence,

$$q_{diff} = -E_{AS}^{*} - 1/2\ RT \tag{3.80}$$

For the purposes of calculating some numerical values, Equation 3.72 for $\bar{t}$ in absence of surface migration, assuming the term due to Knudsen diffusion can be ignored, and Equation 3.77 for $\bar{t}_2'$ can be rewritten in more suitable forms using Equations 3.73 and 3.80 as

$$\log \bar{t} = \log 303 \frac{\ell^2}{d^2} + 0.434 \frac{-E^*_{AS}}{RT} \tag{3.81}$$

and

$$\log \bar{t}'_2 = \log 54.5\ \ell' + 0.217 \frac{-E^*_{AS}}{RT} \tag{3.82}$$

where ℓ and ℓ' are in cm and d is in Å. It was assumed that $\tau_o \simeq 10^{-13}$ sec, a = 3 Å and that the activation energy associated with τ' is equal to $q_{diff}/2$. In Figure 8 values of log $\bar{t}$ and log $\bar{t}'_2$ versus $- E^*_{AS}/RT$ are plotted for d = 5 Å and several values of ℓ and ℓ'.

A more complete discussion of diffusion in capillaries is given by de Boer (69).

G. The Evaluation of S_o and/or Z_o

It has been pointed out that the surface area is not obtained directly from the Henry's Law theory, but a capacity factor is obtained which is the product AS_o or AZ_o. Therefore, S_o must be evaluated external to the theory if the surface area is to be determined. Several methods have been used at various times to evaluate S_o.

Once the value E^*_{AS} is known, S_o can be evaluated from Equation 3.53

$$E^*_{AS} = - \frac{1}{9 \cdot 3^{1/2}} \frac{\pi N_o C}{S_o^3} \tag{3.53}$$

if the constant C which arises from London's (70) formulation of dispersion forces is known. Several formulas have been proposed for the calculation of C, of which the best attempt is due to Kirkwood-Müller (71,72), and are summarized by Margenau (73). Halsey and co-workers have used this method to determine S_o and hence the surface area. As to be expected, the surface area calculated depends upon the particular formula used to calculate C. Since a given adsorbent should have the same surface area available to various adsorbates, it has been proposed (56) that if the capacity factor AS_o is plotted versus the second virial radii of the adsorbates, a straight line should result whose slope is equal to the surface area. In practice, areas thus calculated were lower than those based on the Kirkwood-Müller formula, but comparable areas were obtained if crystal radii were used in place of the second virial radii.

The easiest and simplest method for evaluation of S_o was proposed by Hansen (55) who used the "combining laws" suggested by Hirschfelder, Curtiss and Bird (60) that $\sigma_{AB} = 1/2\ (\sigma_{AA} + \sigma_{BB})$, σ_{AB} being the distance at which the intermolecular potential between molecules A and B is zero. If a 3-9 potential function is used to represent gas-solid interactions, it can be shown that $S_o = 0.7147\ \sigma_{AB}$. Also, $X_o = 0.8584\ \sigma_{AB}$ and $X_o = 1.201\ S_o$. This method was used in the calculation of all Henry's Law surface areas reported.

Values S_o and X_o using this method are given in Table 2 for several adsorbates on carbon and silica gel adsorbents. σ_{AA} for carbon was chosen as equal to the interplanar spacing of graphite or 3.4 Å and σ_{AA} for silica gel was chosen as equal to the crystal diameter of the oxide ion or 2.8 Å.

IV. APPLICATION OF GAS-SOLID CHROMATOGRAPHY TO STUDY OF PHYSICAL ADSORPTION

The application of gas-solid chromatography to the study of physical adsorption makes use of principles laid down by Wilson (74), Weiss (75), De Vault (76) and Glueckauf (77) for liquid-solid chromatography. Although there are several different types of chromatographic processes, only two are of interest in gas-solid chromatography. They are: (1) Elution gas-solid chromatography (alternately known as pulse flow or impulse chromatography) whereby a small sample of adsorbate is injected into the column containing the adsorbent and is carried through the column by an inert carrier gas. (2) Frontal gas-solid chromatography (alternately known as continuous or step flow chromatography) whereby at some given time the adsorbate is injected continuously into the carrier gas stream. The method for continuously injecting the adsorbate depends upon its physical state at room temperature. Henceforth, elution gas-solid chromatography shall be referred to as EGC and frontal gas-solid chromatography as FGC.

The measurement of surface areas by the BET method using FGC to obtain the adsorption data has been developed by Nelson and Eggertsen (78) and extended by Haley (79) to include the size distribution of pores. EGC has also been used by

several authors (80-85) to determine heats of adsorption. The heat of adsorption measured is effectively the isosteric heat of adsorption at zero surface coverage. FGC (86-90) and EGC (91-93, 89,90) have been used to measure adsorption isotherms of adsorbates that are usually liquid at room temperature (e.g. hexane and benzene) over the temperature range 0-600°C. The gas chromatographic methods thus far referred to require that either the chromatographic detector response be linear with partial pressure of adsorbate or that a suitable calibration be made. Schay and co-workers (94,95) have described a FGC method suitable for measurement of adsorption isotherms of permanent gases and light hydrocarbons. Robbins (96) has used a combination of FGC and EGC methods to measure adsorption isotherms at temperatures between 800-1200°C.

The use of gas adsorption chromatography in physical adsorption studies has both advantages and disadvantages. The principal advantages are versatility and applicability to high temperature adsorption studies. Its principal disadvantage is a lack of necessary accuracy under certain conditions.

Now, it is desirable to develop the theoretical relationships between the chromatographic parameters, the adsorption isotherm and the gas-surface virial coefficients as defined in the preceding sections. It shall be convenient to consider

the chromatographic system as consisting of one gram of adsorbent packed in column of length L at a temperature T_c °K. At time zero, a gas mixture containing a partial pressure P of adsorbate is fed into the column at a flow rate F. It shall be assumed that the input temperature equals the output temperature equals the temperature T_o (°K) of the flowmeter at which F is measured.

A differential material balance around the column can then be written as

Input - Output = Amount in dead space + Amount adsorbed at T_c (4.1)

or

$$\frac{F}{RT_o} P\, dt - \frac{F}{RT_o} P_i\, dt = \frac{V_o}{RT_c} dP_a + dn_a \qquad (4.2)$$

where V_o is the dead space volume. Following Robbins (96), integration of Equation 4.2 can be performed using initial conditions as: $t = 0$, $P_i = 0$, $P_a = 0$, $n_a = 0$ and steady state conditions as: $t = t_m$, $P_i = P$, $P_a = P$, $n_a = n_a^*$. Then

$$\frac{F}{RT_o} P \int_o^{t_m} dt - \frac{F}{RT_o} \int_o^{t_m} P_i\, dt = \frac{V_o}{RT_c} \int_o^{P} dP_a + \int_o^{n_a^*} dn_a \qquad (4.3)$$

Performing the integrations, which includes integrating the second integral on the left by parts, gives

$$n_a^* = \frac{F}{RT_o} \int_o^P t dP - \frac{V_o P}{RT_c} \tag{4.4}$$

If the adsorbate is not "adsorbed", then integrating Equation 4.3 gives

$$\frac{V_o P}{RT_c} = \frac{F}{RT_o} \int_o^P t_i dP \tag{4.5}$$

Substitution of Equation 4.5 into Equation 4.4 results in

$$n_a^* = \frac{F}{RT_o} \int_o^P (t - t_i) dP \tag{4.6}$$

In order to determine the amount adsorbed, it is necessary to evalute the integral in Equation 4.6. Under ideal conditions, the integration could be performed graphically, but in most practical cases this is not feasible.

It shall be convenient to consider an injected sample in EGC as an impulse input function. For linear gas chromatography (i.e. the adsorption isotherm follows Henry's Law) the output or response function to an impulse input function can be closely approximated by a Gaussian distribution function as shown in Figure 9(b). Reilley _et al_. (97) have given a very good discussion of gas chromatographic responses for various input functions. Although the response function could

be obtained by replacing the summation of the individual responses by an integration, a more powerful tool is to use a Laplace transform method to obtain the response function. For a step input function the response function obtained is shown in Figure 9(a). Inasmuch as the response functions are symmetrical about t_R (defined as the retention time), Equation 4.6 can be rewritten simply as

$$n_a^* = \frac{F}{RT_o} P \, (t_R - t_R') \tag{4.7}$$

or

$$\frac{n_a^* RT_c}{P} = F(t_R - t_R') \, (T_c/T_o) \tag{4.8}$$

The left hand side of Equation 4.8 is simply the excess volume (V_{ex}) as defined in previous sections. The product Ft_R is defined as the retention volume V_R.

If the maximum partial pressure of the adsorbate in the carrier gas stream lies outside the Henry's Law region, then the interpretation of the retention times becomes more complex. Injected samples of adsorbate exhibiting Type I, II, or IV isotherms (Figure 1) will give asymmetric response peaks with sharp fronts and diffuse tails whereas adsorbates exhibiting Type III or V isotherms (Figure 1) will give response peaks with diffuse fronts and sharp backs. Since Type III and V isotherms are quite rare, the remaining

discussion will be confined to systems exhibiting the other three types of isotherms.

The assignment of t_R' presents no problem since the adsorbate used to determine it is assumed not to be adsorbed and hence must necessarily fall in the Henry's Law region. As the maximum adsorbate concentration in a step input function is increased, the width of the adsorption front will decrease resulting in an increase in the slope of the chromatographic front shown in Figure 9(a). The placement of t_R should be chosen such that the shaded areas (A and A' Figure 9(a)) above and below the output peak are equal. On the idealized chromatogram t_R represents the point of inflection or half-step height of the chromatogram. Although in practice t_R should be chosen so that the areas A and A' are equal, the error introduced by using the half-step height position as equal to t_R is quite small for elongated S-shaped chromatograms.

The use of EGC to measure adsorption isotherms except in Henry's Law region is a questionable application. For a FGC system, the adsorbate partial pressure can be determined either by measuring the flow rate of the input gas stream with and without the adsorbate or by passing the carrier gas through the liquid adsorbate at a given temperature so that it becomes saturated with vapor before entering the column. For a EGC system a scheme must be devised by which the

maximum partial pressure can be calculated. The assignment of t_R also creates considerable problems unless the maximum partial pressure falls within Henry's Law region. The use of Equation 4.6 to determine the amount adsorbed requires that P_m be the same for both adsorbed and nonadsorbed adsorbates. The relationship between response of a chromatographic detector and concentration is such that this is difficult to achieve experimentally. Robbins (96) has proposed that for adsorbate-adsorbent sytems exhibiting Type I, II, or IV isotherms the half-peak height for the sharp front of an EGC peak be used for t_R. This results from an analogy with the corresponding FGC system which in the view of this author is totally unjustified. There is, however, some justification for using the peak maximum. While such effects as longitudinal diffusion and channeling will tend to broaden the chromatographic peak, the position of the peak maximum will remain relatively unchanged.

The identification of the left hand side of Equation 4.8 as equal to V_{ex} is sufficient to relate gas chromatographic retention volumes to the evaluation of gas-surface virial coefficients, two-dimensional gas virial coefficients and Henry's Law constants. A more direct relationship has been given by Hanlan and Freeman (98) who, using the imperfect gas theory of Halsey and co-workers, obtain

$$V_R \text{ (adsorbate)} - V_R \text{ (carrier)} = V_{ex} = V_{ex}^{o} + X_A P \quad C_{AAS}/RT \tag{4.9}$$

where $X_A P$ is the partial pressure of the adsorbate and V_R (carrier) is simply the retention volume for a "nonadsorbed" gas.

In Equation 4.8, the flow rate has in effect been corrected to column temperature. Under normal conditions there will be a small pressure drop across the column necessitating correction of the flow rate to column conditions, hence

$$V_{ex} = F(t_R - t_R') \ (T_c/T_o) \ (P_o/P_c) \tag{4.10}$$

where P_o is the outlet pressure and P_c the column pressure. If it is assumed that flow through the column can be treated as laminar flow through a long capillary, then the pressure correction factor proposed by James and Martin (99) is obtained which is

$$\frac{P_o}{P_c} = \frac{3}{2} P_o \left[\frac{P_i^2 - P_o^2}{P_i^3 - P_o^3} \right] \tag{4.11}$$

where P_i is the column inlet pressure. It can be shown that Equation 4.11 reduces to

$$\frac{P_o}{P_c} = \frac{P_o}{P_m} \left[1 - \frac{1}{12} \left(\frac{\Delta P}{P_m} \right)^2 \right] \tag{4.12}$$

where P_m is the arithmetic mean pressure and $\Delta P = P_i - P_o$. The second term in the brackets of Equation 4.12 can usually be ignored without introducing an appreciable error as it represents a correction for the difference between the arithmetic and the geometric mean pressure. Therefore, the excess volume correct to column conditions is given by

$$V_{ex} = F\ (t_R - t_R')\ \frac{T_c}{T_o}\ \frac{P_o}{P_m}\left[1 - \frac{1}{12}\left(\frac{\Delta P}{P_m}\right)^2\right] \qquad (4.13)$$

All adsorption measurements in the present study taken with the EGC system were presumed to lie in Henry's Law region. The values of t_R and t_R' for the adsorbed and nonadsorbed gases respectively were taken as the positions of the chromatographic peak maxima. Hence, the V_{ex} calculated from Equation 4.13 is equivalent to V_{ex}^o. The FGC system was used to determine the dependence of V_{ex} or n_a^* on P. The value of t_R' was again chosen as the position of the chromatographic peak maximum, while t_R was chosen as the position of half-step height of the chromatographic peak. Hence, each value of V_{ex} calculated from Equation 4.13 gives a point on the adsorption isotherm. Additional points on the adsorption isotherm were obtained by varying the adsorbate partial pressure in the carrier gas stream. The partial pressure of the adsorbate was calculated from

$$P = \frac{F_{adsorbate}}{F_{total}}\ P_m \qquad (4.14)$$

V. EXPERIMENTAL

A. Elution Gas-Solid Chromatography (EGC)

The EGC system used in this work was essentially the same system used by Murphy (59) and described by Hansen et al. (100). For the sake of consistency the system shall be described herein.

The basic system was a Research Specialties Company 600 series gas chromatograph consisting of a M604 main control unit, a M605-1 katharometer (thermal conductivity detector) power supply, a M606 flow controller and a M608-1 recorder unit. The recorder was a Leeds and Northrup Speedomax H with a 9 inch chart. A chart speed of 1 inch/minute was used in all experiments.

A constant temperature bath was used to provide accurate temperature control of the detector-column assembly over the temperature range 25-500°C. The bath consists of a stainless steel tank 9 inches in diameter and 10 inches high placed in a sheet metal box and insulated with fire brick and Zonolite. The tank rested on copper plate which could be heated by a 1500 watt ring heater and was separated from the main insulation by a sheet metal shield and a layer of sand to facilitate the changing of bath material, etc. The top of the tank was insulated with two pieces of 1/2 inch transite.

Fine temperature control was obtained with a 150 watt heater operated by the M607-3 proportional temperature controller using a platinum resistance sensing element. Mineral oil was used as the bath material over the temperature range 25-150°C and a sodium nitrite - potassium nitrate eutectic mixture over the temperature range 150-500°C. Stirring of the bath material was provided by a heavy duty stirring motor with a quartz blade.

The temperature of the bath material was measured by a platinum resistance thermometer and a Müeller bridge calibrated by the National Bureau of Standards. A Leeds and Northrup D.C. Guarded Null Detector (No. 9834) was used to determine the null point. The flow rate was determined by the time required for a film of sodium laurylsulfate to transverse a calibrated volume in a flow meter constructed from a 22 mm OD pyrex tube. The pressure drop across the column was measured by a simple U-tube mercury manometer. A gas sampling valve (Perkin-Elmer Company No. 154-0067) with 0.1 cm^3 sample volume was used to inject the gas samples into the carrier gas stream. This sampling valve is particularly useful in that additional sample loops can be attached quite readily.

The thermoconductivity (katharometer) detector used in the present work was a slight modification of the one described by Hansen et al. (100) and is shown in Figure 10. The detector was a full-flow split-stream model with the two halves of the detector identical. The detector was constructed from a 2 inch

cube of stainless steel. The internal passages of the detector were 1/16 inch in diameter and were constructed by drilling through from one side and then filling in the hole up to the first filament well. The external gas connection fittings (four altogether with one shown in Figure 10) were machined from stainless steel with half-twenty thread on the large end and the small end suitably machined for connection with 1/16 inch Swagelock tube fittings. The filaments used were Gow Mac Instrument Co. type W9225 (tungsten). The detector was assembled by placing a double knife-edge washer (101) in each well, inserting a filament together with a flared 1/4 inch stainless steel tube and finally sealing the assembly with a 1/2 inch hexagonal tube nut with half-twenty thread. The double knife-edge washers were also used to obtain gas tight seals with the input-output gas connection fittings.

A block diagram of the complete chromatographic apparatus is shown in Figure 11. Helium was used as the carrier gas in all chromatographic studies described herein. After the gas sample is injected into the carrier gas stream, it is split in two with each part passing over the filaments normally referred to as the reference filaments, thus producing a sharp negative signal. The two sample streams are then rejoined and passed through the column. After exit the gas stream is again split and passed over the sensing filaments producing the normal chromatographic peak. Typical chromatograms for

an adsorbed and for a non-adsorbed gas are shown in Figure 12 (a). The detector design insures close correspondence between gas concentration and detector response at the temperature of interest while providing a simple means of insulating the electrical leads from the bath material.

The adsorbents used in these studies were Columbia-L activated charcoal, grade LC 20/48, obtained from National Carbon Company and used by Murphy (59), SK activated charcoal obtained from Barnebey-Cheney, and a Fisher Scientific Company Silica Gel that was leached with nitric acid and washed by, but not used by, Murphy (59). All adsorbents were sieved to exclude particles larger than 20 mesh or smaller than 40 mesh. All samples were outgassed at 10^{-3} mm pressure and 400°C for the charcoals and 275°C for the silica gel. The adsorbents were packed into one-quarter inch OD stainless steel tubing of suitable length to give the desired sample size and then the column was coiled into a spiral 5 inch in diameter.

The gases used and their minimum purities were U.S. Bureau of Mines helium (99.999%), Air Reduction Co. research grade neon (99.999%), Matheson Co. C. P. Carbon monoxide (99.5%), C. P. methane (99.5%), prepurified nitrogen (99.996%), prepurified argon (99.998%), C. P. ethane (99.0%), C. P. ethylene (99.5%), instrument grade propane (99.5%), C. P. proplyene (99.0%) and bone dry grade carbon dioxide (99.8%). All gases were used as received.

Neon was chosen for use as the non-adsorbed gas because the more logical choice, hydrogen, gives complex peaks with helium carrier when its concentration is greater than 13 mole per cent (102).

B. Frontal Gas Chromatography (FGC)

The FGC system used in this work was for the most part constructed at this laboratory to provide the desired data. The components of the Research Specialties Company chromatograph used with the FGC system were the M605-1 katharometer power supply, the M607-3 proportional temperature controller and the M608-1 recorder unit.

A constant temperature bath similar to the one described for the EGC system was constructed for the FGC system. The bath container itself was a 2 1/2 gal battery jar. Mineral oil was used as the bath material. Temperature control was maintained either through the use of the M607-3 proportional temperature controller or by use of a Precision Scientific Co. electronic relay coupled with a mercury thermoregulator. Additional temperatures were obtained using an ice bath (0°C), melting bromobenzene (-31°C) and melting diethyl malonate (-50°C). The last two baths were prepared by freezing some of the liquid with liquid nitrogen.

The thermoconductivity detector used with the FGC system was a two filament model which was effectively the

sensing side of the detector used with the EGC system except that the internal passages were 1/8 inch in diameter and gas connections were made by silver soldering Swagelock reducers (No. 200-R-3-316) in the inlet and outlet ports of the detector block. Two 50 ohm Helipots were used as the reference filaments.

Many FGC studies have been carried out using adsorbates that are normally liquids at room temperature, permitting adsorbate concentrations to be easily established by bubbling the carrier gas through the liquid adsorbates at an appropriate temperature. The adsorbates of interest in this study were gases at the convenient experimental temperatures (i.e. 0°C and above). Hence, the gas mixtures were prepared by adding and mixing a carrier gas stream with an adsorbate gas stream. Since the accuracy of the data will reflect changes in the flow rates of the various gas streams, it is necessary to maintain the flow rates as nearly constant as possible. Constant differential type flow controllers Model 63 BU-L produced by Moore Products Co. (Springhouse, Pennsylvania) proved very satisfactory in maintaining constant flow rates. A fine needle valve must be used with the flow controllers, so Matheson Co. Model 621PB1 low flow flowmeters with 610 metering tubes were used to provide a suitable needle valve and at the same time indicated approximate flow rates.

The flow rates were measured by soap bubble flow meters using a solution of sodium laurylsulfate and constructed from 50 ml pyrex burets that were calibrated every 10 ml. The flow meters were housed in an air thermostat constructed from 3/4 inch plywood with a plexiglass sliding front door. The thermostat contained a small fan and a suitable heating element and was maintained at slightly above room temperature using a Precision Scientific Co. electronic relay coupled with a mercury thermoregulator.

The columns were usually U-tubes made from 8 mm OD pyrex tubing of suitable length so as to contain the desired amount of adsorbent. The columns were weighed, filled, outgassed at a suitable temperature with a stream of helium passing through the column and weighed again to determine the sample weight before attaching the column to the FGC system.

One-eighth inch OD stainless steel tubing was used throughout with the exception of sections leading to column input and from the detector output where 1/8 inch ID polyethylene tubing was used to obtain a certain degree of flexibility in that portion of the system. Swagelock tube fittings were used for all metal gas connections with 1/8 inch OD kovar-pyrex graded seals providing connections to the glass components of the system.

A schematic diagram of the FGC system is shown in Figure 13. An experiment is started by the interchange of a pure

carrier gas stream with the carrier gas stream containing a known partial pressure adsorbate by rotating the four-way stopcock S3. Attached to the plug of stopcock S3 was a plexiglass cam which operated a normally closed micro switch wired in series with the chart drive switch of the recorder. Hence, prior to the interchange of the gas streams the chart drive switch was closed and the micro switch opened and time zero can be indicated on the recorder chart. As stopcock S3 is rotated to interchange the gas streams, the cam is also rotated and the micro switch is closed to start the recorder chart. Since the filled column offers a flow resistance and hence, a pressure drop across it, a needle valve (V) was inserted to provide an equivalent pressure drop in the gas mixture stream as measured by the mercury U-tube manometers (M).

The partial pressure of adsorbate could be determined by measuring the flow rate of the adsorbate with flowmeter F1 and of the helium carrier with flow meter F2 before the two streams are added by switching stopcock S1. In practice, it is more convenient to determine the flow rate of the adsorbate by measuring the flow rate of helium carrier with F2, adding the adsorbate stream, and measuring the flow rate of the mixed stream. It is assumed that the partial pressure is given by Equation 4.14.

The dead space volume was determined using samples of neon injected into the carrier gas stream by the Perkin-Elmer gas sampling valve suitably coupled with the micro switch. A typical frontal chromatogram showing a neon peak is shown in Figure 12(b). The adsorbents and gases used in adsorption studies using FGC were the same as those described in the previous section for EGC.

C. Vacuum Microbalance (MB)

A gravimetric adsorption system was constructed to extend the range of adsorption measurements to regions in which chromatographic measurements are impractical. The main components of the gravimetric systems, henceforth referred to as MB, were a No. 2000 Cahn RG Electrobalance enclosed in a vacuum bottle and a Texas Instruments Inc. Model 145 Precision pressure gage equipped with high resolution read-out. The pressure gage was also equipped with a 10,000 ohm restransmitting potentiometer which was not used in these studies. A Type 6 Bourdon tube capsule with a No. 1 Bourdon tube serial No. 1898 was used with the pressure gage. The particular capsule-tube combination used permitted the measurement of absolute pressures of 0-32 inches of Hg with an accuracy of better than 0.01 mm Hg. The remaining components of the MB system were a vacuum pumping system and a gas handling

system. A schematic diagram of the complete system is shown in Figure 14 and a photograph of the system is shown in Figure 15.

The vacuum pumping system consisted of a 3-stage mercury diffusion pump suitably trapped and backed by a mechanical fore pump. The pumping system could be isolated from the MB itself by the large bore valve V2. A certain amount of flexibility was necessary between the valve and the pump-out port on the vacuum bottle and was provided by a pair of one inch ID stainless steel bellows welded to kovar-pyrex graded seals.

Since rather large quantities of gas are required for the MB system, a large gas storage is necessary. The gases used with the MB system were the same as those described for the EGC system. With the particular arrangement of the gas handling system, the gas was first passed through a fine capillary (0.009 inch ID) and then through a dry ice-acetone cold trap before reaching the gas storage bulb. Another section of similar capillary tubing provided control over the rate at which gas entered at the adsorption part of the MB system.

The electrobalance is based on the null-balance principle, using a torque motor to supply a restoring force to counteract changes in weight suspended from the balance beam. Therefore, changes in weight are given by changes in the electrical

signal to the motor. A helipot potentiometer is used to subtract a portion of the electrical signal applied to the motor before output to a recorder. A Mosely Model 7001A X-Y recorder, modified for potentiometric input, was used with the electrobalance in all adsorption measurements. Although the helipot potentiometer was the most accurate available commercially, in light of the present work, its replacement by an accurate voltage divider would permit better use of the accuracy available from the electrobalance and from recorders such as the Mosely Model 7001A.

Static electricity proved to be a serious problem, so the hangdown tubes containing the sample and the tare weight pans were covered with a conductive coating of stannous oxide.

Since the adsorbent sample was not in contact with the hangdown tube surrounding it, the adsorbent temperature could not safely be assumed equal to that of the tube, but was measured by means of a thermocouple located immediately above the sample.

A thermocouple support assembly (similar to Cahn Instrument Co. Cat. No. 2020) was machined to fit into the vacuum bottle standard taper joint for the sample hangdown tube. The assembly supported 2 hole 1/8 inch OD ceramic tubing used to support and insulate the thermocouple wires above the sample. To avoid creation of additional junction potentials, the thermocouple wires were brought out of the

vacuum bottle through a ceramic to metal vacuum feed through. This was soldered to a 1/4 inch OD kovar-pyrex graded seal which was glass blown to the center hangdown tube serving as the vacuum bottle pump-out port.

Copper-constantan was used as the thermocouple material. Twenty-four ga. copper and constantan were soldered in the feed through and connected to the measuring thermocouple made from 30 ga. constantan and 32 ga. Nylclad insulated copper. A reference thermocouple made from the same copper and constantan was kept at 0°C.

A calibration chart covering the temperature range 10-272°K for the particular constantan used was obtained from Dr. B. C. Gerstein at this laboratory. The calibration points in the range 76-86°K were plotted and an excellent straight line could be drawn through the points. The emf of the copper-constantan thermocouple was measured when immersed in liquid nitrogen at a temperature determined by a calibrated platinum resistance thermometer. The thermocouple calibration was then shifted so as to pass through the experimental point. In this way the formula

$$T(°K) = 87.25 - 64.0\ (MV - 5.040) \qquad (5.1)$$

was established, where MV is the emf of the thermocouple in mv.

In the range 0-100°C, the thermocouple was calibrated against the platinum resistance thermometer. The resulting temperature versus emf curve was fit via computer to a tenth degree polynomial in emf. The coefficients are given in Table 3.

A calibration chart is supplied with the Bourdon tube and capsule with points spaced approximately 40 mm apart. The calibration points were divided into three sections and fit via computer to fourth, seventh and fifth degree polynomials in gage readings respectively. The coefficients are given in Table 3.

After the electrobalance was set up according to the instruction manual, an appropriate amount of adsorbent was placed on the sample pan, the standard taper joints greased and the system evacuated with the fore pump. The mercury diffusion pump was then turned on. The adsorbent was outgassed with a tube furnace approximately 10 inches long at 400°C for the charcoals or 275°C for the silica gel for a period of 2 or 3 days. The background pressure with the adsorbent hot was 10^{-6} mm Hg or less. After the initial outgassing, the hangdown tube was wrapped with a neoprene covered heating tape, permitting further outgassing at 225°C between adsorption measurements at different temperatures if the measurements were to be made at 0°C or above. After

an adsorption isotherm at a given temperature was measured, the system was initially evacuated through the gas handling side before the valve to the high vacuum system was opened to avoid excessive filling of cold traps. With this procedure it was found that the system could be repeatedly evacuated without greatly impairing the pumping speed or the magnitude of the background pressure.

The desired temperatures were obtained with a liquid nitrogen bath, an ice bath and a circulating constant temperature water bath. The water bath consisted of two parts. A pyrex battery jar 10 1/8 inch OD and 10 inches deep with a 2 1/2 gal capacity was placed in a 5 gal pail and insulated with Zonolite to act as a reservoir. A lid for the pail was made from 2 inch styrofoam and cut to facilitate its removal. A suitable portion was cut out from one part of the lid to accommodate a Haake Constant Temperature Circulator - Model ED unitherm (distributed by Poly Science Corp.). The second part of the water bath consisted of a 100 mm OD closed pyrex tube 11 inches deep with suitable bottom inlet and top outlet tubes conducive to circular motion placed in a sheet metal box 9 inches square and 14 inches deep and insulated with Zonolite to act as a water jacket around the hangdown tube. The tube was held in place at the top with styrofoam and an additional styrofoam cap was used once the water jacket was

in place. Thickwall vacuum tubing was used to connect the pump of the Circulator to the inlet of the water jacket and for the gravity return from the water jacket to the reservoir. With this arrangement, temperatures could be controlled to within ± 0.05°C for periods of 2-4 hours.

VI. RESULTS

A. Processing of Experimental Data

1. Introduction

Most of the experimental data obtained during the studies described in this dissertation was processed by the use of one or more of the computer programs given in Appendix C. These programs are written in Fortran IV and have been used with IBM Model 360/50 and 360/65 computers. If the programs listed in Appendix C are used, then the symbol (at -@) should be replaced by an apostrophe (') throughout the programs when the Fortran source decks are prepared. The device used to list the source program decks interpreted the (') as an (@).

2. Gas chromatographic data

Most of the gas chromatographic data was processed by a computer program representing a combination of Program 1 (used to process raw data to obtain V_{ex}^{o} as a function of temperature through the use of Equation 4.13) and Program 4 (used to obtain the interaction potential $-E_{AS}^{*}/R$ and the capacity factor AZ_{o} from the V_{ex}^{o} versus temperature data through Equation 3.42). Experimentally, the raw data are obtained and processed in the order temperature/gases but must be in the order gas/temperature to evaluate $-E_{AS}^{*}/R$ and AZ_{o}. The previous computer program contained a machine

language routine to rearrange the data, but it was incompatible with the new computers so the rearrangement was performed by hand. Although, theoretically, it would be possible to write an almost complete program to eliminate bad points, etc., from a practical point of view in cases where the number of data points is relatively small the data should be plotted before deciding which points to use or not to use.

3. Microbalance data

a. General All microbalance (MB) data were processed by Program 2 or Program 3. Both programs make use of the polynomials given in Table 3 to determine the pressure above the adsorbent sample from Pressure Gage readings. There are two methods by which the MB can be set up for operation. The procedural details can be obtained by consulting the instruction manual and the set up methods are referred to as basic or alternate. Generalized equations for total sample weight and weight of gas adsorbed at a given pressure are given respectively as

$$SW = S - E + (D - B)\ M + P \times R$$

Basic method $E = 0,\ B = 0.0$

Alternate method $E \neq 0,\ B = 0.5$

and

$$WA = (D_2 - B)M_2 - (D_1 - B)M_1 + P_2 \times R_2 - P_1 \times R_1$$

Basic method $B = 0.0, \quad M_1 = M_2$

Alternate method $B = 0.5$ (6.2)

with D = Mass dial reading, in %/100 of f.s.

AM = M.D.R., in mg

P = Recorder reading in %/100 of f.s.

R = Recorder range setting, in mg

S = Substitution weight

E = Zero offset

where the notation is the same as used in Programs 2 and 3.

b. Low temperature nitrogen adsorption data

Temperatures near 80°K were calculated by the use of Equation 5.1. Application of the BET equations requires the saturation vapor pressure of nitrogen which between the temperatures 64° and 84°K is given (103) by the equation

$$\log_{10} P_o \text{ (mm)} = -\frac{339.8}{T} - 0.0056286\ T + 7.71057 \qquad (6.3)$$

A value of 15.8 $\mathring{A}^2$ was used as the area covered by a nitrogen molecule.

Program 3 will do a least squares fit using either the '∞ form' of the BET Equation (2.3) or the 'n-layer' BET Equation (2.4) following the method of Joyner et al. (18) with n=1 and n variable. A simple minimum search routine will determine the best value of n. When n=1, the Langmuir Equation (2.16) is obtained.

c. <u>High temperature adsorption data</u> The adsorption data for argon, nitrogen, carbon monoixde, methane, ethylene, ethane and carbon dioxide on Silica Gel, SK charcoal and Columbia-L charcoal were processed by Program 2 to obtain the gas-surface virial coefficients. Program 2, after calculation of the weight adsorbed (W_A) versus pressure (P), fits these data to a suitable nth degree polynomial for two purposes. First of all, the W_A versus P plots would not always pass through the origin and it was necessary to correct the W_A versus P plots by shifting them up (usually) or down. The principal reason for this origin displacement was an unbalanced signal from the MB to the recorder when the initial charge of gas was let into the vacuum bottle containing the MB (i.e. the pressure rise from 10^{-6} mm to 10^{-1} mm or so is almost instantaneous). The filtering and damping in the electrical system necessary to reduce noise level from vibrations, etc. are sufficiently large that the recording system does not recover completely. Possible solutions to the problem are to let in a few mm of He gas prior to actual adsorption measurements, use a variable leak valve such as those produced by Granville-Phillips Co. and using the MB in a more vibration free environment. Secondly, poor points were eliminated before proceeding futher. Suitable weights are applied to the low pressure points before curve fitting. The W_A versus P curve is transformed into a V_{ex} versus P curve (by Equation

3.9) and fit to an n-1 degree polynomial. The intercept or zeroth power term is V_{ex}^{o} and first power coefficient is C_{AAS}/RT. The V_{ex} versus P curve is then transformed into a $(V_{ex} - V_{ex}^{o})/P$ versus P curve and fit to an n-2 degree polynomial or to a first degree polynomial if n=2. The intercept now is equal to C_{AAS}/RT and provides a cross check on the previous value of C_{AAS}/RT. If n is greater than 2, then the first power coefficient is equal to D_{AAAS}/RT, etc., while if n=2, the curve $(V_{ex}-V_{ex}^{o})/P$ versus P should have zero slope. The V_{ex}^{o} versus T data are collected and fit by the same procedure used in Program 4 to obtain $-E_{AS}^{*}/R$ and AZ_{o}.

The experimental values of V_{ex}^{o} and C_{AAS} are used to calculate values of B_2/A versus T which are then fed into Program 5 to calculate the two-dimensional surface area and gas-gas interaction parameters. A brief outline of the method of least squares analysis used will now be given. When experimental and theoretical values of B_2 are equated, Equation 3.60 can be written as

$$\left[\frac{B_2(T_i)}{A}\right]_{exp} = \frac{N\pi\sigma_2^{\,2}}{A}\ \Phi(T_i^{*}) \tag{6.4}$$

where $\Phi(T_i^{*}) = \psi(T_i^{*}) + \psi'(T_i^{*})$ and $\psi'(T_i^{*})$ is zero if the Barker and Everett monolayer potential is used (see section III-D-3 for details on the evaluation of ψ and ψ'). If

$$\tau_i = \left(\frac{N\pi\sigma_2^{2}}{A}\right)_i \tag{6.5}$$

then

$$\tau_i = \left[\frac{B_2(T_i)}{A}\right]_{exp} \Phi(T_i^*) \tag{6.6}$$

Now, define

$$\bar{\tau} = \left(\sum_i^N \tau_i\right)/N \tag{6.7}$$

and

$$S = \sum_i^N (\tau_i - \bar{\tau})^2 \tag{6.8}$$

The procedure now is to minimize S by adjusting $-E_o^*/R$ to obtain the best value of $\bar{\tau}$. Hence, if σ_2 is known, then A can be calculated. For the Barker and Everett monolayer potential

$$\sigma_2 = \sigma_{BE}^* = \sigma\ (E_o/E_o^*)^{1/12} \tag{6.9}$$

and for the Sinanoglu and Pitzer monolayer potential

$$\sigma_2 = \sigma \tag{6.10}$$

where σ is the bulk gas collision parameter obtainable from tabulations of Hirschfelder, Curtiss and Bird (60). σ is not equal to the collision parameter (σ_{SP}^*) for Sinanoglu and Pitzer monolayer potential which can be calculated from Equation 3.58 by setting $E^*(\sigma_{SP}^*) = 0$. In certain cases, the minimization of Equation 6.8 was not performed, but $-E_o^*/R$ was simply incremented over a range such as $(-E_o/R)/2$ - $(-E_o/R)$ and the various parameters printed out with desired values chosen by inspection.

The processing of the MB data to obtain V_{ex}^{o} and C_{AAS} proved to be rather difficult for many of the adsorbate-adsorbent combinations used. Freeman and Halsey (51) showed that a plot of $\ln(-C_{AAS})$ versus 1/T should be linear. This along with the fact that $\ln V_{ex}^{o} T^{-1/2}$ versus 1/T should give a linear plot was used to obtain a consistent set of parameters by repeated trials.

B. Low Temperature Nitrogen Adsorption

The nitrogen adsorption isotherms were measured for all three adsorbents at approximately 80°K by use of the MB and are shown in Figure 16. The corresponding BET and Langmuir plots are shown in Figures 17 and 18 respectively and the best fit parameters obtained from these plots are given in Table 4. The parameters are tabulated with respect to the n-layer BET Equation (2.4) with $n=\infty$ again representing the normal BET Equation (2.3) and with n=1 representing the Langmuir Equation (2.16). The best fit value of n was also determined which in all cases turned out to be less than 1 (~.9). This represents a physically unreal situation (i.e. stating that less than a monolayer can be formed) and hence was ignored.

The BET surface areas are nominal values for adsorbents of this type. The average value of 703 m^2/g for the Silica Gel compares with a value of 650 m^2/g obtained previously using a volumetric adsorption apparatus. The Langmuir surface

areas are proportionally larger than the BET areas as is fully expected. The adsorption data were insufficient to determine a Langmuir surface area for Columbia-L charcoal. As can be seen in Figures 17 and 18, the BET equation fits the data to a relative pressure of 0.2 for Silica Gel and approximately 0.12 for SK charcoal while the Langmuir equation fits the data to relative pressures of 0.5. Hence, the implications are that more faith should be put into the Langmuir areas than the BET areas, but, from the material presented in Chapter II of this dissertation, there are many reasons for not accepting the values given as representing the true areas of the adsorbents, especially for the activated charcoals.

Consider a cylindrical pore of radius r and length ℓ. Its surface area is $2\pi r\ell$ and its volume is $\pi r^2\ell$. Suppose that the "BET or Langmuir" monolayer capacity actually corresponds volume filling of the pore, rather than covering its surface. The surface area calculated, erroneously, on the surface covering model will be

$$A_{app} = \frac{\pi r^2 \ell}{\bar{v}} \; a \qquad (6.11)$$

where $\bar{v}$ = molecular volume of nitrogen in the liquid state (58.2 $\mathring{A}^3$) and a = molecular cross sectional area taken as 15.8 $\mathring{A}$. The ratio of apparent to true area will therefore be

$$\frac{A_{app}}{A_{true}} = \frac{A_{app}}{2\pi r \ell} = \frac{ra}{\bar{v}} = 0.27r \qquad (6.12)$$

Where r is in Å. As will be discussed later, the charcoals apparently have a fraction of the surface area in pores or in large cavities with connecting pores of the order 2 Å in radius, others as large as 20 Å in radius, while the Silica Gel has pores of the order 20 Å in radius. Clearly the ratio of apparent to true surface area could vary from 0.5 to 5.

The values of the parameter C in Table 4 for $n=\infty$ can be related to the net heat of adsorption through Equation 2.2. The validity of Equation 2.2 is questionable at best so that the heats of adsorption were not calculated.

C. Frontal Gas-Solid Chromatography (FGC)

The use of FGC to measure adsorption isotherms (effectively V_{ex} versus P in the low pressure region) was an attempt to extend EGC measurements to determine the third order gas-surface virial coefficient (C_{AAS}) and from this to calculate the surface area of the adsorbent using the two-dimensional gas film model.

Adsorption studies were conducted with FGC using argon, carbon monoxide and methane on Columbia-L charcoal. Some additional studies were conducted using ethylene, ethane and carbon dioxide on Silica Gel and Columbia-L charcoal. With

the latter adsorbates the low pressure portion of the adsorption isotherm could not be sufficiently documented to evalute V_{ex}^{o} and C_{AAS}. The scatter of the experimental data precluded the evaluation of C_{AAS} for argon and carbon monoxide although V_{ex}^{o} could be evaluated with reasonable accuracy. Methane proved to be the only adsorbate giving data sufficiently accurate to permit the evaluation of both V_{ex}^{o} and C_{AAS}.

The methane adsorption isotherms on Columbia-L charcoal are shown in Figure 19 and the gas-surface virial coefficients thus determined are given in Table 13 along with values of V_{ex}^{o} obtained by use of injected samples with the FGC system. The data plotted according to Equation 3.42 are shown in Figure 20, which also shows the corresponding plots obtained for methane on Columbia-L charcoal with the EGC and MB systems. The surface areas and interaction potentials evaluated for the Henry's Law model by application of Equation 3.42 and for the two-dimensional gas film model are given in Tables 11 and 12 respectively.

D. Elution Gas-Solid Chromatography (EGC)

The Henry's Law constants for the adsorption of argon, nitrogen, oxygen, carbon monoxide, methane, ethane, ethylene, propane, propylene and carbon dioxide on Silica Gel, SK charcoal and Columbia-L charcoal were determined over wide temperature ranges by EGC. Columbia-L charcoal was used as

a check out adsorbent before proceeding with other adsorbents. All adsorbates used gave symmetrical chromatographic peaks at temperatues such that reasonable retention times with minimum peak broading were obtained thereby indicating that the measurements were indeed being made in the Henry's Law region. The one exception to the previous statement was carbon dioxide on SK charcoal. This system gave chromatographic peaks with nearly symmetrical tops but with the bottom portions exhibiting long sloping tails. Also, a portion of the first sample injected appeared to be irreversibly adsorbed. The anomalous behavior of carbon dioxide on SK charcoal is apparently due, in part, to strong quadrupole interaction with the π-bonds of the carbon surface (104).

Experimental values of V_{ex}^{o} versus T are given in Tables 17, 18, 19 for Silica Gel, Columbia-L charcoal and SK charcoal respectively. The same data are plotted according to Equation 3.42 in Figures 21-28. The surface areas and gas-solid interaction potentials evaluated for the Henry's Law model by application of Equation 3.42 are given in Table 11.

The reliability of the EGC determination of the Henry's Law constant, V_{ex}^{o}, depends on the particular adsorbate-adsorbent combination; the temperature range and carrier gas flow rate must also be considered. For the activated charcoals, as shall be discussed later, the gas molecules apparently do not "see" all of the available surface even at temperatures of 350°K.

Hence, the basic question arises as to just what is actually being measured by EGC using the charcoal adsorbents.

For the Silica Gel adsorbent, a general statement can be made that within broad limits the Henry's Law surface areas and gas-solid interaction potentials obtained from EGC and MB data are in reasonable agreement (compare values summarized in Tables 5 and 8). In general, the surface area values vary somewhat randomly with the usual trend of lower surface areas for larger gas molecules being partially observed. A more orderly variation for the gas-solid interaction potentials (Table 8) is observed. The gas-solid interaction values (as well as surface areas) for the gases Ar-CH_4 should be lightly regarded since the amount adsorbed was small at the temperatures used resulting in large relative errors. The values were calculated using only the three or four points which gave the best straight line. From Equation 3.42 it can be seen that a small error in the gas-solid interaction potential can be considerably magnified when the surface area is calculated. The random scatter in the Henry's Law surface areas (Table 5) for the two different runs (1 and 2) most probably reflects differences in sample preparation (e.g. length and temperature of sample outgassing).

E. Vacuum Microbalance (MB)

In addition to measuring the low temperature nitrogen adsorption isotherms on Silica Gel, Columbia-L charcoal and SK charcoal, the high temperature adsorption isotherms of some or all of the gases argon, nitrogen, carbon monoxide, methane, ethylene, ethane and carbon dioxide on the same three adsorbents were measured at four temperatures between 0-100°C by the MB system. Only the low pressure (0-300 mm) range was investigated.

The numerical high temperature adsorption isotherms are given in Tables 20, 21 and 22 for Silica Gel, Columbia-L charcoal and SK charcoal respectively. If it was necessary to correct the measured isotherms, then the corrected data are given in the tables. The gas-surface virial coefficients determined from the MB adsorption data are given in Tables 14, 15 and 16 for Silica Gel, Columbia-L charcoal and SK charcoal respectively. The surface areas and interaction potentials evaluated for the Henry's Law model by application of Equation 3.42 and for the two-dimensional gas film model are given in Tables 11 and 12 respectively. The V^{o}_{ex} versus T data plotted according to Equation 3.42 are shown in Figures 29-32.

The gravimetric measurement of adsorption isotherms using the MB has the advantage that the excess volume is unambiguously defined by

$$V_{ex}\ (cm^3/g\ adsorbent) = \frac{W_A \cdot RT}{M \cdot P} \qquad (6.13)$$

where M is the molecular weight of the adsorbate. If M = 3×10^4 mg and T = 300°K, then the change in V_{ex} for a change in W_A of 0.001 mg is given by

$$\Delta V_{ex}\ (cm^3/0.001\ mg\ g) = \frac{0.623}{P(mm)} \qquad (6.14)$$

Therefore, for V_{ex} = 10 cm^3/g, an error of 1% in V_{ex} reflects an error of approximately 0.002 mg/g if P = 10 mm.

The maximum sample weight that could be used with the present MB system set up was 750 mg prior to outgassing. The samples lost between 20-50 mg in weight upon outgassing thereby setting an effective limit of 0.001 mg on the accuracy obtainable with the MB system in its present environment, although the MB has a quoted sensitivity of 0.0001 mg for a 1 g load.

The MB adsorption data on Silica Gel were sufficiently accurate that good values of V_{ex}^{o} could be calculated, but not sufficiently accurate to evalute C_{AAS}. Within the accuracy of the measurements, the adsorption isotherms could be considered to obey Henry's Law over the pressure range used, although sufficiently accurate data would undoubtedly show that the adsorption isotherms exhibited a slight curvature. The calculated Henry's Law surface areas are comparable to those obtained from the EGC data.

The MB adsorption data on Columbia-L charcoal and SK charcoal were very similar with the same trends observed in the calculated parameters for both adsorbents.

The gases argon, nitrogen and carbon monoxide were adsorbed sufficiently by both adsorbents to permit the evalution of both V^o_{ex} and C_{AAS}. There is an estimated 10-20 per cent error in the C_{AAS} values obtained while the V^o_{ex} values are accurate within 2-3 per cent. The Henry's Law surface areas calculated are approximately 50 per cent larger than those calculated from the EGC data. The two-dimensional surface areas calculated reflect the uncertainty in the C_{AAS} values.

The Henry's Law surface areas calculated for methane from MB data were larger, by factors of 3-7, than those calculated from the EGC data. The two-dimensional surface areas were smaller, by factors of 6-20, than the Henry's Law surface areas calculated from the same data.

The high temperature adsorption isotherms for ethylene, ethane and carbon dioxide were measured only on SK charcoal. The calculated Henry's Law surface areas are from 30 per cent less to 75 per cent greater than the corresponding EGC values. The two-dimensional surface areas for ethylene and ethane are less by factors of 2 and 5 respectively than the Henry's Law surface areas. The two-dimensional and Henry's Law surface area for carbon dioxide differ by only 30 per cent.

The gas-surface virial coefficients evaluated from the MB data appear to be precise to within 1 - 2 per cent. However, even at the highest temperatures at which data were taken, the amounts adsorbed even in the low pressure range were sufficiently large to make it uncertain that the intercept and initial slope of the plot of V_{ex} versus P were correctly established.

See Tables 5, 6 and 7 for more direct comparisons of the previously stated observations. Possible explanations for these observations will be presented in the next section.

The gas-solid interaction potentials calculated from the MB data are lower than the corresponding EGC values. The larger MB Henry's Law surface area values reflect, in part, the decrease in the gas solid interaction potentials. The same trends are observed for both the MB and EGC gas-solid interaction potentials.

VII. DISCUSSION

A. General

The Henry's Law and two-dimensional surface areas calculated for the adsorbents Silica Gel, Columbia-L charcoal and SK charcoal from the EGC, FGC and MB data are summarized in Tables 5, 6 and 7 respectively. The corresponding gas-solid interaction potentials are summarized in Tables 8, 9 and 10.

A detailed error analysis of the experimental data and calculated parameters will not be made. Brief discussions of the accuracy of the data obtained by the various experimental techniques have been give in the appropriate places. Apart from the questions that have arisen pertaining to the interpretation with the EGC and MB systems, the principal errors in the evaluation of the gas-solid interaction potentials result from curve fitting of the experimental data. But, as Equation 3.42 shows, a small error in the gas-solid interaction potential is magnified in the evaluation of the intercept of the experimental plot and hence, in the evaluation of AZ_o from which the surface area is calculated once a value for Z_o is known. The calculation of Z_o as well as the uncertainties in the values calculated has been discussed in Section III-G. Therefore, after all things have been considered, it can be estimated

that there is a 10-20 per cent uncertainty in the surface area values given in Tables 5, 6 and 7, but nowhere near the factors of 6 to 20 that arise if either of the BET areas given in Table 4 are accepted as representing the true area of the adsorbent.

Also, all theoretical derivations of the two-dimensional gas and gas-solid virial coefficients have assumed that the solid acted as a homogeneous continuum and that a uniform potential energy field exists over the entire surface. But, it is almost certainly true that the surfaces of most adsorbents can be classified as heterogeneous rather than homogeneous. Surface heterogeneity can result from the existence of capillaries, different crystal planes exposed, variation in surface chemical composition and a number of other sources. The capillary surface problem has, in principle, been solved in Section III D-2(b). Freeman (54) has expressed the view that "within limits, this high temperature approach to physical adsorption is not bothered by surface heterogeneity". The treatment of the solid adsorbent as a continuum has converted the 6-12 molecular-molecular interacting potential law into a 3-9 molecular-surface potential law. It has also been necessary to assume that the gas molecule can be represented as a point particle. Spherical molecules such as the rare gases and nearly spherical molecules such as methane can be represented as point particles without stretching the analogy very far.

For gases such as nitrogen, carbon monoxide, ethylene, ethane, propylene, propane, and carbon dioxide the approximation as point particles does indeed become strained. Hence, for these molecules the theoretical potential energy curves should be derived with the inclusion of molecular orientation effects which present formidable, if not insurmountable, theoretical problems. Everett (105) has given an excellent, but simple, discussion on the effect of surface heterogeneity on the adsorption isotherm and on the theoretical evaluation of the adsorption potential energy curve.

Some discussion has been given at various times as to the applicability and accuracy of the experimental methods described in this dissertation. There are two basic approaches that can be taken in physical adsorption studies and they are (1) study the adsorption of a single adsorbate by series of adsorbents of the same structural type or (2) study the adsorption of a series of adsorbates on a single adsorbent. The usual approach to a study of physical adsorption is to take a combination of the two basic approaches. If the amount adsorbed for a specific adsorbate by an adsorbent at a given temperature is known, then rough estimates can be made as to adsorption of other adsorbates on other adsorbents and at other temperatures. It is this inner relationship between amount adsorbed, adsorbate, adsorbent and temperature that governs the applicability and accuracy of an experimental method. The experimental methods described in

this dissertation have a practical lower temperature limit of 0°C. Although various liquid N_2 and dry ice slushes can be prepared to obtain lower temperatures, considerable difficulties are encountered in maintaining constant temperatures for extended periods of time. In order to maintain constant temperatures between -196 and 0°C, it is necessary to use a suitably designed cryostat. A high precision adsorption apparatus for studying "high temperature" adsorption over this temperature range has been described by Constabaris et al. (106). The previous statements indicate, in part, the desirability of initially studying the high temperature adsorption of various adsorbates on different adsorbents by different experimental techniques. Ideally, if from the Henry's Law and/or two-dimensional gas film models the surface area(s) calculated can be specified as representing the "true" area of the adsorbent, then instead of changing the temperature range and/or experimental method to accommodate the adsorbent, the adsorbate could be changed to accomplish the same purpose.

The advent of modern high speed computers has made use of theories requiring long and complicated calculations practicable. Through the use of Equation 3.42, Henry's Law surface areas and gas-solid interaction potentials can be readily determined without recourse to a computer, but the application of the two-dimensional gas film model will, in

general, require the use of a computer.

B. Silica Gel

Summaries of the Henry's Law surface areas and gas-solid interaction potentials are given in Tables 5 and 8 respectively.

In Table 8 containing the gas-solid interaction potentials, there are two principle points of interest. For the gases argon, nitrogen and carbon monoxide the trend of increasing gas-solid interaction potentials is essentially the opposite to that observed for the corresponding gas-gas interaction potentials (see Table 14) indicating that orientation effects are more important in gas-surface interactions than in gas-gas interactions. The second region of interest is the change of the gas-solid interaction potentials over the series methane - propane. Both the gas-gas interaction potentials and gas-solid interaction potentials for the activated charcoals (Tables 9 and 10) show a trend of increasing potential over the series, but for Silica Gel the interaction potentials for ethylene and propylene are greater than the interaction potentials for ethane and propane respectively. The polarizabilities* parallel to the C-C bonds of ethylene and ethane are 5.61 and 5.48 x 10^{-24} cm^3 respectively, while the corresponding average polarizabilities are 4.76 and 4.47 x 10^{-24} cm^3.

---

*See table on page 179 of Reference 5.

Hence, it is insufficient to simply wave off the anomalous behavior as due to the polarizabilities of the molecules. A more reasonable explanation should include the basic differences in the bonding of the surface atoms. The surface of carbon adsorbents is presumed to have a graphite structure with π-electron orbitals determining the adsorption properties while the surface of the Silica Gel consists of oxide ions bonded through a crystal lattice. The possibility that the carbon surface contains various oxygenated species can not be completely excluded.

There isn't a great deal that can be said about the surface area values given in Table 5. The choice is between accepting the BET area of 700 m^2/g, the Langmuir area of ~1000 m^2/g or a value of 70-90 m^2/g from Table 5. The low temperature nitrogen adsorption isotherm in Figure 16 is clearly of Type I. A large amount of the difference among the values for a given gas can be attributed to variations in the exposed surface caused by differences in sample outgassing as well as length of time over which the experimental data were taken. Observations on the rate of adsorption with the MB system indicated almost instantaneous equilibration with all adsorbates used at temperatures above 0°C. Although no specific data on the pore size distribution for the Silica Gel was determined, minimum pore radii for similar Silica Gels have been given as 10-30 Å. The pores of Silica Gel are

usually found to be slit-shaped versus cylindrically shaped. Steele and Halsey (52) have shown that slit-shaped pores have considerably less effect in terms of an apparent area as shown in Figure 6 than cylindrical pores. Therefore, although considerable variation occurs among the Henry's Law surface areas, there are several reasons to expect that they more closely represent the true surface area of the Silica Gel than do either the BET or Langmuir values of the surface area.

None of the experimental techniques used in the present studies on Silica Gel provided sufficiently accurate data over the temperatures used to permit the evaluation of the surface area using the two-dimensional gas film model.

C. The Activated Charcoals

Summaries of the surface areas evaluated by application of the Henry's Law and two-dimensional gas film models for the Columbia-L charcoal and SK charcoal are given in Tables 6 and 7 respectively. Summaries of the corresponding gas-solid interaction potentials are given in Tables 9 and 10. The two-dimensional gas film model gas-gas interaction parameters are summarized in Table 12. Included in the summaries are the parameters evaluated by Hansen _et al_. (100) that have been corrected for an incorrect chart speed. Since, for practical purposes, any trends or anomalies observed for one charcoal

were also observed in the other charcoal, the discussion will consider both charcoals together, except for the FGC results which were limited to methane on Columbia-L charcoal.

A comparison of the gas-solid interaction potentials determined by EGC in the present study and by Hansen et al. (100) shows some anomalous but not readily explainable features. The gas-solid interaction potentials (as well as corresponding Henry's Law surface areas) agree perfectly for ethylene and propane, but there is considerable disagreement for the other gases where direct comparisons can be made. It would be expected that small differences would occur on the Columbia-L charcoal simply because of slight differences in sample preparation and general experimental procedures between the present and past investigators, although the samples were taken from the same batch of charcoal. The large difference observed for nitrogen is disturbing, but the fact that near perfect agreement is observed for ethylene and propane is encouraging. While the gas-solid as well as gas-gas interaction potential for ethane is larger than that for ethylene, the effective diameter of the ethylene molecule is larger than that for ethane (4.52 versus 3.95) as determined by the gas-gas collision parameter. Hence, the observations that all molecules that are effectively smaller than ethylene show greater interaction potentials for the present set of data, but with the magnitude of the difference decreasing as the size of the

molecule increases, most certainly indicates the effect of a porous structure.

The gas-solid interaction potentials for a given experimental technique generally increase as the size of the gas molecule increases (ethane and propane are exceptions). The gas-gas interaction potentials for the light hydrocarbons follow a similar trend.

A few comments on the interaction parameters evaluated for the two-dimensional gas film model are in order. It had been hoped that FGC would provide sufficiently accurate data to permit the application of the two-dimensional gas film model and that the MB system would expand the range over which useful data could be obtained. As can be seen from the error limits placed on surface areas in Table 12, the application of the model was not very successful for the charcoal adsorbents. The experimental errors have been discussed previously and the effect of the various types of surfaces will be discussed later. The second parameter of importance is ξ which relates the gas-gas and gas-gas surface interaction parameters through $E_o^* = \xi^2 E_o$ and $\sigma^* = (\xi)^{-1/6} \sigma$. The values of ξ approximately equal to 0.9 are in agreement with values obtained by other workers using various carbon adsorbents.

It remains to discuss the values given in Tables 6 and 7 for the surface area of the charcoal adsorbents. The relationship between the Henry's Law surface area and gas-solid

interaction potential $-E^{*}_{AS}/R$ is given by Equation 3.42. Hence, the discussion of the Henry's Law surface areas will indirectly reflect the values of $-E^{*}_{AS}/R$. It shall be convenient to compare the Henry's Law surface areas calculated from the experimental data in the following order: 1) EGC and MB, 2) EGC and FGC and 3) FGC and MB. Secondly, the change in the surface area calculated for the series of gases for a particular experimental method will be discussed. Last of all, the surface areas calculated from the MB data using the two-dimensional gas film model will be compared with the Henry's Law surface areas calculated from the same data. All of the surface area values given in Tables 6 and 7 were calculated from a plane surface model. The use of the MB system permits visual observation of the relative rates of adsorption through the time required for the system to achieve equilibrium. The gases argon, nitrogen and carbon monoxide came to equilibrium very rapidly with the addition of more gas to the adsorption system. The gases methane, ethane, ethylene and carbon dioxide required considerable time for equilibrium to be achieved after each addition of gas to the adsorption system, although approximately 70-80 per cent of each addition was adsorbed quite rapidly. A general decrease in equilibration times was observed as the temperature was increased.

It is immediately obvious that a plane surface model alone cannot explain the differences in the Henry's Law

surface areas calculated from the MB and EGC data for a given adsorbate. Hence, the capillary surface model of Steele and Halsey (52) was extended (Section III - A -2) to include a repulsive potential to aid in the interpretation of the calculated Henry's Law surface areas. The apparent area ($A_{app} = A_{plane}/A_{cap.}$) and the apparent interaction potential ($E^{*\prime}_{AS}/E^{*}_{AS}$) as a function of the capillary radius R divided by S_o are shown in Figures 6 and 7 respectively. In order for an adsorbate-adsorbent system to achieve true equilibrium, the adsorbate must be able to get to the available surface area. The average time of passage for a gas molecule through a capillary was developed (Section III - F) and is shown as a function of $-E^{*}_{AS}/RT$ in Figure 8. It shall be assumed that any capillaries present in the adsorbents are cylindrical in shape. Cross sections of three possible ideal surfaces are shown in Figure 33. Figure 33(a) shows the plane surface model, Figure 33(b) shows a capillary surface model consisting of two capillaries with different radii and Figure 33(c) shows a capillary surface model consisting of sections of capillaries with large radii connected by short sections with small radii.

The experimental values of V^{o}_{ex} and the observations on the time required to achieve equilibrium indicate the presence of capillaries with very small diameters. A possible model for the surface of the charcoals is as follows. If A is the true

area, including capillary walls, of a porous adsorbent, then the area A' obtained from a plane model satisfies

$$A' < A \tag{7.1}$$

Now, if it is assumed that the charcoal surface area consists of a fraction α in capillaries with mean radii of $R \leq 5$ Å and of a fraction $(1-\alpha)$ in capillaries with mean radii large compared to S_o, then for the MB data

$$A'_{MB} = A\,[\alpha \times A_{app}(R/S_o) + (1-\alpha)] \tag{7.2}$$

where it has been assumed that the entire area is available to the gas molecule. In the EGC column, the adsorbate sample spends only a small amount of time in the vicinity of an adsorbent particle. Hence, if the true gas-solid interaction potential $-E^{*}_{AS}/R$ was determined from Figure 7 for the small capillaries, the use of Figure 8 would show that a molecule would not penetrate very far into the capillary in the available time. Therefore, if it is assumed that the small capillaries are not seen in the EGC data,

$$A'_{EGC} = A \times (1-\alpha) \tag{7.3}$$

Now,

$$\frac{A'_{MB}}{A'_{EGC}} = \frac{\alpha \times A_{app}(R/S_o) + (1-\alpha)}{(1-\alpha)} \tag{7.4}$$

Equation 7.4 predicts that the ratio A'_{MB}/A'_{EGC} should decrease

as S_o increases. The ratios calculated for the series argon, nitrogen, methane, ethane and ethylene on SK charcoal are 1.85, 2.68, 4.25, 1.55 and 1.28 respectively. Therefore, although the adsorption data indicates the presence of capillaries with very small diameters, cylindrical capillaries alone cannot account for the large differences in the Henry's Law surface areas which is especially noticeable for methane on Columbia-L charcoal.

The calculation of a larger Henry's Law surface area from the MB data than from the EGC data reflects an increase in the amount adsorbed at a given temperature. It is also observed that the ratio $(V^o_{ex})_{MB}/(V^o_{ex})_{EGC}$ increases as the temperature increases. The significance of the last statement is difficult to ascertain. As the temperature of the adsorbent is increased, more of the internal surface existing in capillaries should become available to the gas molecules with the EGC system and hence, it would be expected that the excess volume ratio should increase if anything. It should also be pointed out that the MB data was taken over the temperature range of 273-350°K while the EGC data was taken over the temperature range 350-500°K.

It has been observed that extremely low values ($\leq 1\ m^2/g$) are obtained for the BET surface areas of some coals when calculated from low temperature nitrogen adsorption data, but more nominal values ($\sim 100\ m^2/g$) of the surface

areas are obtained when calculated from the heat of immersion in methonal. Maggs (107,108) has concluded that the surface area values calculated from the low temperature nitrogen adsorption data were in error. Gregg and Pope (109) have calculated the BET surface areas for a series of vitrains from the adsorption of nitrogen at -196°C, nitrogen at -183°C and butane at 0°C and the BET surface areas for each vitrain continuously increase as the temperature of the adsorption is increased. Maggs (110) and Zwietering et al. (111) have explained this anomalous behavior in terms of an capillary surface model such as the one shown in Figure 33(c) with narrow constrictions connecting enlarged sections. The passage of gas molecules through the narrow constrictions is considered to be an activated process which reflects the time required for the molecules to pass through the constriction, if the size of the molecule will permit to to pass through the capillary.

While in the present adsorption studies an increase in adsorption is not observed as the temperature is increased, the fact that a larger V^{o}_{ex} calculated from the MB data than from the EGC data may result from this effect. Hence, although the behavior of the ratio of the Henry's Law surface areas A'_{MB}/A'_{EGC} cannot be explained through the presence of cylindrical capillaries, the behavior of the Henry's Law ratio can be explained, in part, through a combination of

the adsorbent surface models (Figure 33) consisting of portions of plane, large cylindrical capillaries and cylindrical capillaries containing enlarged sections. The enlarged sections of the capillary must be, by necessity, quite large. Relatively small spherical shaped sections would have an even greater effect on the apparent area (Figure 6) than simple cylindrical capillaries. The trend of increasing Henry's Law ratio from argon-methane followed by smaller ratios for ethane and ethylene indicates the presence of constrictions with diameters in the range of 3-5 Å, i.e., large enough to permit passage of molecules the size of methane or smaller, but not molecules that are very much larger than methane. Whether or not a molecule can pass through a constriction will, of course, reflect the true value of the gas-solid interaction potential $-E^{*}_{AS}/R$ to the extent that it can be determined from Figure 7 and the time of passage through the constriction as indicated by Figure 8.

It would appear that the Henry's Law surface areas calculated from the EGC data are incorrect since apparently the injected gas sample spends insufficient time in the presence of an adsorbent particle for the gas to "see" all of the available surface area. At the same time, the question arises as to what the Henry's Law surface areas calculated from the MB data mean, especially in the case of methane. It appears that in the MB data the gases argon, nitrogen and

carbon monoxide can "see" all or most of the available surface. Methane "sits on the fence" so to speak between the lighter gases and the C_2 and C_3 hydrocarbons in regard to all experimentally determined gas-gas and gas-solid interaction parameters. The size and gas-solid interaction potentials for the C_2 and C_3 hydrocarbons are apparently sufficiently large to prevent the molecules from "seeing" all of the available surface.

In view of the previous discussion, comparisons of the Henry's Law surface areas calculated from FGC-EGC data and from FGC-MB data will be considered together. The Henry's Law surface areas calculated for methane on Columbia-L charcoal (Table 6) from data taken on the FGC system lie between the the EGC and MB values. Hence, it is apparent that more of the available surface is being "seen" in the FGC data than in the EGC data but not as much as in the MB data. This reflects an increase in the amount of time in which equilibrium can be achieved, but since the experimental V^o_{ex} values are determined from the appearance of the adsorption front, insufficient time existed for true equilibrium to be achieved. But, values of V^o_{ex} determined on the FGC system for argon and carbon monoxide on Columbia-L charcoal at 0 and 25°C agree with the MB values within 5 per cent.

In view of the previous discussion, it is not surprising that there is a general trend of decreasing surface area with increasing size of the adsorbate molecule. Similar effects

have been observed in BET surface areas evaluated for "porous" adsorbents (112) and in low area "non-porous" adsorbents (113).

The surface areas calculated using the two-dimensional gas film model and the Henry's Law model should be equivalent. As can be seen in Tables 6 and 7, the values for the Henry's Law and two-dimensional gas film surface areas calculated from the MB and FGC data do not show very good agreement. Once again, methane represents the dividing line between normal and abnormal results. While the surface areas for the gases argon, nitrogen and carbon monoxide should be accepted only as approximate values, they do indicate that most of the available surface is being seen by the gas molecules. In many respects, the two-dimensional gas film surface area values for methane, ethane and ethylene simply reflect the anomalous behavior of the Henry's Law surface areas for the same gases. The low values for the two-dimensional gas film surface areas can arise from either low values of V^{o}_{ex} or high values of C_{AAS}. For the larger gas molecules, the values of C_{AAS} are probably too high due to the simultaneous interaction of more than two molecules in the capillaries. Hence, while the exact reasons for the anomalous behavior may be obscure, it can be safely stated that capillaries with narrow constrictions must be present to explain the results.

What are the true surface areas of the charcoal adsorbents? For SK charcoal, the choices lie between the BET and Langmuir values of ~900 and ~1100 m^2/g adsorbent respectively or the 200-250 m^2/g adsorbent calculated from the high temperature adsorption of the smaller gas molecules. For Columbia-L charcoal, the corresponding choices are ~1200 and an estimated value of 1600 m^2/g adsorbent or 250-300 m^2/g adsorbent. In view of the problems associated with the interpretation of the high temperature adsorption data, it is no wonder that the interpretation of low temperature adsorption presents even greater problems with the theoretical ambiguities in addition to effects such as capillary condensation. Hence, while there exists some uncertainties in the surface areas calculated from the high temperature adsorption data, there is no reason not to accept the surface areas calculated as being more representative of the true surface area of the adsorbents than the BET and Langmuir surface areas.

VIII. SUMMARY

Three high temperature gas adsorption techniques, namely elution gas-solid chromatography, frontal gas - solid chromatography and microbalance gravimetry, have been studied as sources of surface area measurements. Surface areas have been calculated from high temperature adsorption data both from the temperature dependence of the initial isotherm slope (Henry's Law constant), which also provides gas-solid interaction potentials, and from the third virial coefficients for gas-solid interaction. Surface areas of all adsorbents studied were also obtained by the standard Brunauer-Emmett-Teller (BET) method based on nitrogen adsorption at liquid nitrogen temperatures.

The adsorbents studied were two activated charcoals and a silica gel; all were known to be porous adsorbents. All high temperature methods gave surface areas less, by factors as large as twenty, then the BET surface areas. For a given adsorbent, areas obtained by different techniques were in the order BET > microbalance > frontal gas-solid chromatography > elution gas-solid chromatography. The results obtained for the charcoals were consistent with an adsorbent model featuring large cavities connected by channels of molecular dimensions. The connecting channels introduce a transit

time requirement such that adsorption methods with short characteristic times, such as elution gas-solid chromatography, will not measure appreciable fractions of the cavity surface area, particularly if the adsorbate molecule is larger. It was found that the surface areas obtained from the high temperature techniques agreed more closely if the adsorbate molecule was larger than methane then if the adsorbate molecule was smaller than methane. The results obtained for the Silica Gel were not greatly affected by its porous structure.

The BET surface areas are probably unreasonably high and the indicated "monolayer capacity" on which these areas are based may actually represent a filling of cavity volumes by liquefied adsorbate. In principle, there appears to be no basis for considering BET surface areas more accurate than areas based on high temperature adsorption using techniques such as microbalance gravimetry with long equilibration times.

IX. LITERATURE CITED

1. Young, D. M. and A. D. Crowell. Physical Adsorption of Gases. Washington, D.C., Butterworths, Inc. 1962.

2. McBain, J. W. The Sorption of Gases and Vapors by Solids. London, England, Routledge and Sons, Ltd. 1932.

3. Brunauer, S. The Adsorption of Gases and Vapors, Vol. 1, Physical Adsorption. Princeton, N.J., Princeton University Press. 1945.

4. Gregg, S. J. and K. S. W. Sing. Adsorption, Surface Area and Porosity. New York, N.Y., Academic Press, Inc. 1967.

5. Ross, S. and J. P. Olivier. On Physical Adsorption. New York, N.Y., Interscience. 1964.

6. Dubinin, M. M. Quarterly Reviews (London). 9:101. 1955.

7. Dubinin, M. M. Chemical Reviews. 60:235. 1960.

8. Brunauer, S., L. S. Deming, W. S. Deming and E. Teller. Journal of the American Chemical Society. 62:1723. 1940.

9. Brunauer, S. and P. H. Emmett. Journal of the American Chemical Society. 57:1745. 1935.

10. Emmett, P. H. and S. Brunauer. Journal of the American Chemical Society. 59:1553. 1937.

11. Langmuir, I. Journal of the American Chemical Society. 40:1361. 1918.

12. Brunauer, S., P. H. Emmett and E. Teller. Journal of the American Chemical Society. 60:309. 1938.

13. Halsey, G. D., Jr. Discussions of the Faraday Society. 8:54. 1950.

14. Hill, T. L. Journal of Chemical Physics. 14:263. 1946.

15. Guggenheim, E. A. Modern Thermodynamics by the Methods of Willard Gibbs. London, England, Methuen and Co., Ltd. 1933.

16. Gurvitsch, L. G. Zhurnal Russkogo Fiziko - Khimiecheskogo Obshchestva, Chast'Khimicheskogo. 47:805. 1915.

17. McKee, D. W. Journal of Physical Chemistry. 63:1256. 1959.

18. Joyner, L. G., E. B. Weinberger and C. W. Montgomery. Journal of the American Chemical Society. 67:2182. 1945.

19. Lippens, B. C. and J. H. de Boer. Journal of Catalysis. 4:319. 1965.

20. de Boer, J. H., B. G. Linsen and Th. J. Osinga. Journal of Catalysis. 4:643. 1965.

21. Thomson, W. (Lord Kelvin). London, Edinburgh, and Dublin Philosophical Magazine. Series 4, 42:448. 1871.

22. Kistler, S. S., E. A. Fischer and I. R. Freeman. Journal of the American Chemical Society. 65:1909. 1943.

23. Derjaguin, B. V. International Congress of Surface Activity Proceedings. 2nd, 2:153. 1957.

24. Dubinin, M. M. and E. G. Zhukovskaya. Bulletin of the Academy of Sciences of the USSR, Division of Chemical Sciences. 10:1636. 1959.

25. Harvey, E. N. Journal of the American Chemical Society. 65:2343. 1943.

26. Barrett, E. P., L. G. Joyner, and P. P. Halenda. Journal of the American Chemical Society. 73:373. 1951.

27. Cranston, R. W. and F. A. Inkley. Advances in Catalysis. 9:413. 1957.

28. Broekhoff, J. C. P. and J. H. de Boer. Journal of Catalysis. 9:8. 1967.

29. Broekhoff, J. C. P. and J. H. de Boer. Journal of Catalysis. 9:15. 1967.

30. Innes, W. B. Analytical Chemistry. 29:1069. 1957.

31. Lippens, B. C., B. G. Linsen and J. H. de Boer. Journal of Catalysis. 3:32. 1964.

32. de Boer, J. H. and B. C. Lippens. Journal of Catalysis. 3:38. 1964.

33. Lippens, B. C. and J. H. de Boer. Journal of Catalysis. 3:44. 1964.

34. de Boer, J. H., A. van den Henvel and B. G. Linsen. Journal of Catalysis. 3:268. 1964.

35. Pierce, C., J. W. Wiley and R. N. Smith. Journal of Physical Chemistry. 53-669. 1949.

36. Polanyi, M. Verhandlungen der Deutschen Physikalischen Gesellshaft. 16:1012. 1914.

37. Dubinin, M. M. The porous structure and adsorption properties of active carbons. Industrial Carbon and Graphite. Pp. 219-230. London, England, Society of Chemical Industry. 1958.

38. Dubinin, M. M. Russian Journal of Physical Chemistry. 39:697. 1965.

39. Kaganer, M. G. Proceedings of the Academy of Sciences of the USSR, Section: Physical Chemistry. 116:603. 1957.

40. Kaganer, M. G. Russian Journal of Physical Chemistry. 33:352. 1959.

41. Kaganer, M. G. Proceedings of the Academy of Sciences of the USSR, Section: Physical Chemistry. 138:419. 1961.

42. Harkins, W. D. and G. Jura. Journal of the American Chemical Society. 66:1366. 1944.

43. Barrer, R. M. and I. S. Kerr. Transactions of the Faraday Society. 55:1915. 1959.

44. Sing, K. S. W. Chemistry and Industry. 829. 1967.

45. de Boer, J. H., B. G. Linsen, Th. van der Plas and G. J. Zondervan. Journal of Catalysis. 4:649. 1965.

46. Steele, W. A. and G. D. Halsey, Jr. Journal of Chemical Physics. 22:979. 1954.

47. Barker, J. A. and D. H. Everett. Transactions of the Faraday Society. 58:1608. 1962.

48. Sams, J. R., Jr., G. Contabaris and G. D. Halsey, Jr. Journal of Chemical Physics. 36:1334. 1962.

49. Bond, R. L. and D. H. T. Spencer. The ultra-fine capillary structure of coals and carbonized coals. Industrial Carbon and Graphite. Pp. 231-251. London, England, Society of Chemical Industry. 1958.

50. Hansen, R. S. Journal of Physical Chemistry. 55:1195. 1951.

51. Freeman, M. P. and G. D. Halsey, Jr. Journal of Physical Chemistry. 59:181. 1955.

52. Steele, W. A. and G. D. Halsey, Jr. Journal of Physical Chemistry. 59:57. 1955.

53. De Marcus, W. C., E. H. Hopper and A. M. Allen. U.S. Atomic Energy Commission Report K-1222. [Carbide and Carbon Chemicals Corp., K-25 Plant, Oak Ridge, Tenn.] 1955.

54. Freeman, M. P. Journal of Physical Chemistry. 62:723. 1958.

55. Hansen, R. S. Journal of Physical Chemistry. 63:743. 1959.

56. Sams, J. R., Jr., G. Constabaris, and G. D. Halsey, Jr. Journal of Physical Chemistry. 64:1689. 1960.

57. Sinanoglu, O. and K. S. Pitzer. Journal of Chemical Physics. 32:1279. 1960.

58. Hansen, R. S. and J. A. Murphy. Journal of Chemical Physics. 39:1642. 1963.

59. Murphy, J. A. Chromatographic Measurement of Gas-Solid Interaction Potentials. Unpublished Ph.D. thesis. Ames, Iowa, Library, Iowa State University of Science and Technology. 1963.

60. Hirschfelder, J. O., C. F. Curtiss and R. B. Bird. Molecular Theory of Gases and Liquids. New York, N.Y., John Wiley and Sons, Inc. 1954.

61. Freeman, M. P. Journal of Physical Chemistry. 62:729. 1958.

62. Johnson, J. D. and M. L. Klein. Transactions of the Faraday Society. 60:1964. 1964.

63. Krizan, J. E. and A. D. Crowell. Journal of Chemical Physics. 41:1322. 1964.

64. Wolf, R. and J. R. Sams, Jr. Journal of Physical Chemistry. 69:1129. 1965.

65. Clausing, P. Annalen der Physik. Series 5, 7:489. 1930.

66. Clausing, P. Annalen der Physik. Series 5, 7:521. 1930.

67. Kruyer, S. Nederlandse Akademie van Wetenschappen Proceedings. 56B:274. 1953.

68. Everett, D. H. Transactions of the Faraday Society. 46:453. 1950.

69. de Boer, J. H. The Dynamical Character of Adsorption. London, England, Oxford University Press. 1953.

70. London, F. Zeitschrift für Physikalische Chemie (Leipzig). Series B, 11:222. 1930.

71. Kirkwood, J. G. Physikalische Zeitschrift. 33:57. 1932.

72. Müller, A. Proceedings of the Royal Society (London). Series A, 154:624. 1936.

73. Margenau, H. Reviews of Modern Physics. 11:1. 1939.

74. Wilson, J. N. Journal of the American Chemical Society. 62:1583. 1940.

75. Weiss, J. Journal of the Chemical Society. 297. 1943.

76. De Vault, D. Journal of the American Chemical Society. 65:532. 1943.

77. Glueckauf, E. Journal of the Chemical Society. 1302. 1947.

78. Nelson, F. M. and F. T. Eggertsen. Analytical Chemistry. 30:1387. 1958.

79. Haley, A. J. Journal of Applied Chemistry (London). 13:392. 1963.

80. Greene, S. A. and H. Pust. Journal of Physical Chemistry. 62:55. 1958.

81. Habgood, H. W. and J. F. Hanlan. Canadian Journal of Chemistry. 37:843. 1959.

82. Eberly, P. E., Jr. Journal of Physical Chemistry. 65:68. 1961.

83. Eberly, P. E., Jr. and C. N. Kimberlin, Jr. Transactions of the Faraday Society. 57:1169. 1961.

84. Ross, S., J. K. Saelens and J. P. Olivier. Journal of Physical Chemistry. 66:696. 1962.

85. Gale, R. L. and R. A. Beebe. Journal of Physical Chemistry. 68:555. 1964.

86. James, D. H. and C. S. G. Phillips. Journal of the Chemical Society. 1066. 1954.

87. Gregg, S. J. and R. Stock. Sorption isotherms and chromatographic behavior of vapors. In Desty, D. M. Ed. Gas Chromatography, 1958. Pp. 90-98. New York, N.Y., Academic Press, Inc. 1958.

88. Eberly, P. E., Jr. Journal of Physical Chemistry. 65:1261. 1961.

89. Saint-Yrieix, Alain. Bulletin de la Societe Chimique de France. 3407. 1965.

90. Roginskii, S. Z., M. L. Yanovskii, Lu Piei-Chang, V. W. Brazhnikow, I. E. Neimark and M. A. Piontkovskaya. Kinetics and Catalysis. 1:261. 1960.

91. Cremer, E. and H. F. Huber. Gas Chromatography, International Symposium. 3:169. 1962.

92. Beljakova, L. D., A. V. Kiselev and N. V. Kovaleva. Bulletin de la Societe Chimique de France. 285. 1967.

93. Huber, J. F. K. and A. I. M. Keulemans. Nonlinear ideal chromatography and the potentialties of linear gas-solid chromatography. In Swaay, M. van, ed. Gas Chromatography, 1962. Pp. 26-34. London, England, Butterworths. 1962.

94. Schay, G. and G. Szekely. Acta Chimica Hungarica. 5:167. 1954.

95. Schay, G., P. Fejes, I. Halasz and J. Kiraly. Acta Chimica Hungarica. 11:381. 1957.

96. Robbins, L. A. Gas Adsorption and Polymorphism in the Reductive Decomposition of Calcium Sulfate. Unpublished Ph.D. thesis. Ames, Iowa, Library, Iowa State University of Science and Technology. 1966.

97. Reilley, C. N., G. P. Hildebrand and J. W. Ashley, Jr. Analytical Chemistry. 34:1198. 1962.

98. Hanlan, J. F. and M. P. Freeman. Canadian Journal of Chemistry. 37:1575. 1959.

99. James, A. T. and A. J. Martin. Biochemical Journal. 50:679. 1952.

100. Hansen, R. S., J. A. Murphy and T. C. McGee. Transactions of the Faraday Society. 60:597. 1964.

101. Jackson, D. M., G. Wells and D. Soseman. Unpublished multilithed paper. U.S. Atomic Energy Commission. Ames Laboratory. Contribution No. 957. 1960.

102. Hansen, R. S., R. R. Frost and J. A. Murphy. Journal of Physical Chemistry. 62:2028. 1964.

103. Melville, Sir Harry and B. G. Gowenlock. Experimental Methods in Gas Reactions. New York, N.Y., St. Martin's Press, Inc. 1964.

104. Amberg, C. H., D. H. Everett, L. H. Ruiter and F. W. Smith. International Congress of Surface Activity Proceedings. 2nd, 2:3. 1957.

105. Everett, D. H. The interaction of gases and vapours with solids. In Goldup, A. ed. Gas Chromatography, 1964. Pp. 219-237. London, England, The Institute of Petroleum. 1965.

106. Constabaris, G., J. H. Singleton and G. D. Halsey, Jr. Journal of Physical Chemistry. 63:1350. 1959.

107. Maggs, F. A. P. Nature (London). 169:269. 1952.

108. Maggs, F. A. P. Nature (London). 169:793. 1952.

109. Gregg, S. J. and M. I. Pope. Fuel. 38:501. 1959.

110. Maggs, F. A. P. Research Applied in Industry (London). Research Correspondence. 6:13S. 1953.

111. Zwietering, P., J. Overeem and D. W. van Krevelen. Fuel. 35:66. 1956.

112. Emmett, P. H. Chemical Reviews. 43:69. 1948.

113. Emmett, P. H. and M. Cines. Journal of Physical Chemistry. 51:1329. 1947.

X. ACKNOWLEDGMENTS

The author wishes to express his gratitude to Dr. Robert S. Hansen for his encouragement and invaluable suggestions during the course of this research. Dr. Hansen's patience in certain situations during the course of the author's graduate study is deeply appreciated.

The author wishes to acknowledge James "Rummy" Gambell for many enjoyable hours of discussion at the Veenker Memorial Laboratory.

Special thanks are due the Ames Open DBC for providing many hours of stimulating discussion which usually occurred on the fifth day of the week.

APPENDIX A: FIGURES

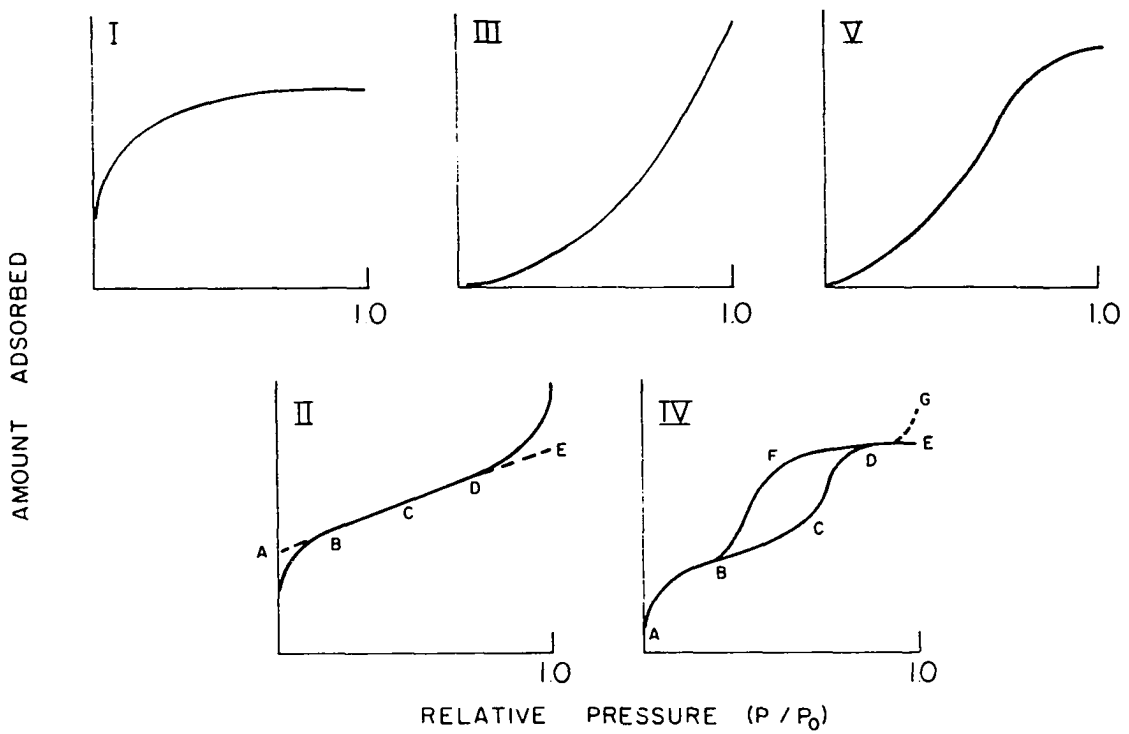

Figure 1. The five types of adsorption isotherms according to the classification of Brunauer, Deming, Deming and Teller (BDDT)

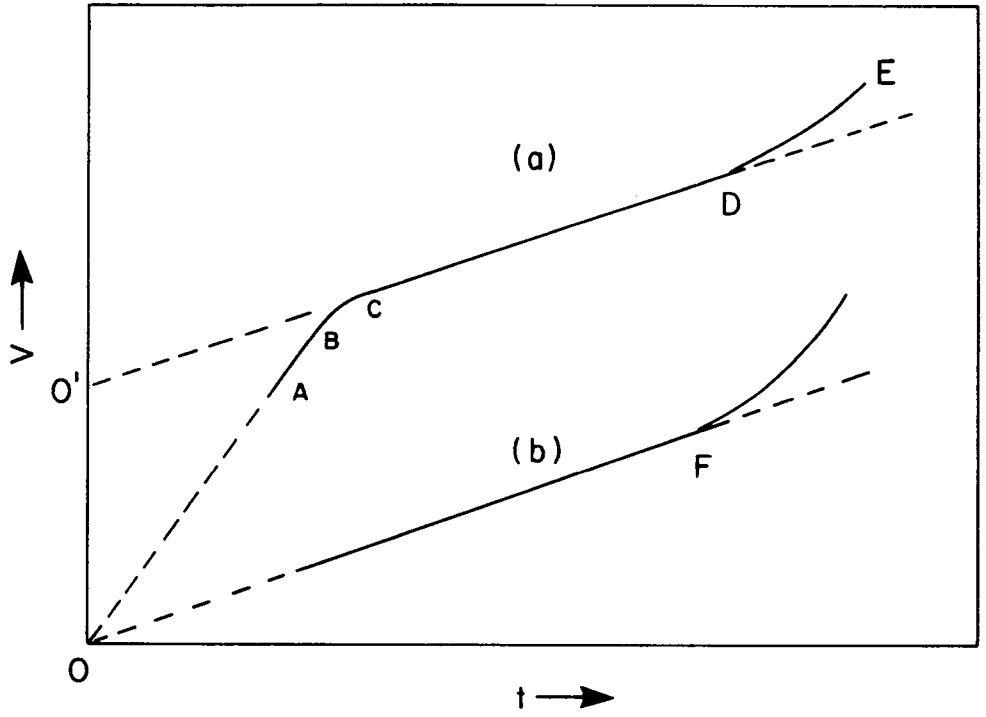

Figure 2. Typical t-plots for (a) a porous adsorbent and (b) a non-porous adsorbent

Figure 3. (a) The potential energy of a molecule as function of the distance from the surface.

(b) The average concentration of molecules as a function of the distance from the surface as calculated by the Boltzmann distribution law for $-E^{*}_{AS}/kT = 3$. C_o is the bulk gas concentration and the shaded area represents the surface excess of gas molecules

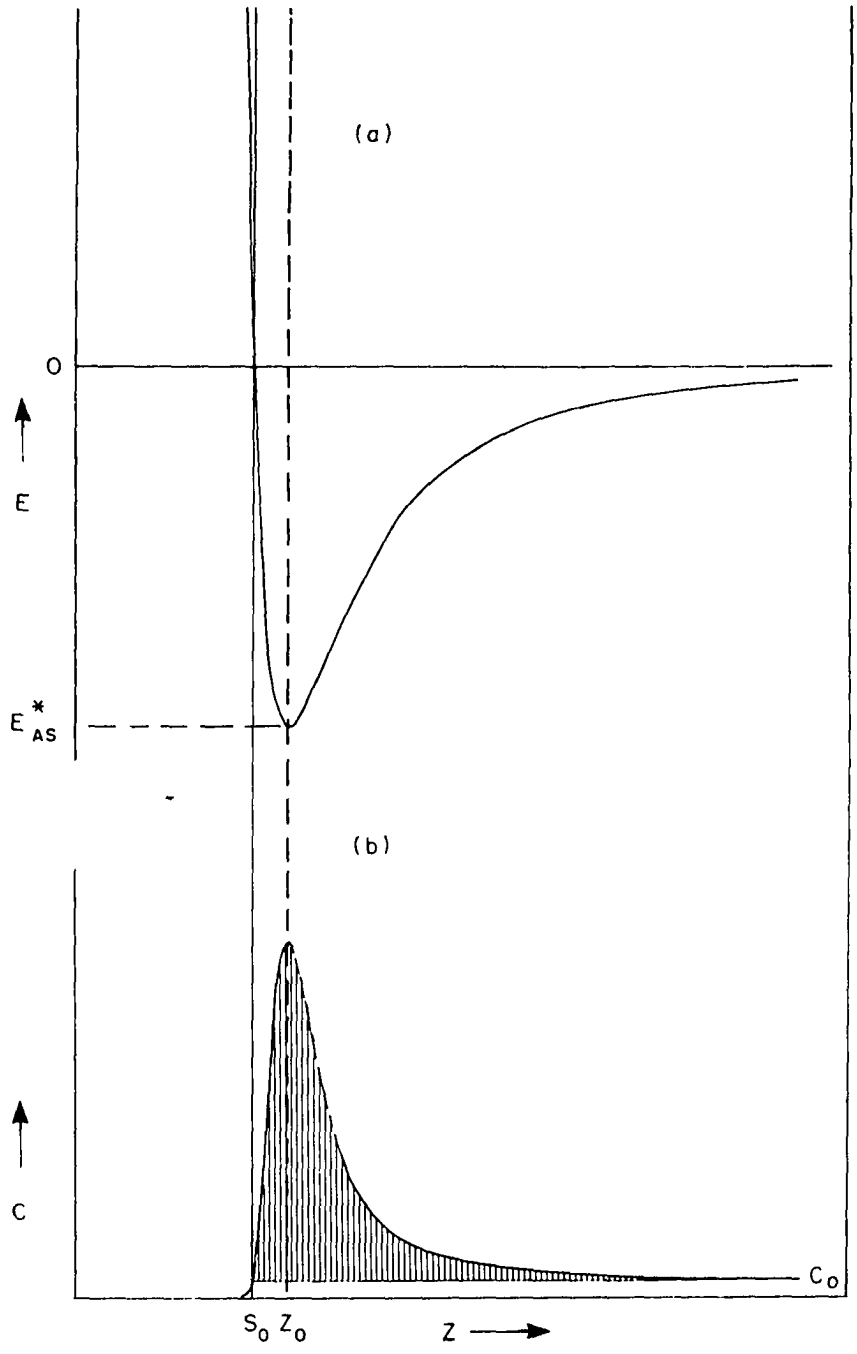
(a)
O
E
E^*_{AS}
(b)
C
C_0
S_0 Z_0
Z

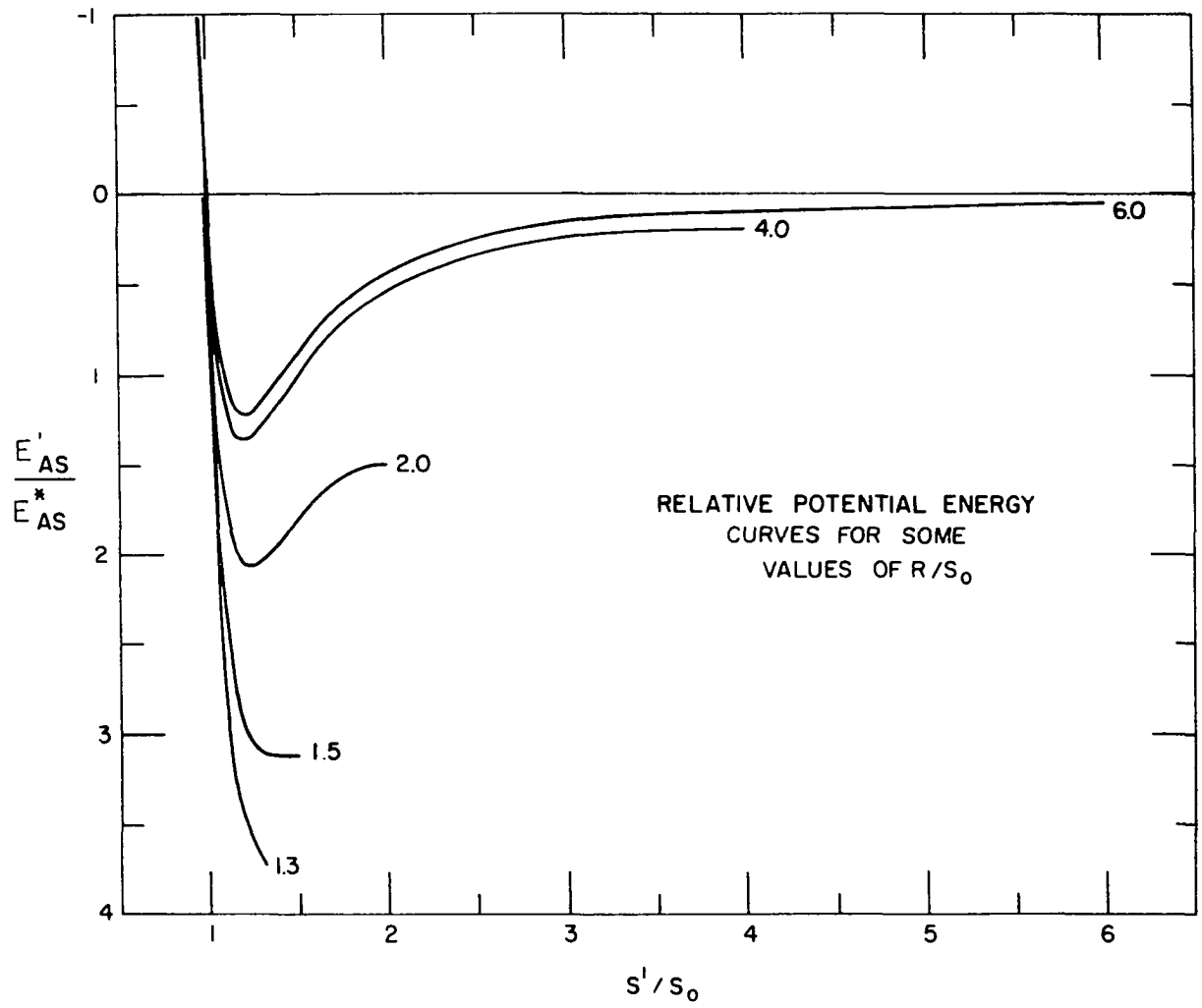

Figure 4. The potential energy of a molecule in capillaries of various radii (R) as a function of the distance from the surface of the capillary. E^*_{AS} and S_o are gas-plane surface interaction parameters

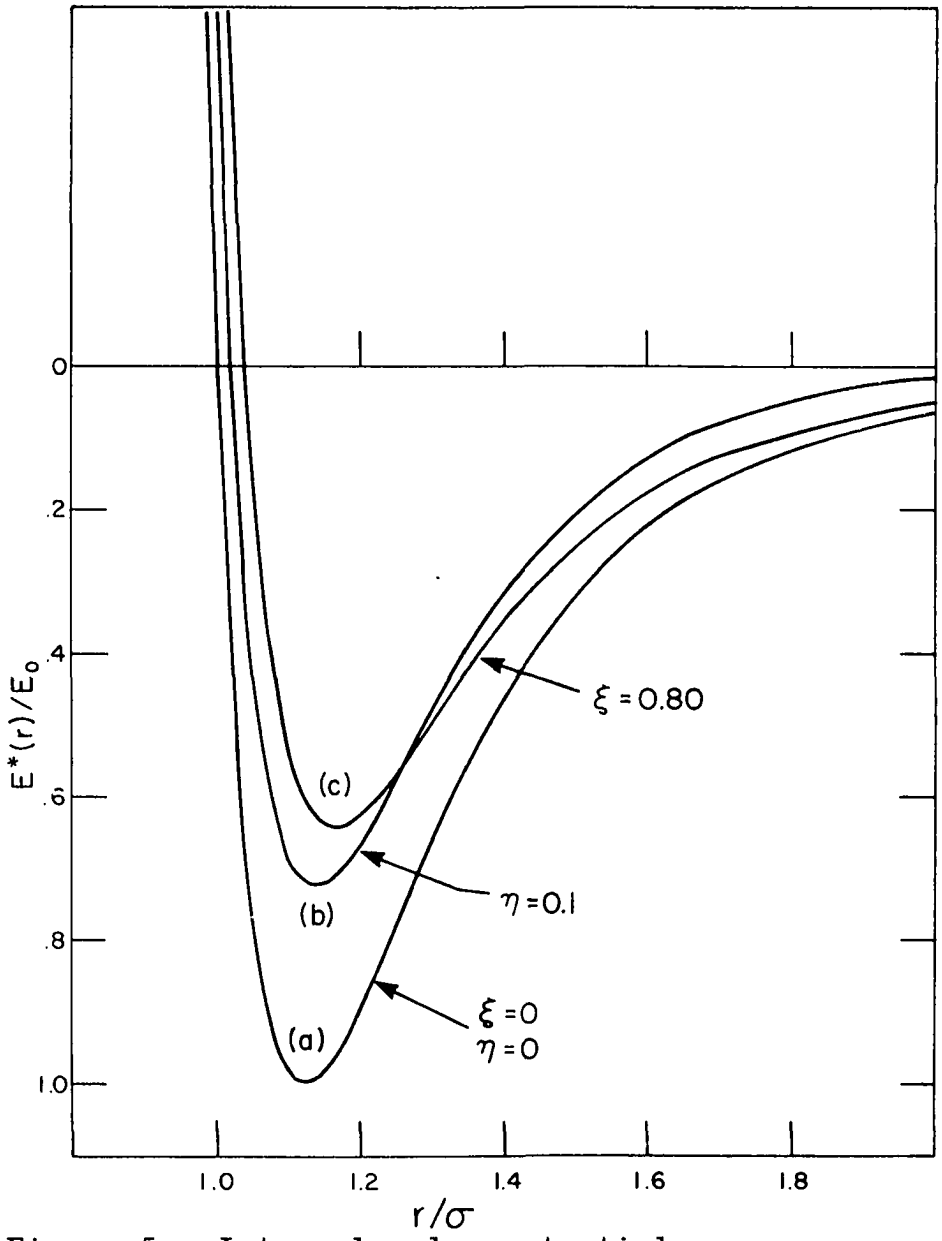

Figure 5. Intermolecular potential energy curves for (a) Lennard-Jones (6-12) bulk gas potential, (b) Sinanoglu and Pitzer monolayer potential and (c) Barker and Everett monolayer potential

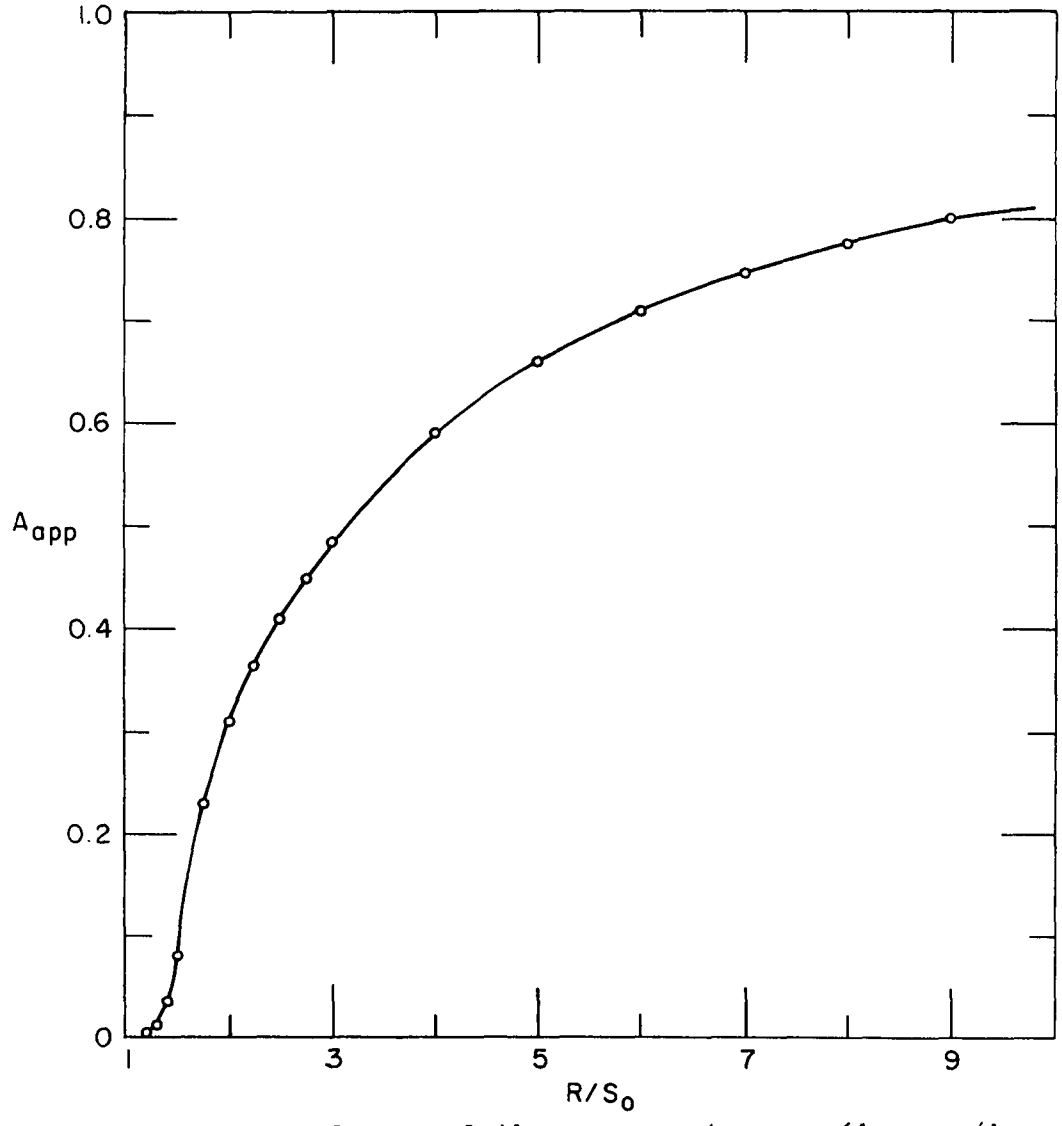

Figure 6. Dependence of the apparent area ($A_{plane}/A_{cap.}$) of a cylindrical capillary on capillary size.

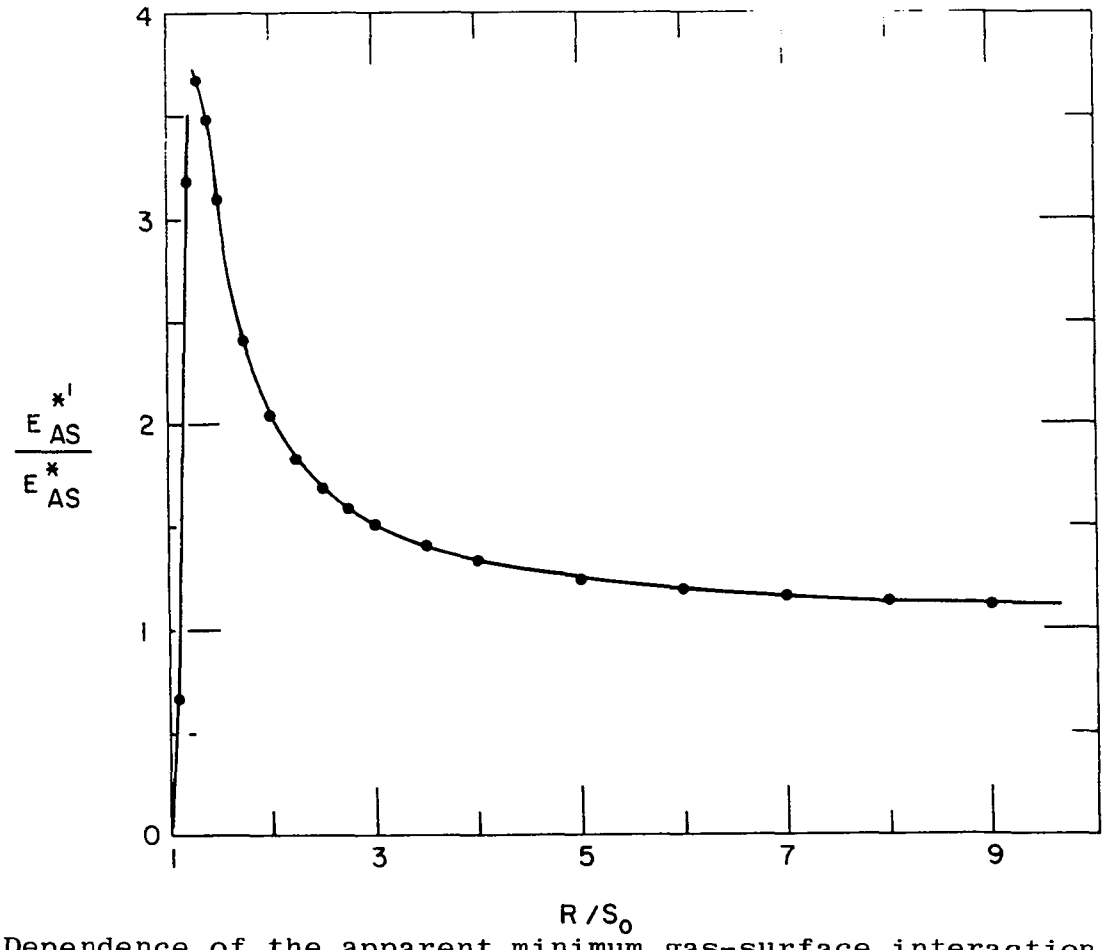

Figure 7. Dependence of the apparent minimum gas-surface interaction potential of a cylindrical capillary on capillary size

Figure 8. The average time required for a molecule to pass through a capillary of length ℓ or ℓ' as a function of the minimum gas-surface potential energy. The primes (ℓ') indicate that the diffusion coefficient has been corrected to include surface migration by a hopping molecule mechanism

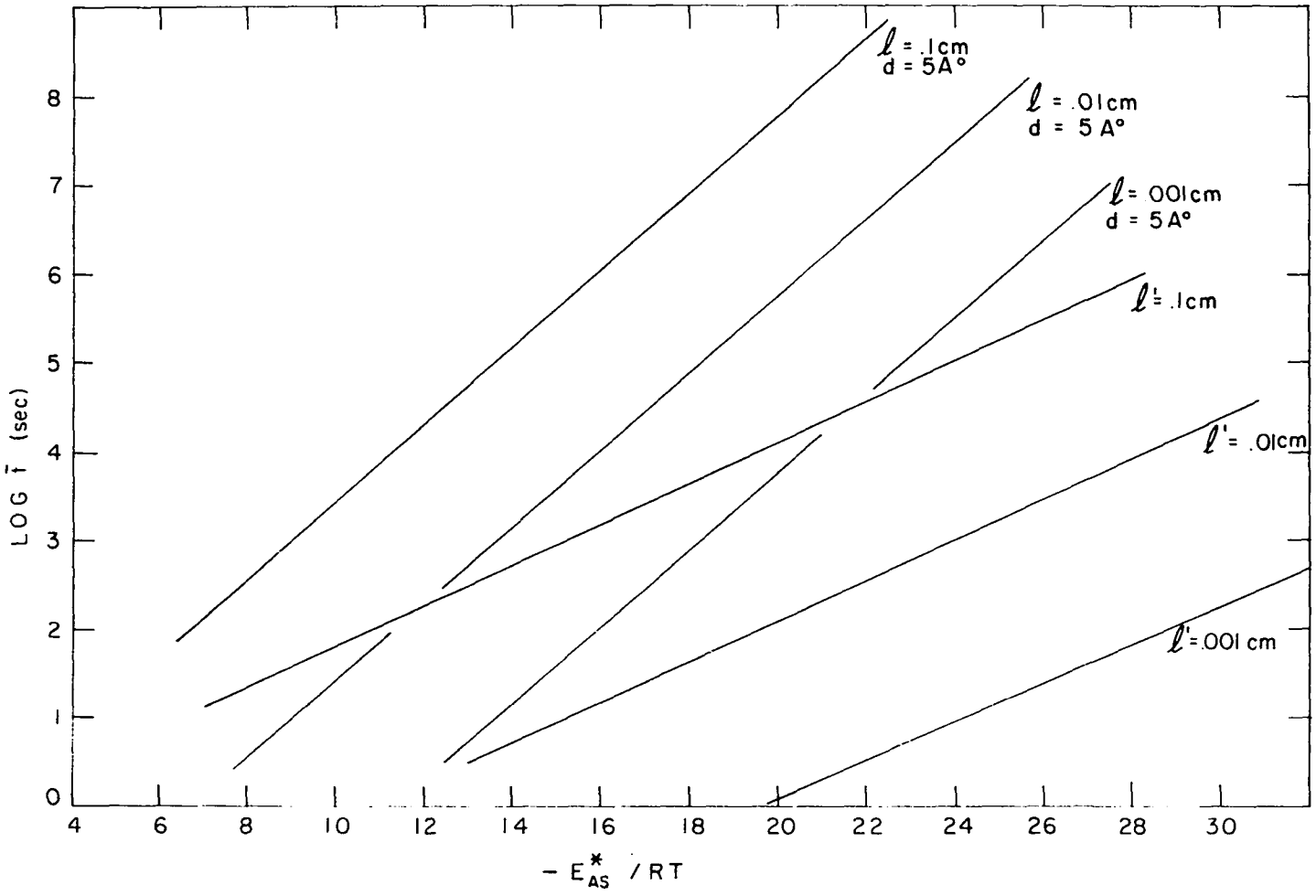
ℓ = .1cm
d = 5A°
ℓ = .01cm
d = 5 A°
ℓ = 001cm
d = 5A°
ℓ' = .1cm
ℓ' = .01cm
ℓ' = .001 cm
LOG t̄ (sec)
0
1
2
3
4
5
6
7
8
4
6
8
10
12
14
16
18
20
22
24
26
28
30
− E*AS / RT

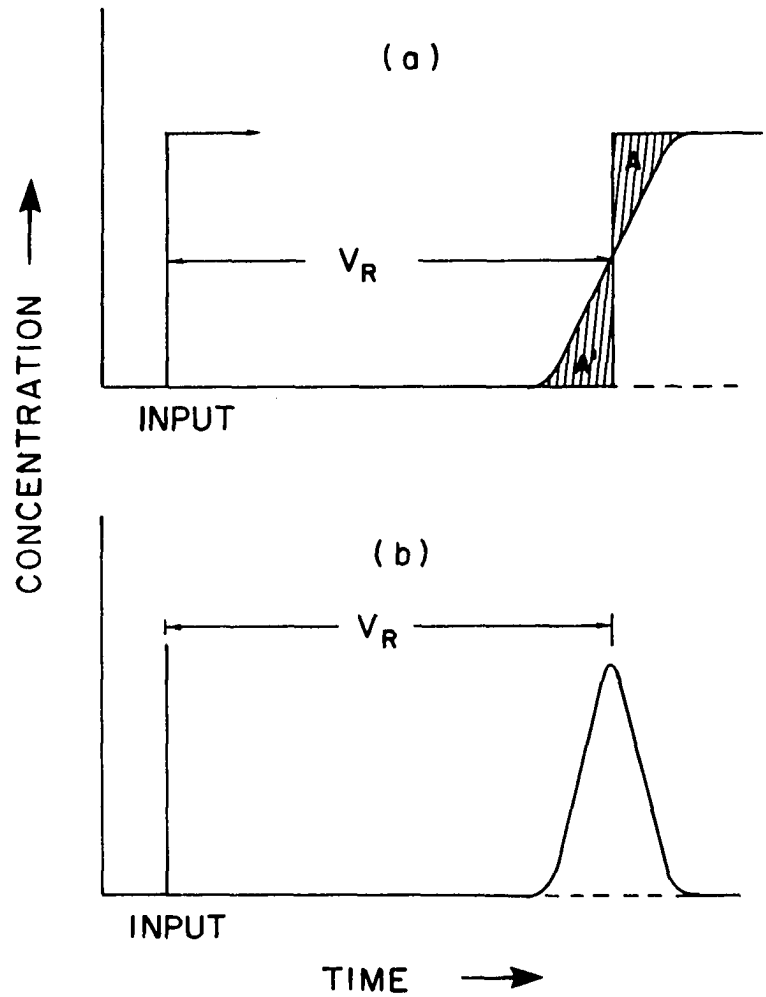

Figure 9. Ideal chromatograms for linear gas-solid chromatography obtained from (a) step and (b) impulse input functions

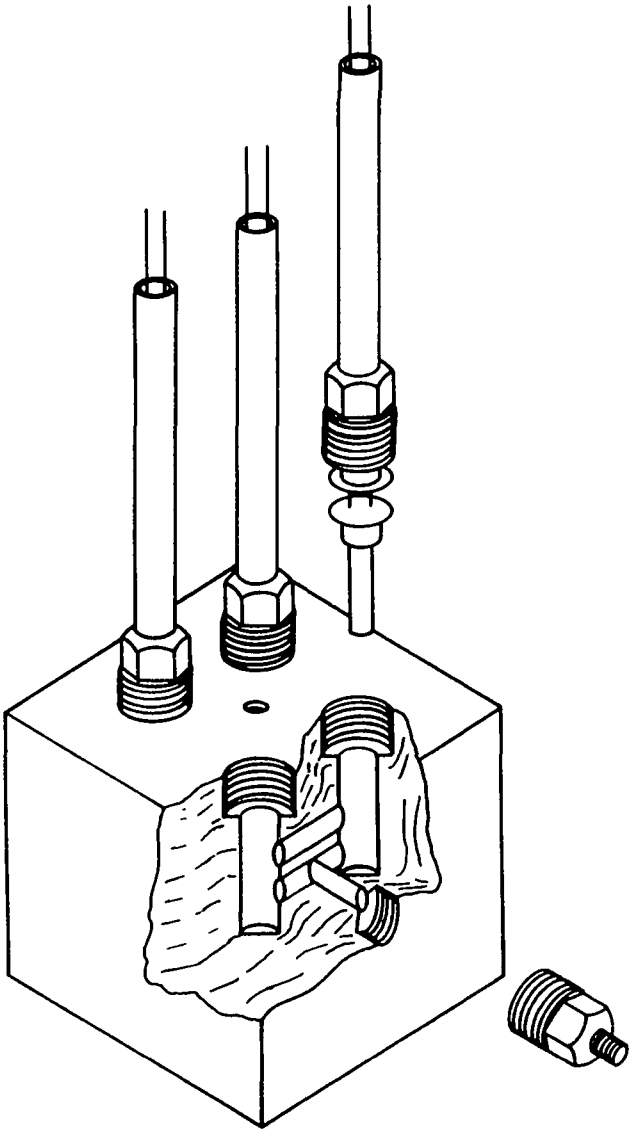

Figure 10. Thermal conductivity detector design

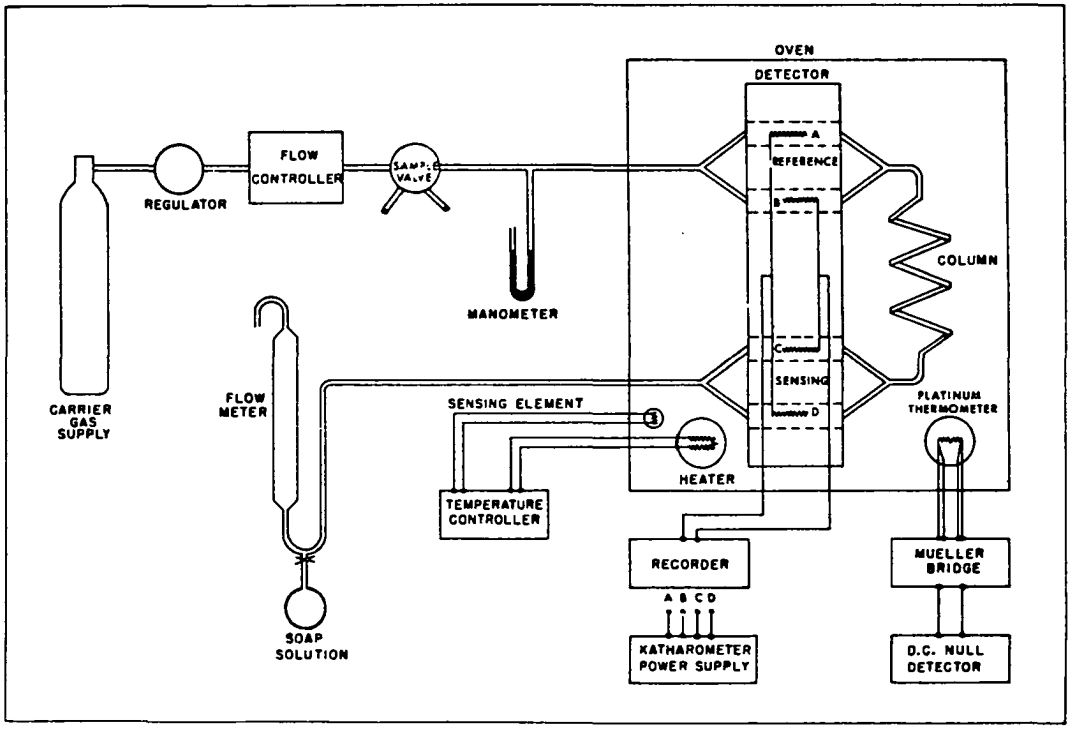

Figure 11. Block diagram for elution gas chromatography system. (courtesy of J. A. Murphy)

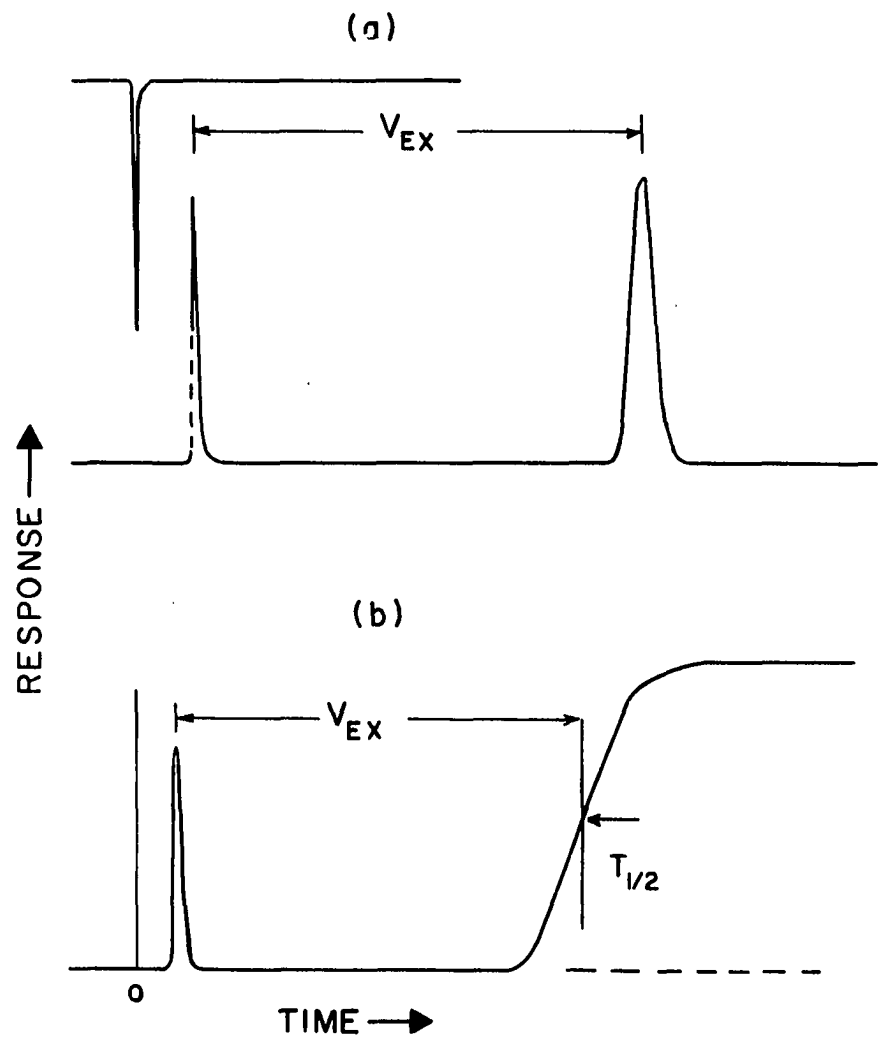

Figure 12. Experimental chromatograms with superimposed neon peaks for (a) elution gas chromatography and (b) frontal gas chromatography

Figure 13. A schematic diagram of the frontal gas chromatography system with the following components:

C	chromatographic column
D'S	differential flow controllers
F'S	microvalve-flowmeters
F1,F2,F3	soap film flowmeters
G1,G2	helium carrier gas supply
G3	adsorbate gas supply
M's	mercury U-tube manometers
S1	high vacuum stopcock - Eck + Krebs Inc. #4870
S2	" " " " " " #4916
S3	" " " " " " #4902
TC	thermoconductivity detector
V	needle valve

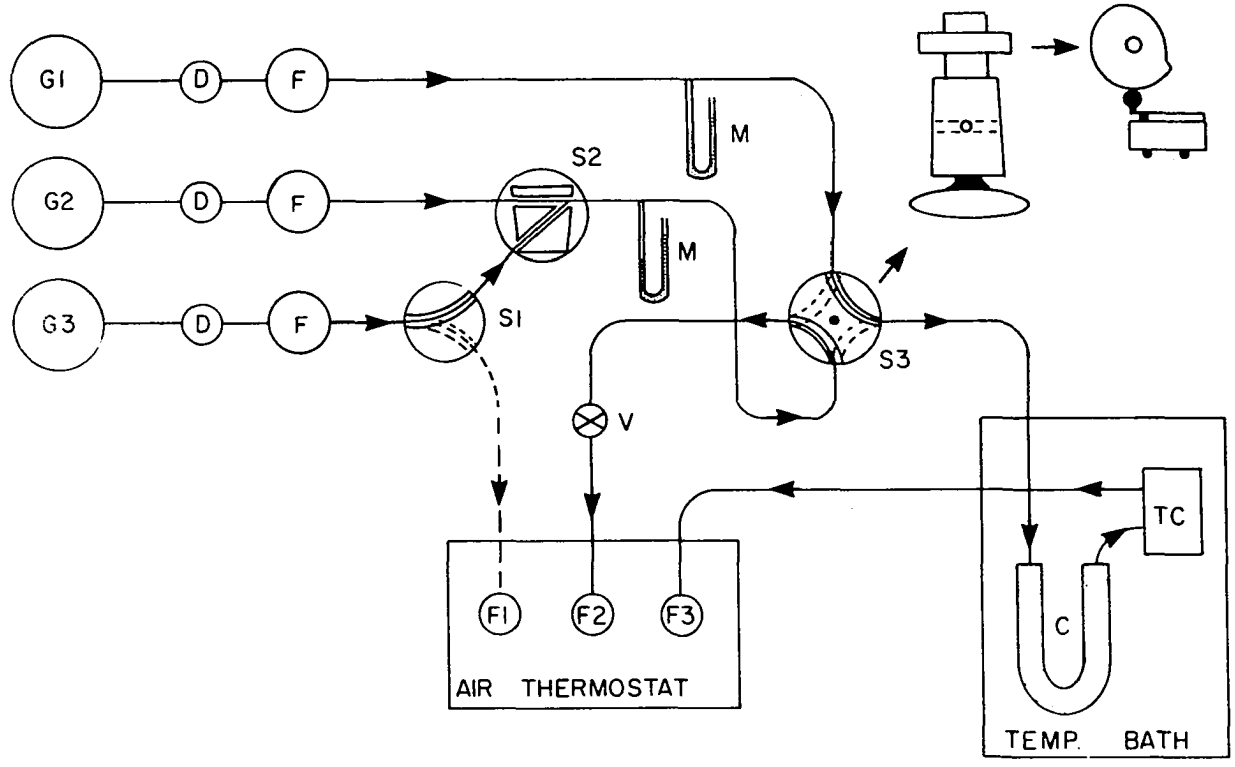
G1
D
F
G2
D
F
G3
D
F
S2
S1
M
M
S3
V
F1
F2
F3
AIR THERMOSTAT
TC
C
TEMP. BATH

Figure 14. A schematic diagram of the gravimetric adsorption system with the following components:

B	1 in. ID stainless steel bellows
BPG	bourdon tube pressure gage
C's	0.009 in. ID capillary tubing
CPG	compound pressure gauge 30 in. vac. -0-15 p.s.i.g.
DP	3-stage mercury diffusion pump - GE M 22DP120
FP's	fore pumps - Welch M-1400
GS	adsorbate gas supply
IG	ion gauge
MB	microbalance encased in vacuum bottle
PG	pressure gauge 0-30 p.s.i.g.
S1	large bore high vacuum stopcock
ST	5 liter pyrex gas storage bulb
T1's	liquid nitrogen traps
T2	dry ice - acetone trap
V1's	Vecco FR-38-S vacuum valves
V2	Vecco FR-150-S vacuum valve

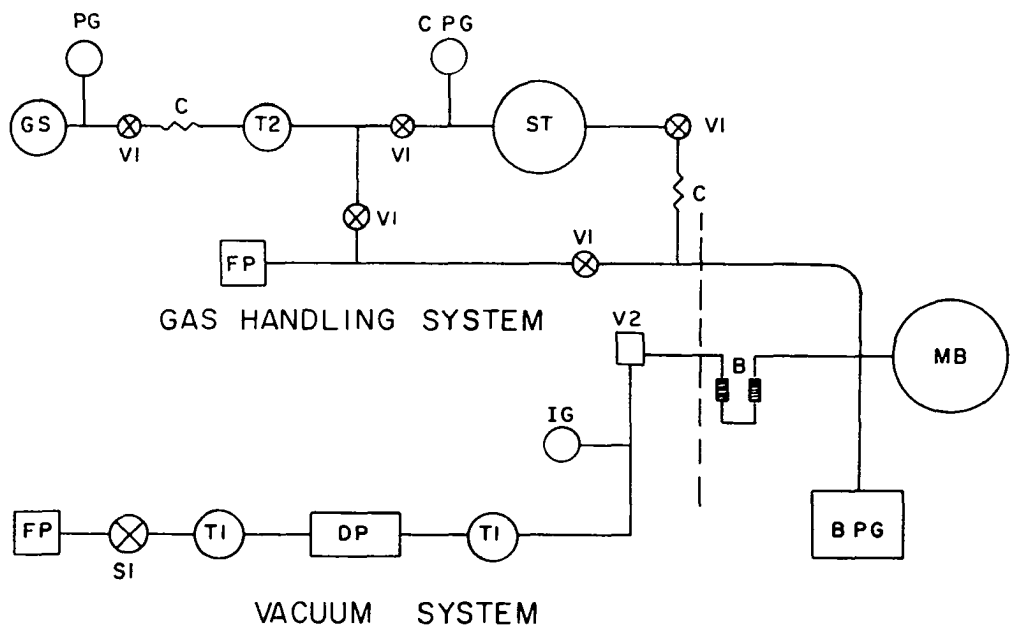
PG
C PG
GS
V1
C
T2
V1
ST
V1
C
V1
FP
V1
GAS HANDLING SYSTEM
V2
B
MB
IG
FP
S1
T1
DP
T1
B PG
VACUUM SYSTEM

Figure 15. Photograph of the gravimetric adsorption system

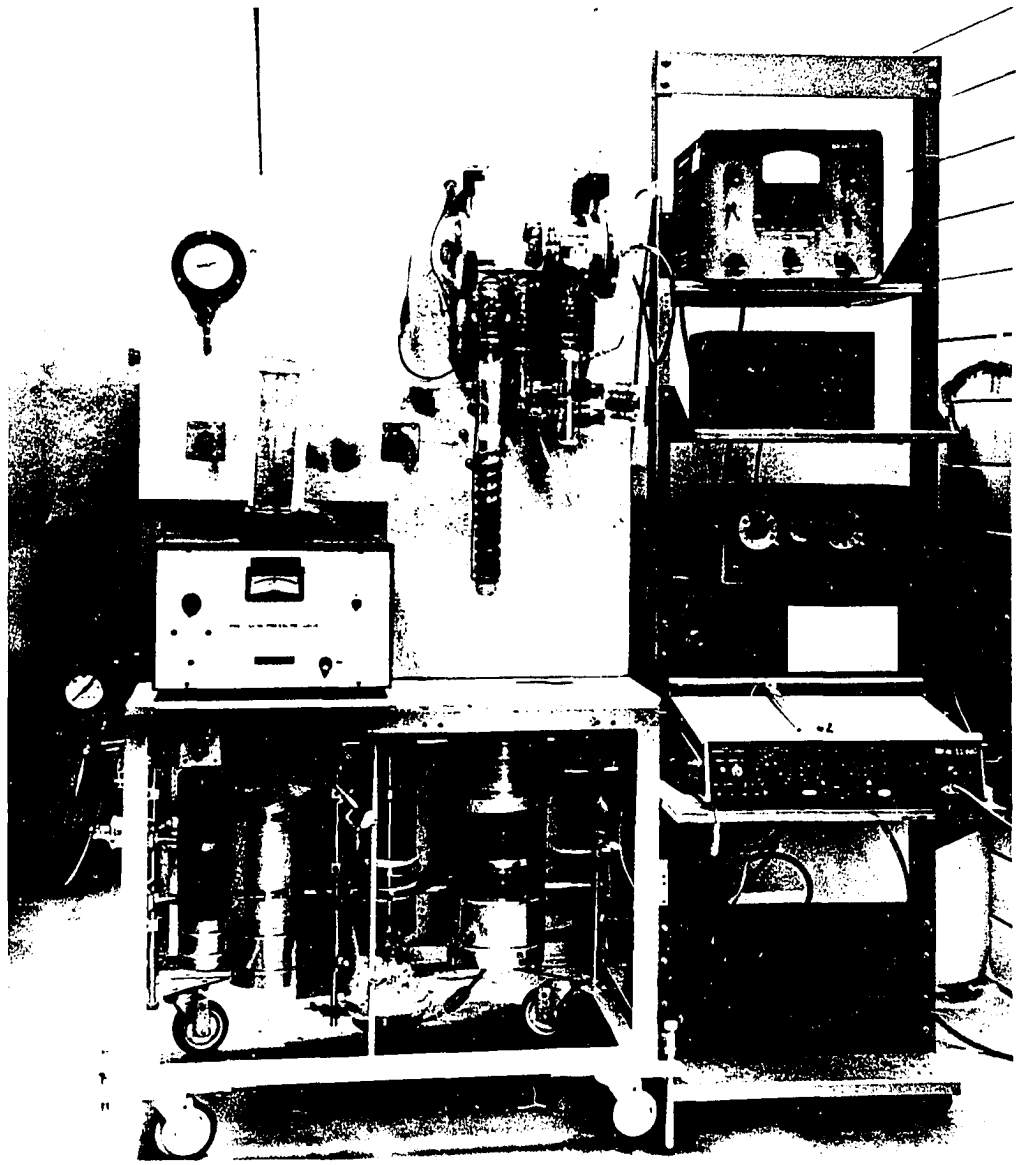

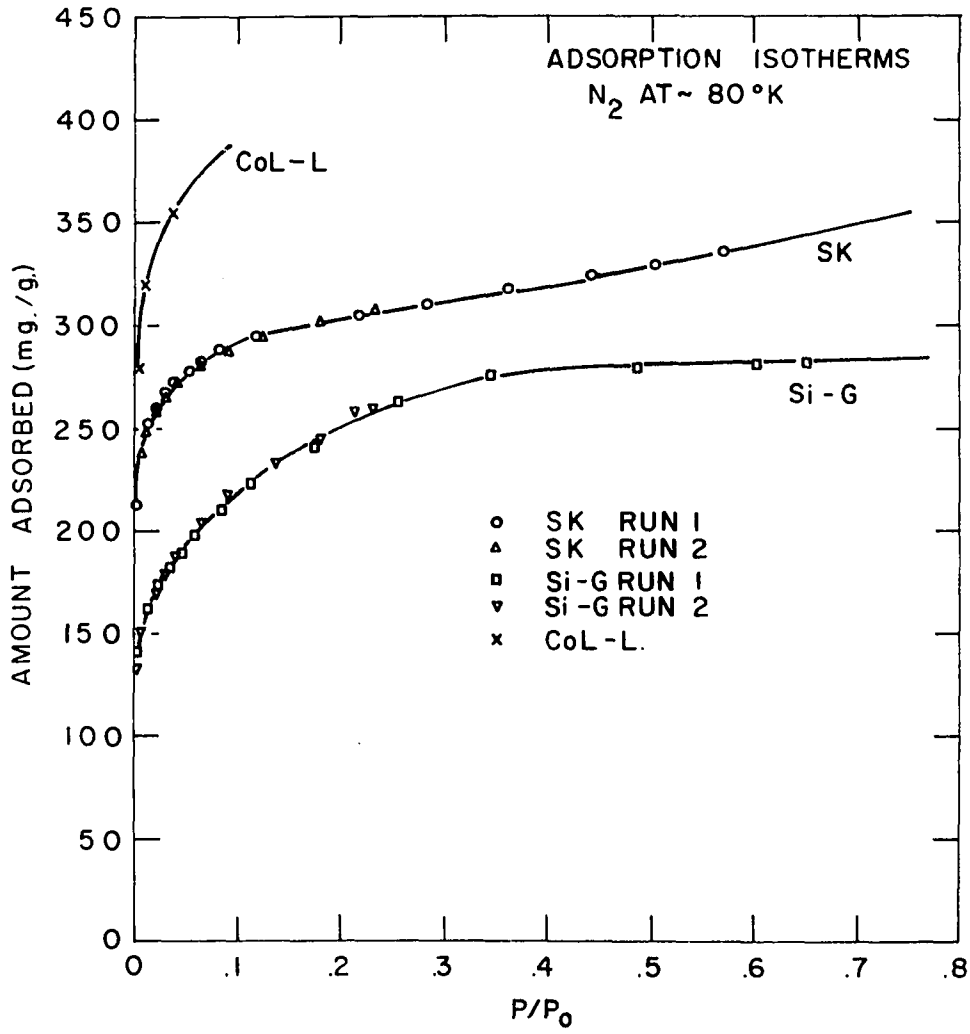

Figure 16. Low temperature nitrogen adsorption isotherms obtained using the gravimetric adsorption system

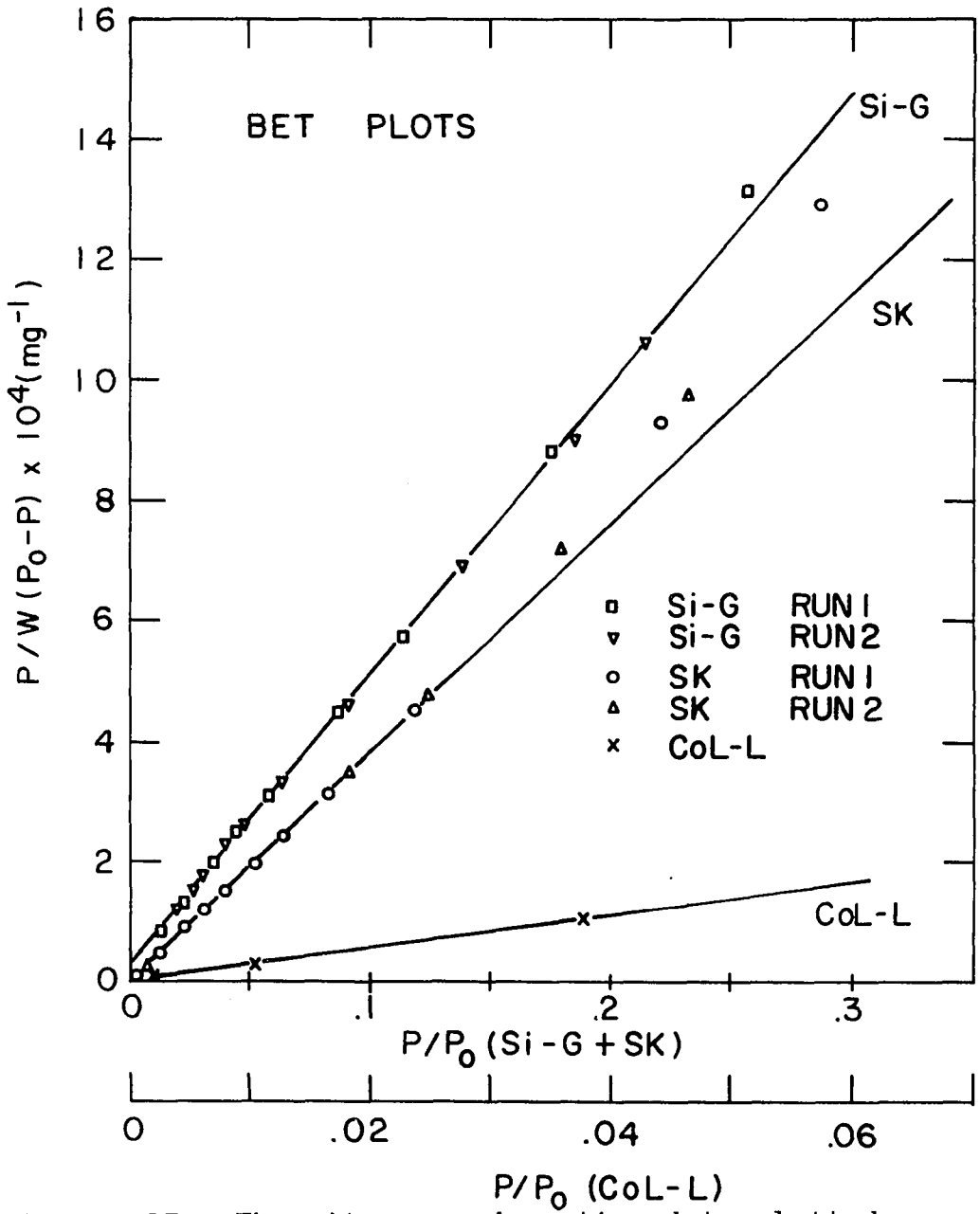

Figure 17. The nitrogen adsorption data plotted according to the BET Equation (2.3)

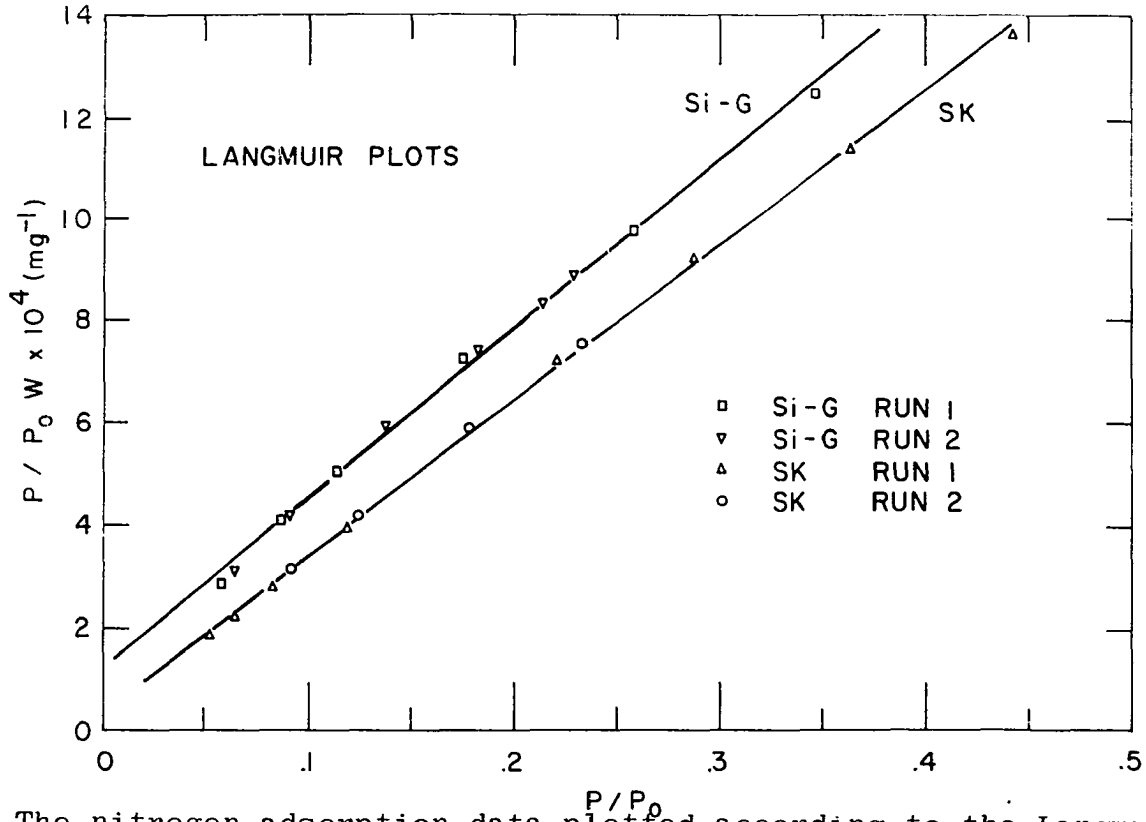

Figure 18. The nitrogen adsorption data plotted according to the Langmuir Equation (2.16)

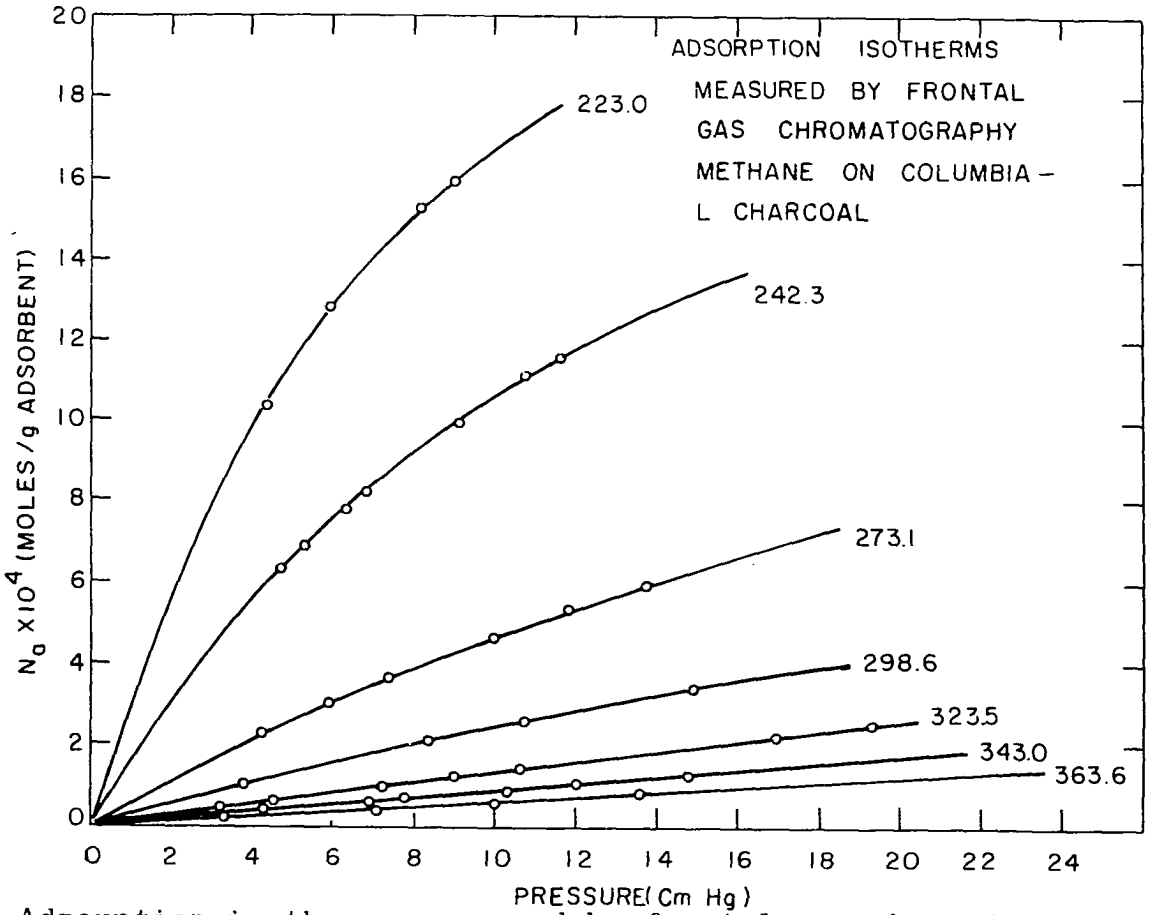

Figure 19. Adsorption isotherms measured by frontal gas chromatography. Methane on Columbia-L charcoal

Figure 20. Dependence of the excess volume in the limit of zero pressure on temperature. Values of V^{o}_{ex} are per g adsorbent. Open circles are experimental data points while the solid lines represent the limiting tangents calculated by use of Equation 3.42

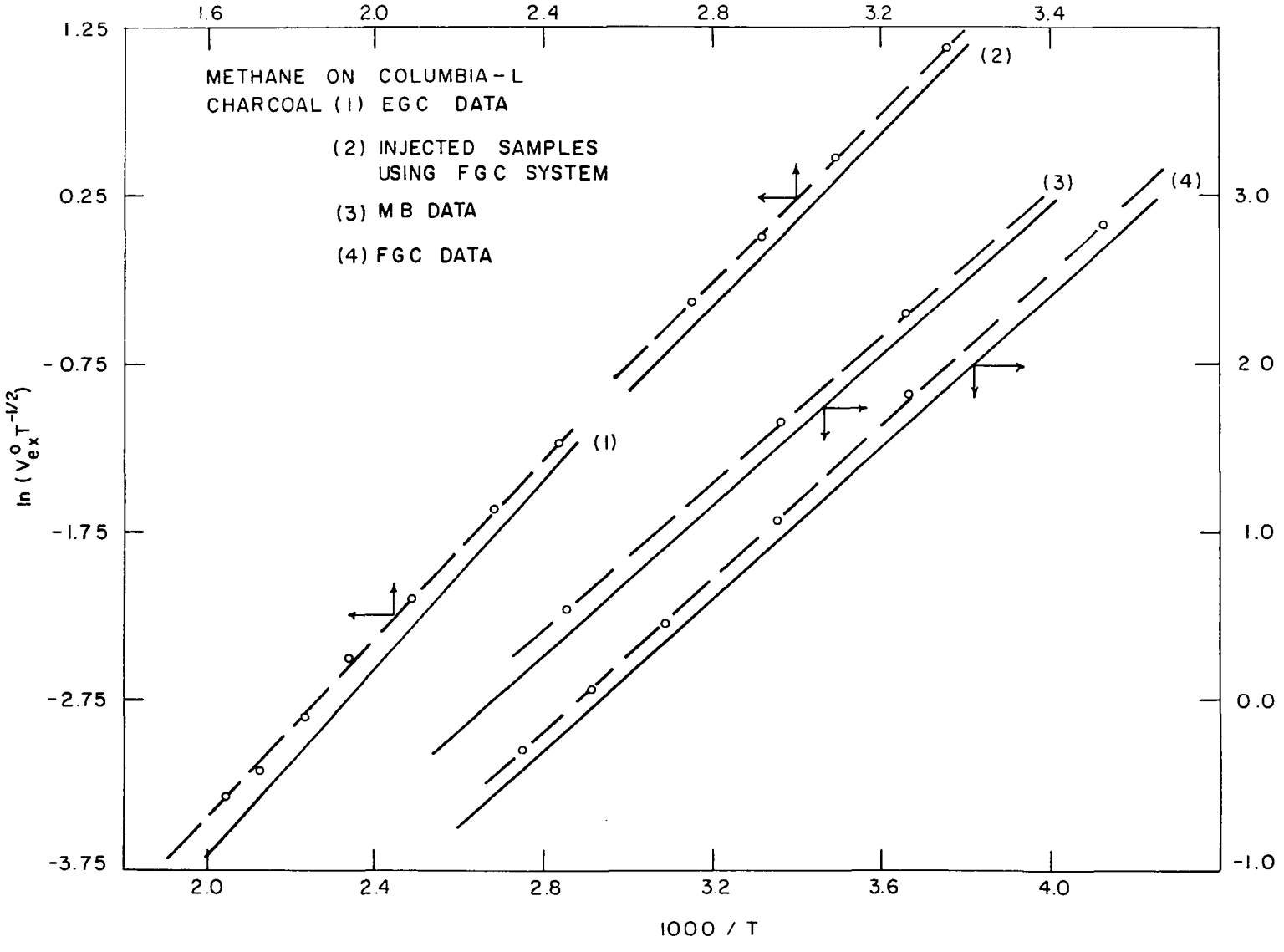
METHANE ON COLUMBIA-L
CHARCOAL (1) EGC DATA
(2) INJECTED SAMPLES
USING FGC SYSTEM
(3) MB DATA
(4) FGC DATA
(1)
(2)
(3)
(4)
1.6
2.0
2.4
2.8
3.2
3.4
1.25
0.25
-0.75
-1.75
-2.75
-3.75
3.0
2.0
1.0
0.0
-1.0
2.0
2.4
2.8
3.2
3.6
4.0
1000 / T
ln ($V_{ex}^{o} T^{-1/2}$)

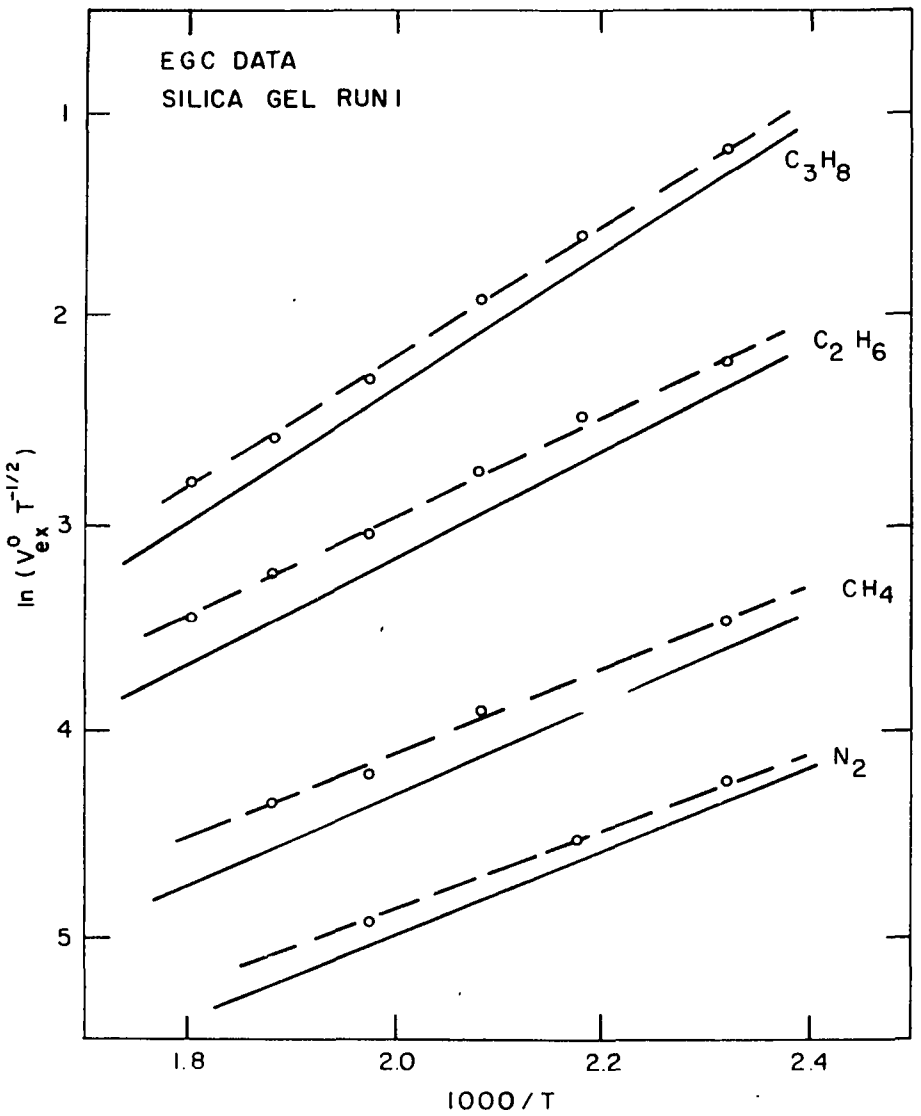

Figure 21. (see Figure 20)

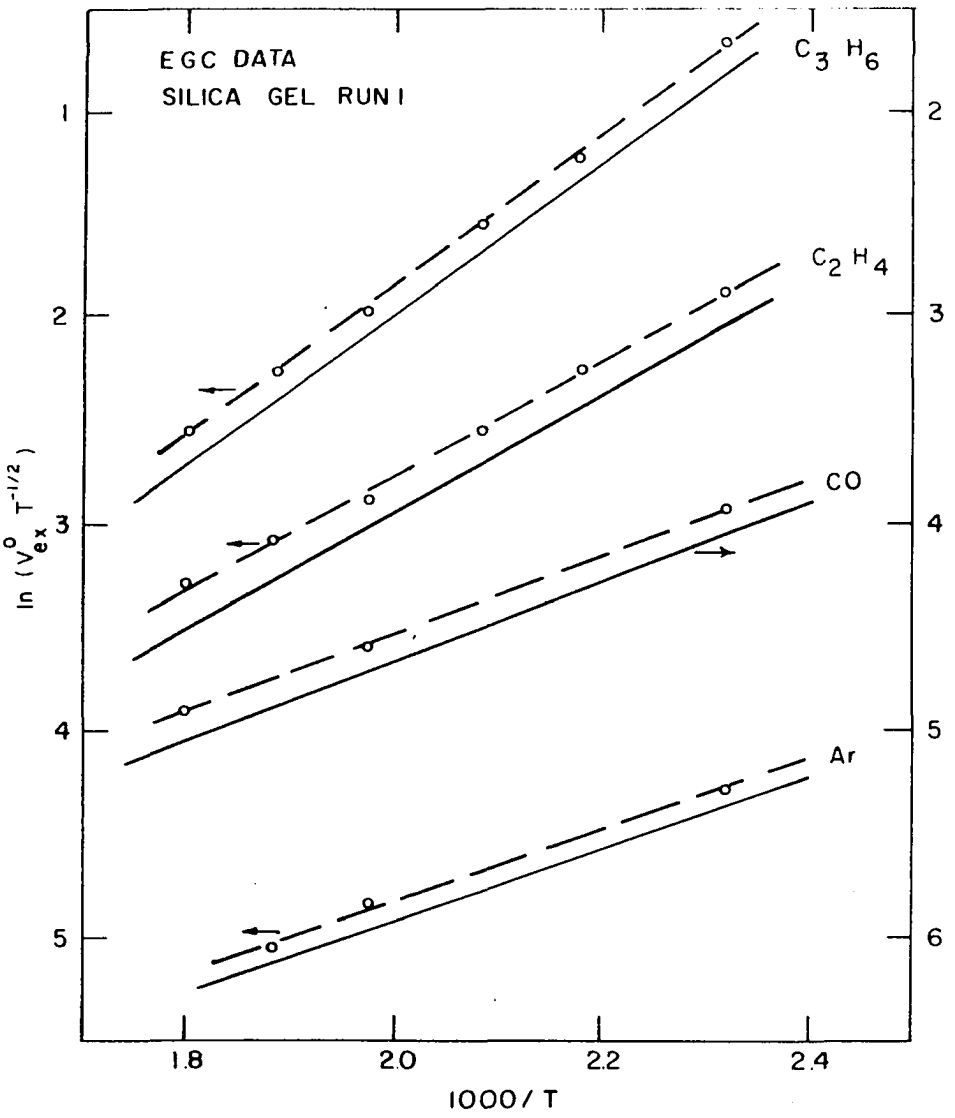

Figure 22. (see Figure 20)

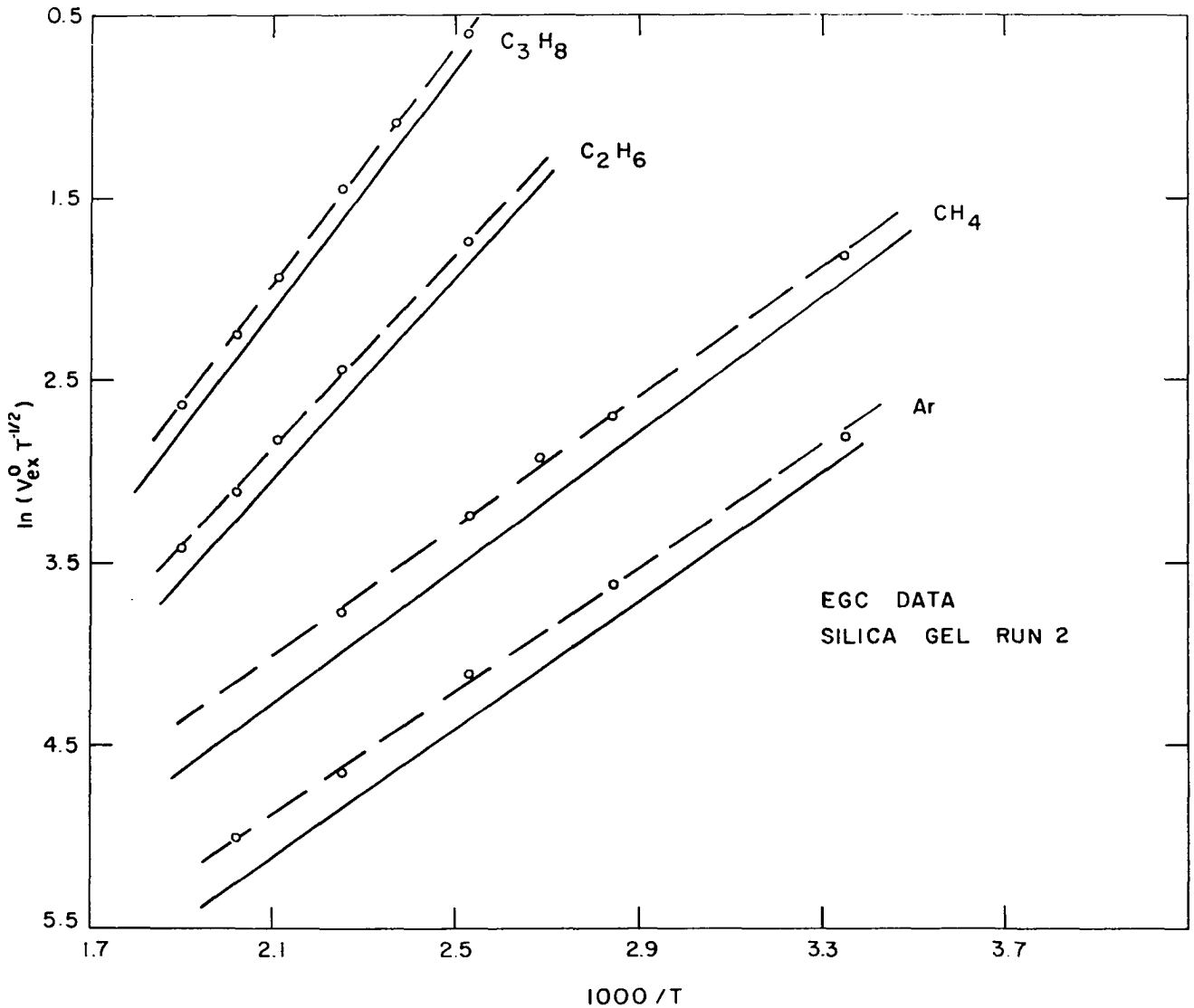

Figure 23. (see Figure 20)

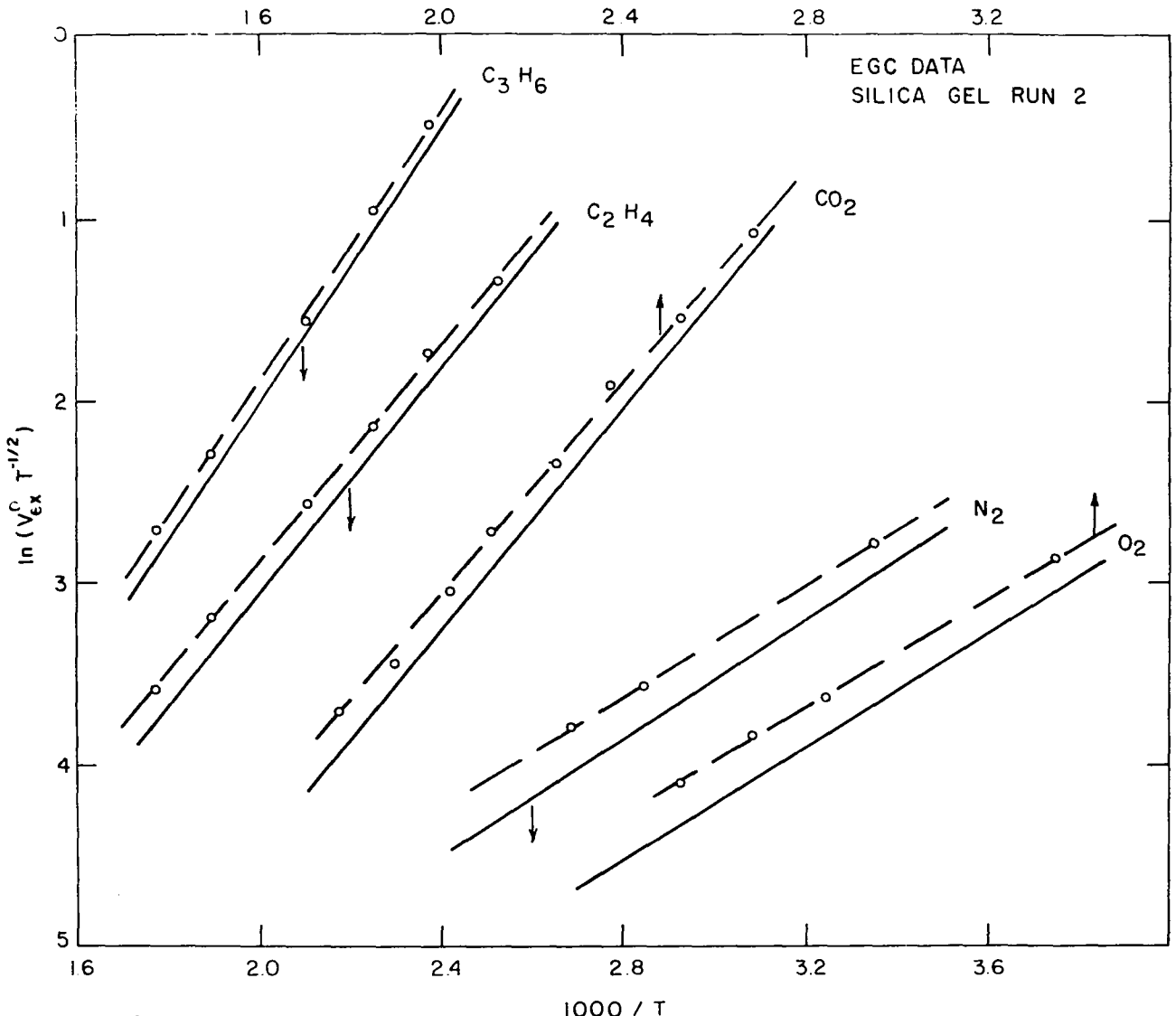

Figure 24. (see Figure 20)

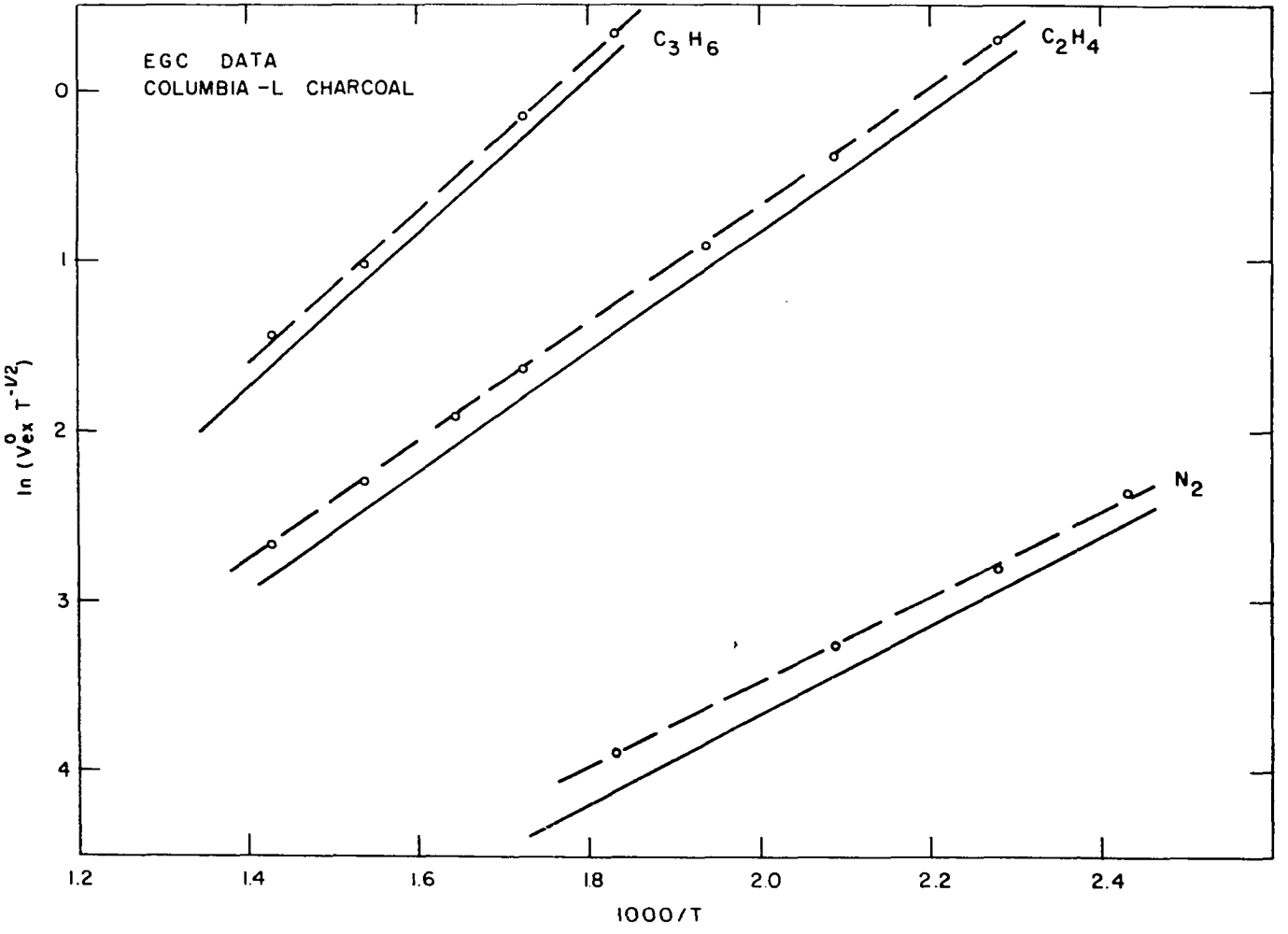

Figure 25. (see Figure 20)

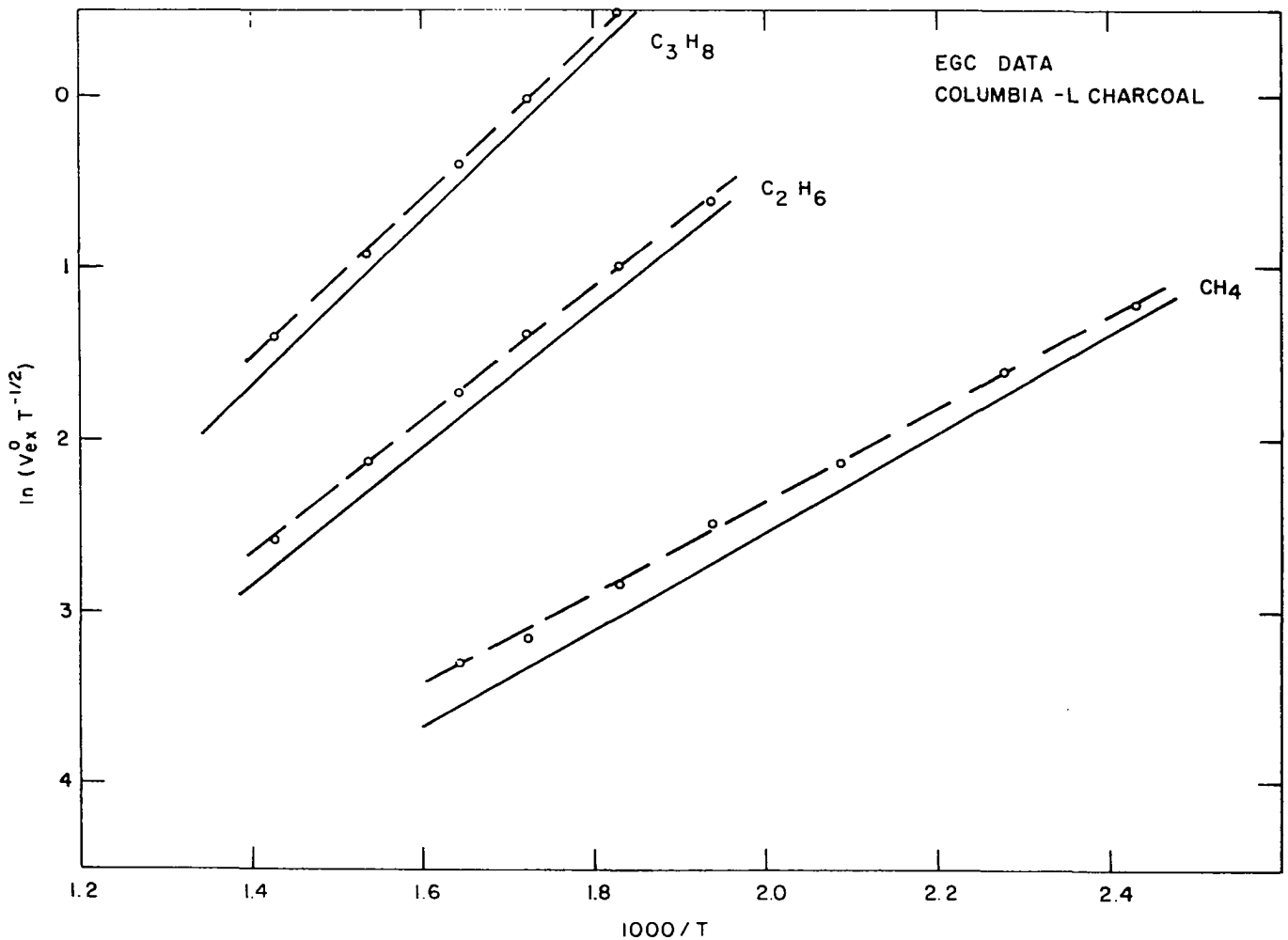

Figure 26. (see Figure 20)

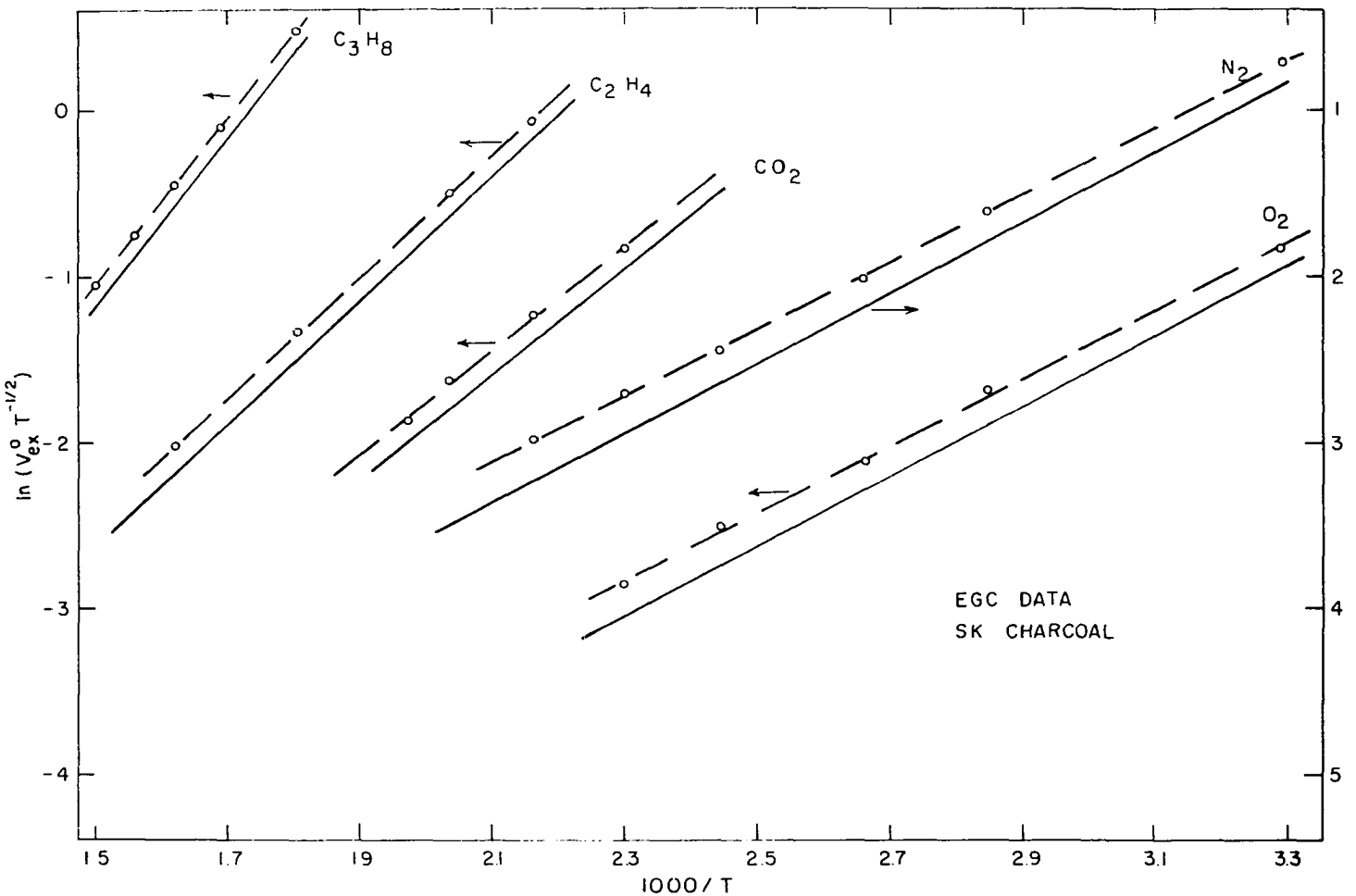

Figure 27. (see Figure 20)

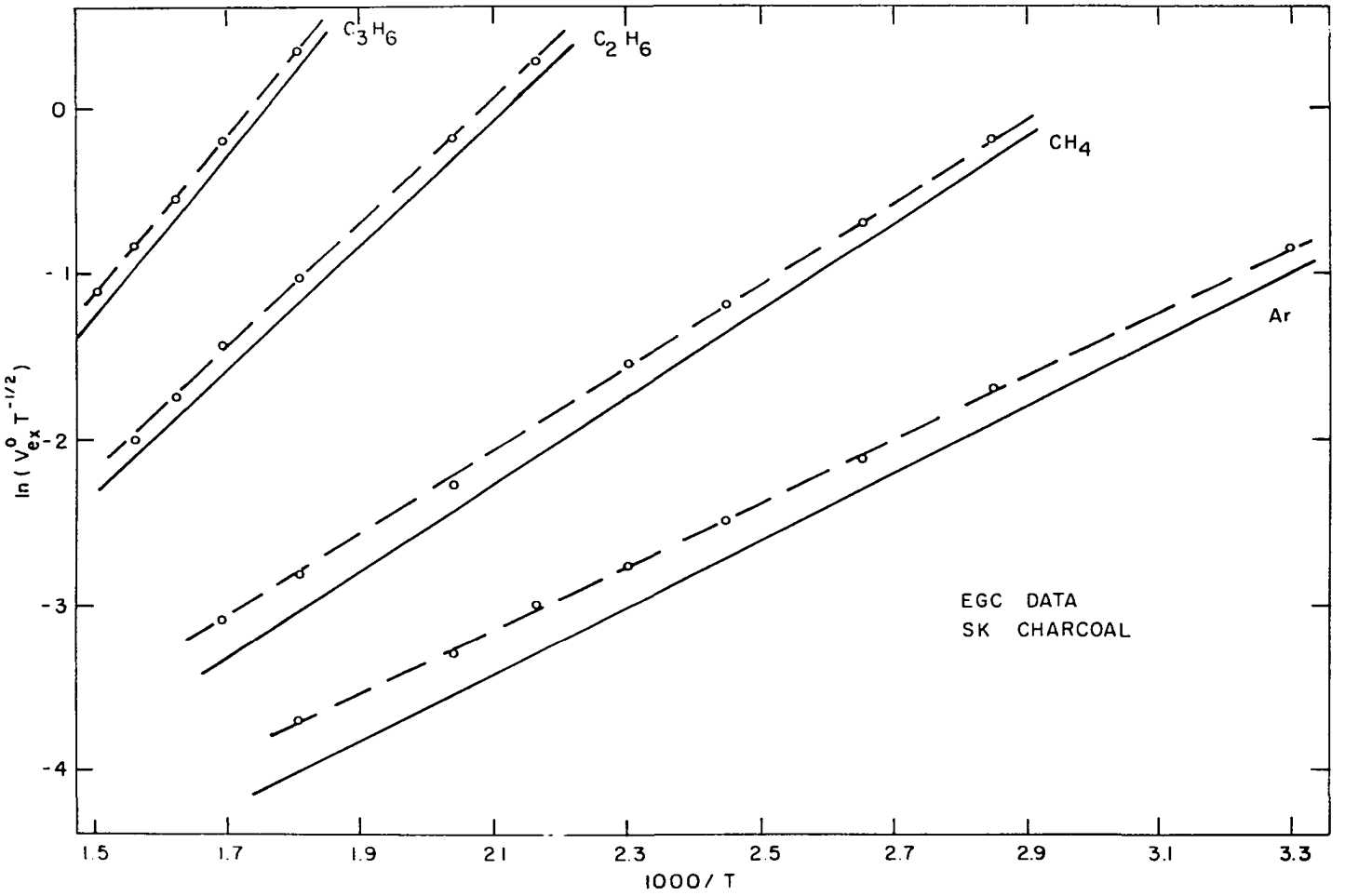

Figure 28. (see Figure 20)

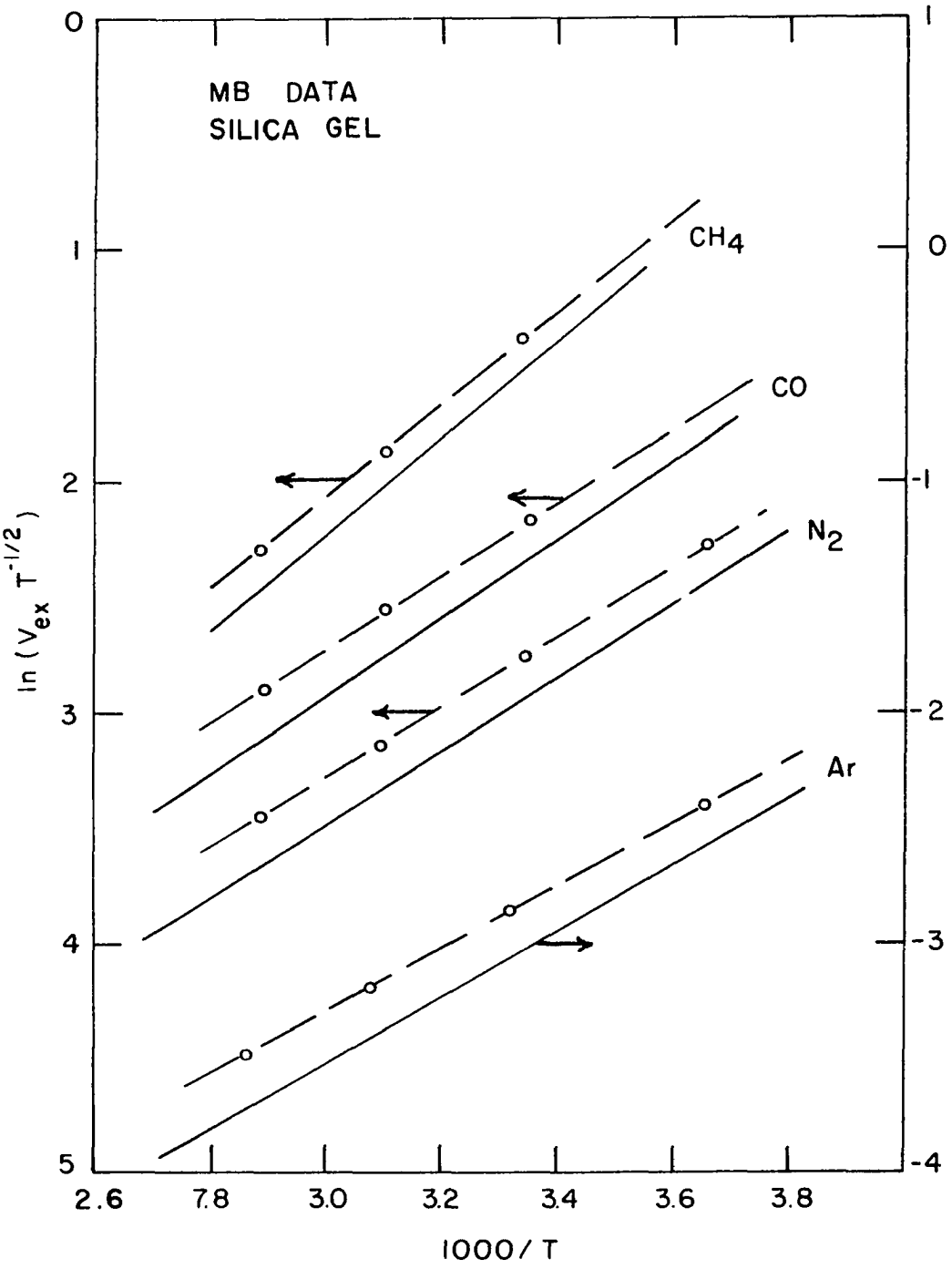

Figure 29. (see Figure 20)

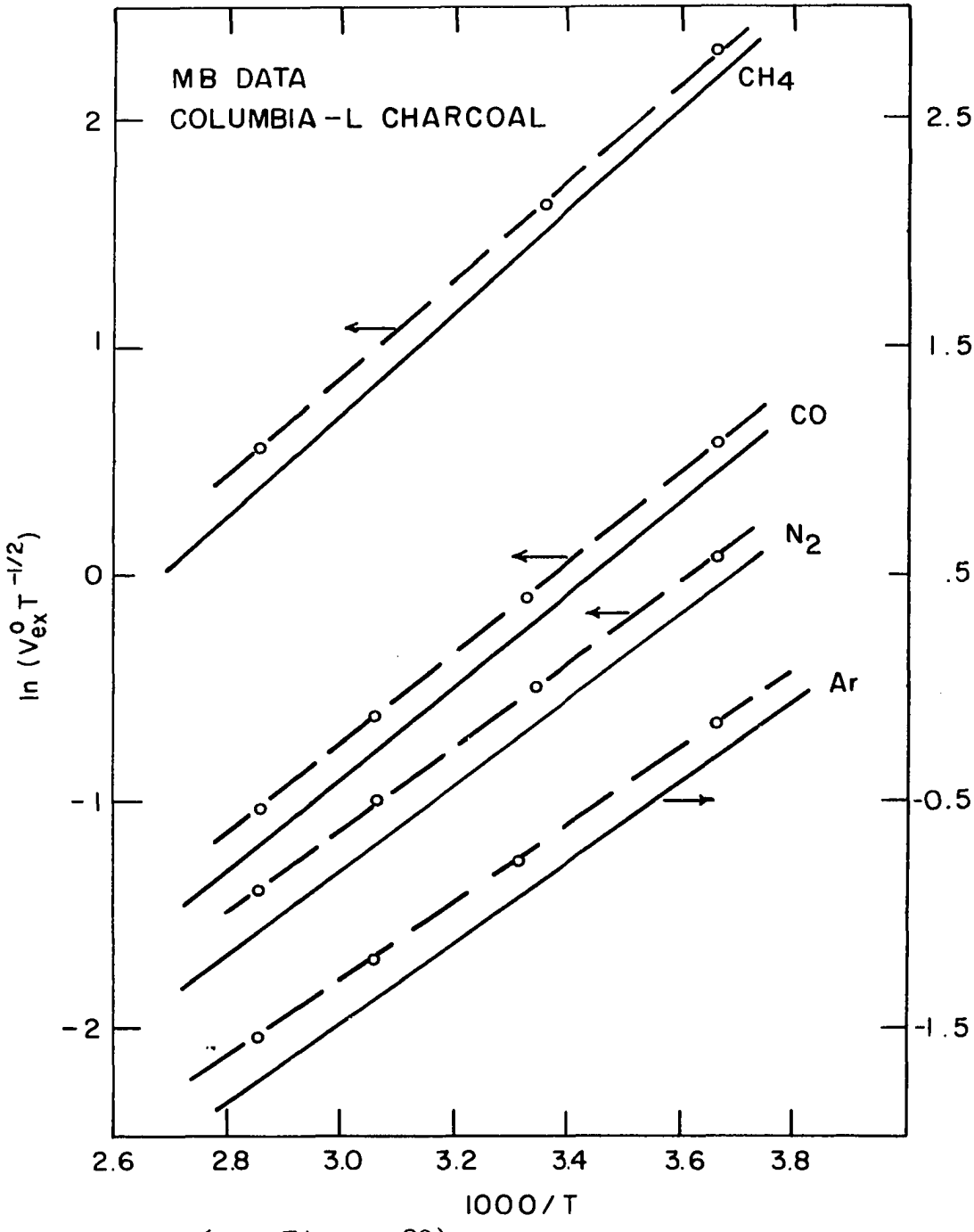

Figure 30. (see Figure 20)

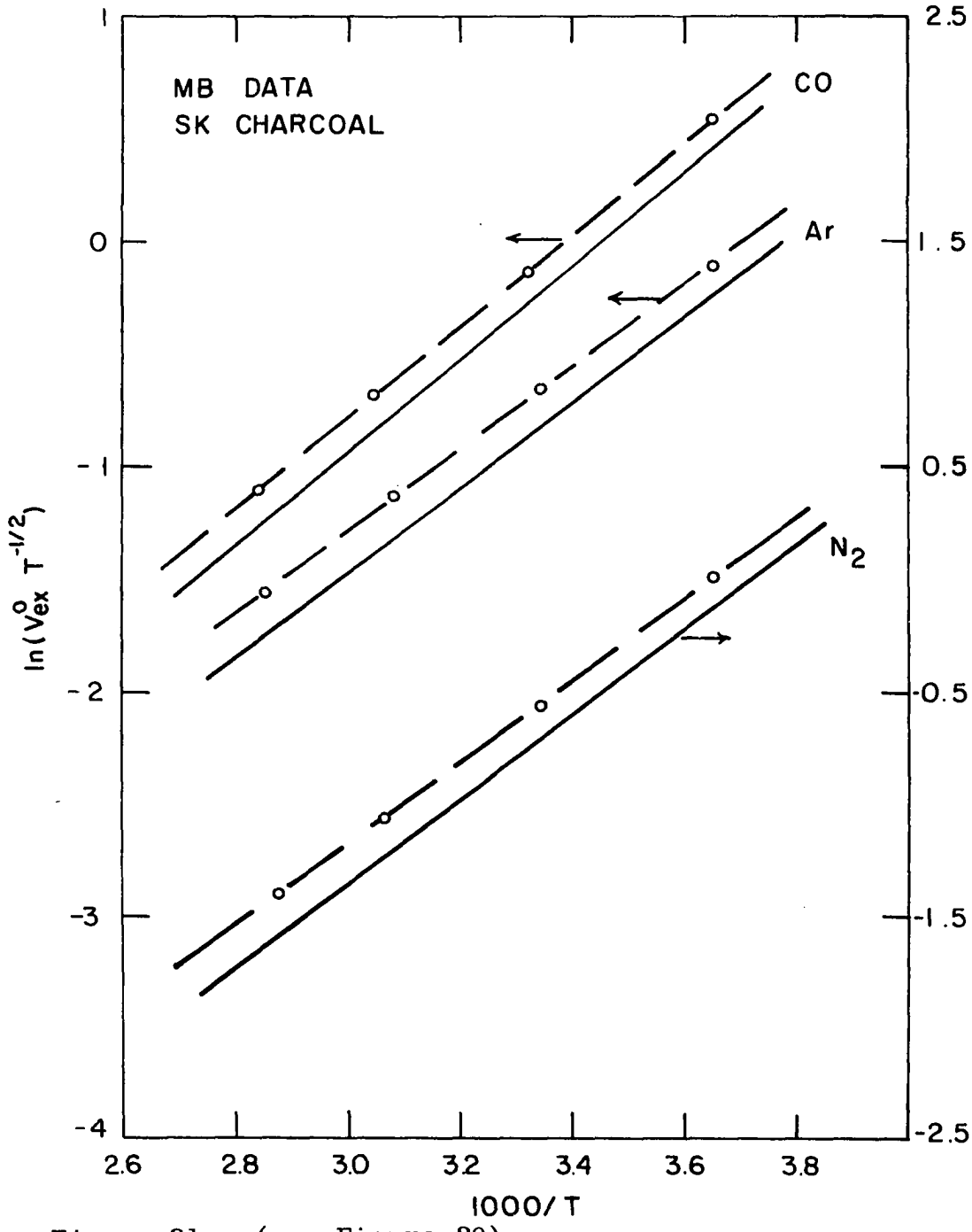

Figure 31. (see Figure 20)

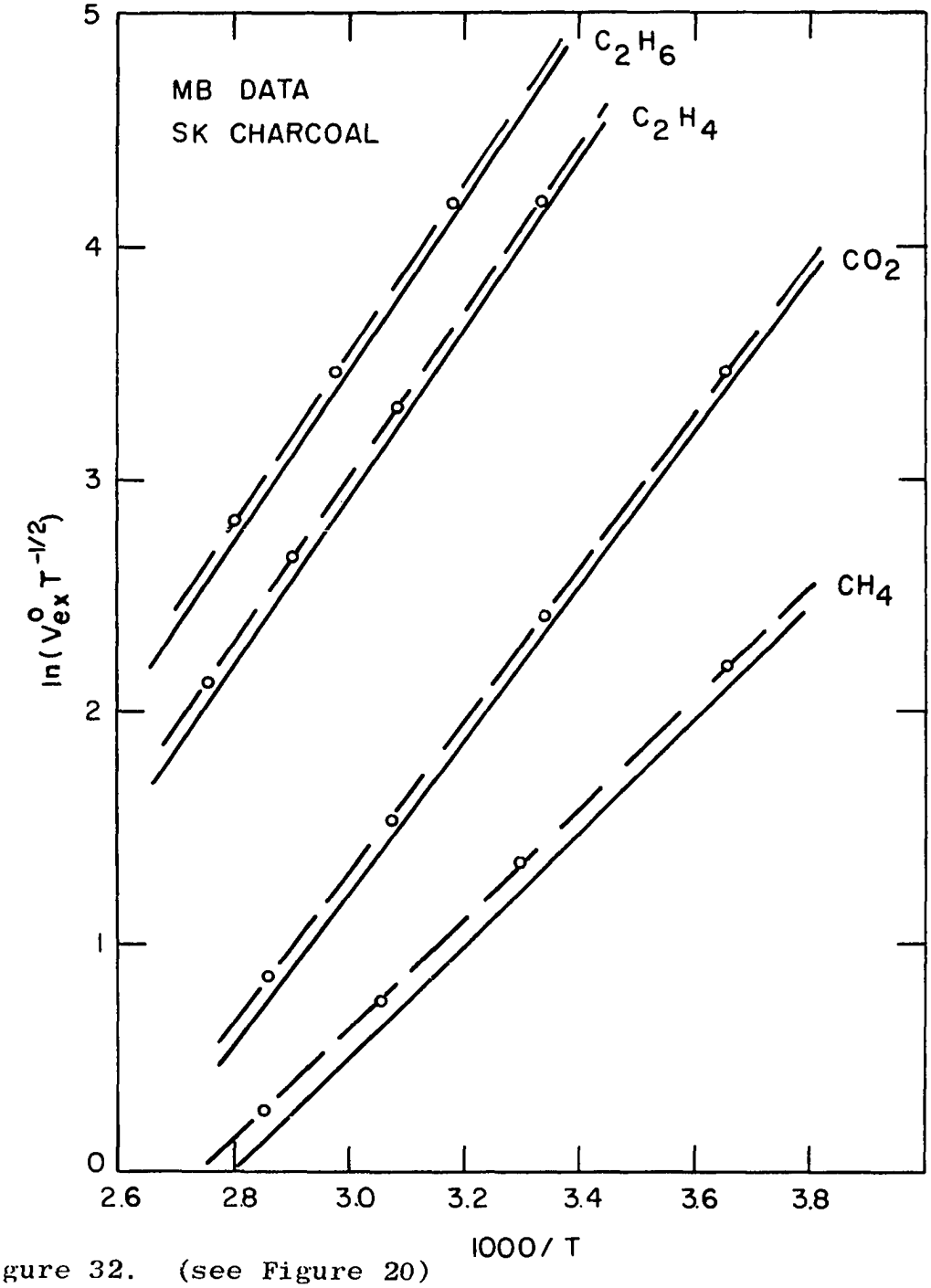

Figure 32. (see Figure 20)

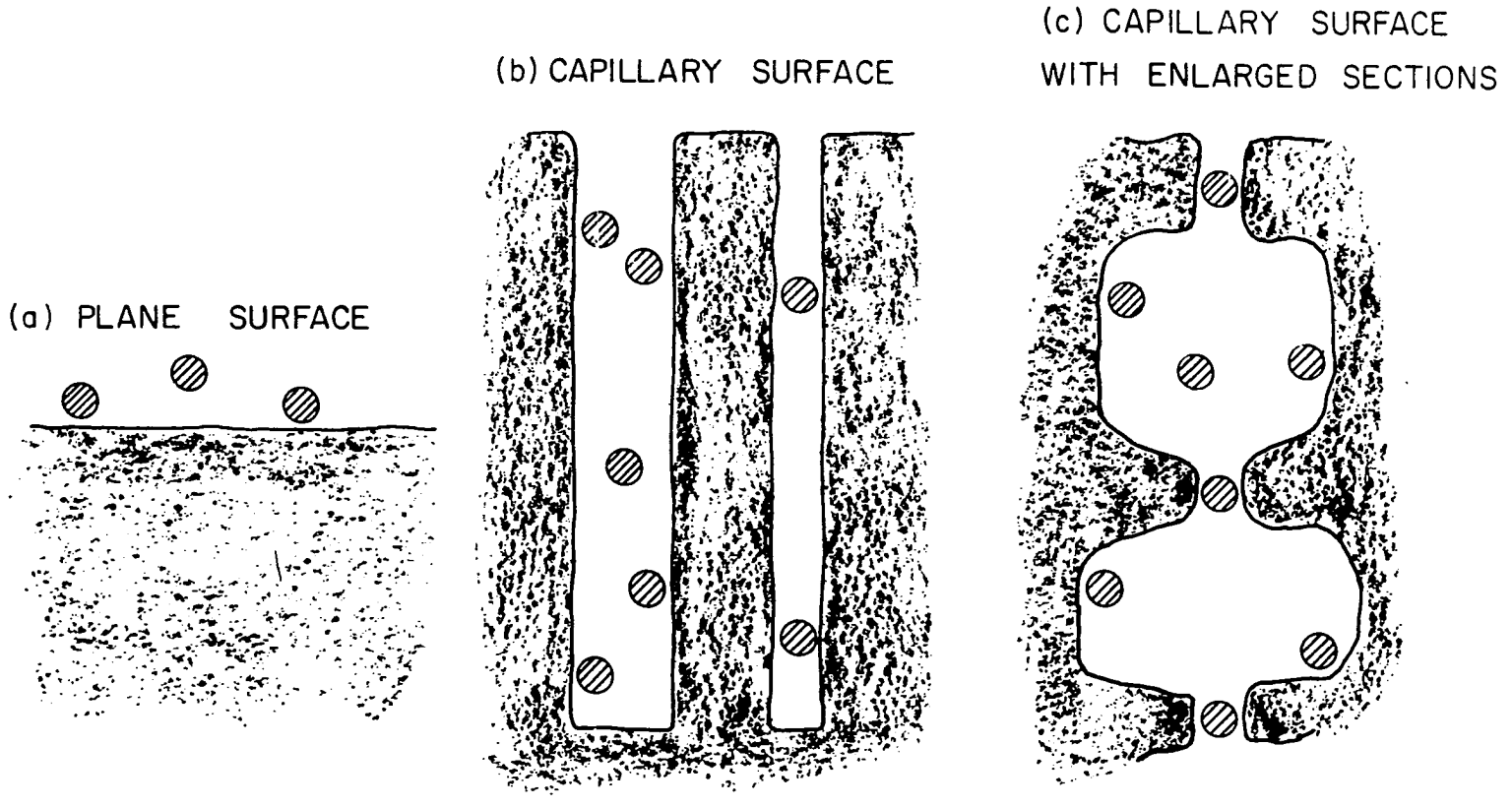

CROSS SECTIONS OF IDEAL SURFACES - ⊘ DENOTES ADSORBATE MOLECULES

Figure 33. Possible models for an adsorbent surface

APPENDIX B. TABLES

Table 1. Two-dimensional virial coefficient $B_2/(N\pi\sigma^2)$ for the Sinanoglu and Pitzer monolayer potential

$4\ E_o/kT$ $\eta=$	0.00	0.01	0.02	0.03	0.04	0.05
1.0	.2774	.2888	.3001	.3115	.3228	.3340
1.2	.2481	.2618	.2756	.2893	.3029	.3165
1.4	.3166	.2328	.2490	.2651	.2811	.2971
1.6	.1833	.2020	.2207	.2393	.3578	.2762
1.8	.1483	.1696	.1980	.2120	.2330	.2539
2.0	.1116	.1356	.1595	..1833	.2069	.2304
2.2	.0734	.1002	.1268	.1532	.1795	.2057
2.4	.0337	.0633	.0927	.1220	.1510	.1799
2.6	-.0076	.0250	.0573	.0894	.1213	.1530
2.8	-.0504	-.0148	.0206	.0556	.0904	.1250
3.0	-.0978	-.0560	-.0176	.0206	.0584	.0960
3.2	-.1408	-.0987	-.0571	-.0158	.0252	.0658
3.4	-.1884	-.1430	-.0980	-.0534	-.0092	.0347
3.6	-.2377	-.1888	-.1404	-.0924	-.0445	.0024
3.8	-.2888	-.2362	-.1842	-.1327	-.0816	-.0310
4.0	-.3417	-.2853	-.2296	-.1743	-.1197	-.0655

Table 2. Values of X_o and S_o

Adsorbent	Gas	X_o (Å)	S_o (Å)
Carbon	Ar	2.92	2.43
	N_2	3.04	2.53
	CO	3.07	2.56
	CH_4	3.10	2.58
	C_2H_4	3.40	2.83
	C_2H_6	3.16	2.63
	C_3H_6	3.78	3.15
	C_3H_8	3.88	3.23
	CO_2	3.38	2.82
	O_2	3.00	2.49
Silica Gel	Ar	2.66	
	N_2	2.79	
	CO	2.82	
	CH_4	2.84	
	C_2H_4	3.14	
	C_2H_6	2.87	
	C_3H_6	3.52	
	C_3H_8	3.58	
	CO_2	3.13	
	O_2	2.74	

Table 3. Coefficients of polynomials resulting from curve fitting thermocouple and pressure gage calibrations.

$$T(°C) = \sum_{o}^{n} C_i \, (EMF)^i \text{ and } P(mm) = \sum_{o}^{n} C_i \, (Gage)^i$$

C_i	Thermocouple (0 - 4 mv)	Pressure Gage (3 sections) 0.0 - 40.654	40.654 - 131.807	131.807 - 202.366
0	0.015482	0.000000	-2.234061×10^{3}	-6.698958×10^{3}
1	20.582000	4.080819	6.326739	24.775299
2	3.328350	-1.004453×10^{-3}	-9.602928×10^{-2}	-0.252695
3	-7.628977	2.798809×10^{-4}	2.202006×10^{-3}	1.522414×10^{-2}
4	6.636682	-3.291307×10^{-7}	-2.929498×10^{-5}	-4.528038×10^{-5}
5	-2.751990		2.254286×10^{-7}	5.326712×10^{-8}
6	0.355424		-9.274017×10^{-9}	
7	0.113904		1.574392×10^{-11}	
8	-0.043864			
9	0.004211			

Table 4. Best fit values obtained by use of the BET equations

Adsorbent	n	W_m (mgg^{-1})	Surface area ($m^2\ g^{-1}$)	C	St. dev. x 10^4
Silica Gel Run 1	1	303.021	1029.4	28	.16
Silica Gel Run 2	1	289.558	983.6	35	.09
SK charcoal Run 2	1	330.277	1122.0	83	.10
Columbia-L charcoal	∞	349.603	1187.6	1377	.08
SK charcoal Run 1	∞	265.643	902.4	1836	.02
SK charcoal Run 2	∞	262.745	892.5	2116	.02
SK charcoal Run 1 and 2	∞	264.067	897.0	2090	.02
Silica Gel Run 1	∞	204.531	694.8	235	.06
Silica Gel Run 2	∞	209.328	711.1	178	.03

Table 5. Summary of surface ares (m^2/g) calculated from experimental Henry's Law (HL) constants for Silica Gel

Gas	MB-HL	EGC-HL Run 1	EGC-HL Run 2
Ar	112.2	73.6	50.3
N_2	74.0	37.0	69.5
O_2			75.9
CO	90.2	63.3	
CH_4	67.8	55.7	87.7
C_2H_4		62.0	35.1
C_2H_6		92.2	51.6
C_3H_6		33.8	24.4
C_3H_8		47.1	35.6
CO_2			32.8

Table 6. Summary of surface areas (m^2/g) calculated from experimental Henry's Law (HL) constants and B_2/A (2D) values for Columbia-L charcoal

	Surface Areas						
Gas	EGC-HL	EGC-HL[a]	FGC-HL[b]	FGC-HL	FGC-2D	MB-HL	MB-2D
Ar		210				314.5	260
N_2	46.4	143				279.5	240
CO		148				253.0	276
CH_4	101.1	148	170.5	418.7	204	794.8	40
C_2H_4	125.5	129					
C_2H_6	80.9	137					
C_3H_6	106.6	76					
C_3H_8	77.7	78					

[a]Taken from Hansen *et al.* (100), but corrected for proper chart speed.

[b]Injected samples.

Table 7. Summary of surface areas (m^2/g) calculated from experimental Henry's Law (HL) constants and B_2/A (2D) values for SK charcoal

	Surface Areas		
Gas	EGC-HL	MB-HL	MB-2D
Ar	144.9	227.3	188
N_2	130.9	243.3	270
O_2	113.9		
CO		216.6	245
CH_4	139.0	367.7	60
C_2H_4	102.6	135.5	76
C_2H_6	117.4	192.0	43
C_3H_6	70.2		
C_3H_8	59.1		
CO_2	77.4	55.2	44

Table 8. Summary of gas-solid interaction potentials for Silica Gel

Gas	MB	$-E^*_{AS}/R$ EGC Run 1	EGC Run 2
Ar	1448	1736	1748
N_2	1598	2055	1614
O_2			1564
CO	1731	1934	
CH_4	2086	2199	1860
C_2H_4		2846	3097
C_2H_6		2550	2788
C_3H_6		3634	3785
C_3H_8		3247	3340
CO_2			3031

Table 9. Summary of gas-solid interaction potentials for Columbia-L charcoal

Gas	MB	EGC	$-E^*_{AS}/R$ EGC[a]	FGC	FGC[b]
Ar	1790		1931		
N_2	1887	2627	2122		
CO	2062		2191		
CH_4	2233	2800	2585	2267	2566
C_2H_4		3570	3562		
C_2H_6		3986	3744		
C_3H_6		4560	4780		
C_3H_8		4824	4829		

[a]Taken from Hansen *et al*. (100).

[b]Injected samples.

Table 10. Summary of gas-solid interaction potentials for SK charcoal

Gas	$-E^*_{AS}/R$ EGC	MB
Ar	2036	1907
N_2	2103	1908
O_2	2122	
CO		2100
CH_4	2631	2430
C_2H_4	3706	3600
C_2H_6	3845	3695
C_3H_6	4889	
C_3H_8	5053	
CO_2	3246	3321

Table 11. Gas-solid interaction parameters evaluated for the Henry's Law model

Adsorbent and system	Gas	$-E^*_{AS}/R$	$-\ln AZ_o$	AZ_o (cm^3)	A (m^2/g)	St. dev.
Silica Gel (MB)	Ar	1448	3.5116	0.03985	112.2	0.011
	N_2	1598	3.8805	.02064	74.0	.004
	CO	1731	3.6712	.02544	90.2	.004
	CH_4	2086	3.9505	.09125	67.8	.006
Columbia-L charcoal (MB)	Ar	1790	2.3878	.09183	314.5	.01
	N_2	1887	2.4656	.08496	279.5	.01
	CO	2062	2.5552	.07768	253.0	.005
	CH_4	2233	1.4008	.2464	794.8	.016
SK charcoal (MB)	Ar	1907	2.7125	.06637	227.3	.014
	N_2	1908	2.6041	.07397	243.3	.007
	CO	2100	2.7107	.06649	216.6	.007
	CH_4	2430	2.1713	.1140	367.7	.014
	C_2H_4	3600	3.0778	.04606	135.5	.012
	C_2H_6	3695	2.8025	.06066	192.0	.002
	CO_2	3321	3.9815	.01866	55.2	.009

Table 11. (Continued)

Adsorbent and system	Gas	$-E^*_{AS}/R$	$-\ln AZ_o$	AZ_o (cm^3)	A (m^2/g)	St. dev.
Silica Gel Run 1 (EGC)	Ar	1736	3.9327	0.01959	73.6	.284
	N_2	2055	4.5748	.01031	37.0	.167
	CO	1934	4.0252	.01786	63.3	.19
	CH_4	2199	4.1459	.01583	55.7	.07
	C_2H_4	2846	3.9392	.01946	62.0	.02
	C_2H_6	2550	3.6322	.02646	92.2	.03
	C_3H_6	3634	4.4322	.01189	33.8	.02
	C_3H_8	3247	4.0829	.01686	47.1	.02
Silica Gel Run 2 (EGC)	Ar	1748	4.3132	.01339	50.3	.07
	N_2	1614	3.9435	.01938	69.5	.02
	O_2	1564	3.8721	.02081	75.9	.04
	CH_4	1860	3.6928	.02490	87.7	.035
	C_2H_4	3097	4.5089	.01101	35.1	.02
	C_2H_6	2788	4.2117	.01482	51.6	.02
	C_3H_6	3785	4.7573	.00859	24.4	.01
	C_3H_8	3340	4.3635	.01273	35.6	.03
	CO_2	3031	4.5799	.01026	32.8	.04
Columbia-L charcoal (EGC)	N_2	2627	4.2617	.01410	46.4	.025
	CH_4	2800	3.4625	.03135	101.1	.03
	C_2H_4	3570	3.1541	.04268	125.5	.008
	C_2H_6	3986	3.5722	.02810	80.9	.02
	C_3H_6	4560	3.2118	.04029	106.6	.025
	C_3H_8	4824	3.5015	.03015	77.7	.008
SK charcoal (EGC)	Ar	2036	3.1627	.04231	144.9	.02
	N_2	2103	3.2239	.03980	130.9	.013
	O_2	2122	3.3765	.03417	113.9	.03
	CH_4	2631	3.1445	.04309	139.0	.02
	C_2H_4	3706	3.3554	.03489	102.6	.009
	C_2H_6	3845	3.2940	.03710	117.4	.028
	C_3H_6	4889	3.6288	.02655	70.2	.005
	C_3H_8	5053	3.7747	.00294	59.1	.005
	CO_2	3246	3.6437	.02615	77.4	.026
Columbia-L charcoal (FGC)	CH_4	2267	2.0419	.1298	418.7	.055
Columbia-L charcoal (FGC) Injected Samples	CH_4	2566	2.9403	.05285	170.5	.013

Table 12. Parameters evaluated for the two-dimensional gas film model

Gas	E_o/R	E^*/R	σ_o (Å)	σ_o^* (Å)	ξ	$A(m^2\ g^{-1})$	St. dev.
CH_4[a]	148.2	128.3	3.817	3.863	.93	204±9	71.4
Ar[b]	119.9	98.8	3.40	3.46	.91	188±10	-
N_2	95.0	78.4	3.70	3.76	.91	270±10	-
CO	100.2	83.0	3.76	3.82	.91	245±30	-
CH_4	148.2	131.7	3.817	3.855	.94	60±1	83.7
C_2H_4	199.2	157.1	4.523	4.613	.89	76±3	245.3
C_2H_6	243.0	170.1	3.95	4.09	.84	43±3	-
CO_2	189.0	150.2	4.486	4.573	.89	44±0	5.7
Ar[c]	119.9	93.0	3.40	3.48	.88	260±30	-
N_2	95.0	76.0	3.70	3.77	.89	240±5	-
CO	100.2	82.7	3.76	3.82	.91	276±20	-
CH_4	148.2	148.2	3.82	3.82	1.00	40±1	-

[a]Columbia-L charcoal FGC data.

[b]SK charcoal MB data.

[c]Columbia-L charcoal MB data.

Table 13. FGC data on Columbia-L charcoal, dependence of gas-surface virial coefficients on temperature

Gas	T(°K)	V_{ex}^o $(cm^3 g^{-1})$	$-C_{AAS} \times 10^{-6}$ $(cm^6\ g^{-1}\ mole^{-1})$	$B_2/A \times 10^{-2}$ $(g\ mole^{-1})$
CH_4	223.0	410.0	25.3	.753
	242.3	265.0	16.15	1.15
	273.1	102.5	4.17	1.99
	298.6	51.0	1.16	2.23
	323.5	29.0	.43	2.54
	343.0	20.0	.278	3.48
	363.6	14.4	.149	3.60
	392.0	11.2	.090	5.06

Table 13. (Continued)

Gas	T(°K)	V^o_{ex} $(cm^3 g^{-1})$	$-C_{AAS} x 10^{-6}$ $(cm^6\ g^{-1}\ mole^{-1})$	$B_2/A \times 10^{-2}$ $(g\ mole^{-1})$
Injected samples CH_4	298.0	53.9		
	323.5	28.2		
	343.0	18.7		
	363.6	13.0		

Table 14. MB data on Silica Gel, dependence of V^o_{ex} on temperature

Gas	V^o_{ex} (cm^3/g)	T(°K)
Argon	1.499	273.50
	1.004	301.36
	.737	324.80
	.579	349.04
Nitrogen	1.680	273.39
	1.094	298.74
	.775	322.80
	.587	346.69
Carbon monoxide	1.995	298.92
	1.382	322.13
	1.018	345.41
Methane	4.322	299.38
	2.752	322.21
	1.852	346.53

Table 15. MB data on Columbia-L charcoal, dependence of gas-surface virial coefficients on temperature

Gas	T(°K)	V^o_{ex} (cm^3g^{-1})	$-C_{AAS}x10^{-4}$ ($cm^6g^{-1}mole^{-1}$)	$B_2/Ax10^{-2}$ (g $mole^{-1}$)
Ar	273.36	14.132	7.925	1.984
	301.90	8.138	2.431	1.836
	327.26	5.498	1.382	2.286
	350.52	4.002	.845	2.638
N_2	273.28	17.911	18.41	2.869
	299.56	10.540	6.918	3.114
	326.64	6.641	2.780	3.151
	350.33	4.667	1.159	2.662
CO	273.26	29.373	45.89	2.659
	300.99	15.693	13.06	2.652
	326.74	9.669	4.778	2.555
	349.98	6.665	2.500	2.814
CH_4	273.36	167.37	2993.0	5.343
	297.66	88.16	7236.0	7.951
	350.33	32.63	345.5	11.53

Table 16. MB data on SK charcoal, dependence of gas-surface virial coefficients on temperature

Gas	T(°K)	V^o_{ex} (cm^3 g^{-1})	$-C_{AAS}x10^{-4}$ (cm^6 g^{-1} $mole^{-1}$)	$B_2/Ax10^{-2}$ (g $mole^{-1}$)	$D_{AAAS}x10^{-10}$ (cm^9 g^{-1} $mole^{-2}$)
Ar	273.36	14.893	10.63	2.397	
	298.33	8.956	4.615	2.877	
	323.57	5.792			
	348.69	3.987			
N_2	273.31	16.818	14.77	2.611	
	298.53	9.849	5.175	2.668	
	325.12	6.242	2.093	2.687	
	346.10	4.561	1.193	2.867	
CO	273.28	28.520	48.00	2.950	
	300.48	15.183	13.65	2.961	
	327.33	9.125	5.175	3.107	
	350.68	6.176	2.161	2.833	
CH_4	273.23	148.21	2553.0	5.810	330.0
	302.93	67.73	702.1	7.652	65.6
	326.99	39.24	258.1	8.378	16.8
	350.28	24.53	112.5	9.352	6.1
C_2H_4	299.56	1137.57	130.3	5.034	101.1
	323.69	493.06	29.43	6.054	14.0
	343.97	267.02	11.08	7.767	4.7
	362.15	158.70	4.423	8.780	2.2
C_2H_6	314.04	1190.76	166.0	5.852	765.
	335.04	581.91	49.16	7.259	37.
	356.44	316.69	20.18	10.06	15.
CO_2	273.36	524.29	36.38	6.616	25.15
	299.51	193.88	7.433	9.887	4.94
	325.37	82.71	.978	7.149	.21
	348.83	44.09	.237	6.078	.03

Table 17. EGC data on Silica Gel, dependence of V^o_{ex} on temperature.

Run No.	Gas	V^o_{ex} (cm^3/g)	T(°K)
1	Argon	0.286	430.86
		.178	506.67
		.149	530.95
1	Nitrogen	.296	430.86
		.230	459.22
		.160	506.67
1	Carbon monoxide	.407	430.86
		.227	506.67
		.177	554.79
1	Methane	.646	430.86
		.436	479.57
		.330	506.66
		.292	530.93
1	Ethylene	3.174	430.86
		2.249	458.24
		1.698	479.56
		1.262	506.66
		1.064	530.95
		0.878	554.78
1	Ethane	2.240	430.86
		1.776	458.23
		1.380	479.56
		1.070	506.66
		0.897	530.95
1	Propylene	10.474	430.86
		6.216	458.22
		4.620	479.55
		3.136	506.66
		2.416	530.94
		1.847	554.79
1	Propane	6.324	430.86
		4.275	458.22
		3.170	479.55
		2.232	506.65
		1.741	530.94
		1.430	554.75
2	Argon	1.035	298.61
		0.504	351.44
		.326	395.57
		.200	443.62
		.149	494.89

Table 17. (Continued)

Run No.	Gas	V^o_{ex} (cm^3/g)	T(°K)
2	Nitrogen	1.070	298.61
		.529	351.46
		.436	372.11
2	Oxygen	0.980	298.64
		.516	351.44
		.422	372.13
		.331	395.56
2	Methane	2.817	298.62
		1.250	351.44
		1.036	372.11
		.778	395.58
		.486	443.62
2	Ethylene	5.262	395.53
		3.610	420.72
		2.494	443.67
		1.690	473.54
		.956	526.24
		.660	561.77
2	Ethane	3.524	395.54
		1.835	443.66
		1.285	473.52
		.992	494.88
		.756	526.26
2	Propylene	12.574	420.68
		8.042	443.71
		4.824	473.54
		2.348	526.21
		1.582	561.77
2	Propane	10.829	395.51
		6.882	420.70
		4.982	443.67
		3.106	473.54
		2.278	494.87
		1.634	526.21
2	Carbon dioxide	6.573	372.12
		4.266	395.56
		3.008	420.76
		2.037	443.61
		1.416	473.49
		1.060	494.89
		.735	526.25
		.590	561.78

Table 18. EGC data on Columbia-L charcoal, dependence of V^o_{ex} on temperature

Gas	V^o_{ex} (cm^3/g)	T(°K)
Nitrogen	1.930	410.87
	1.274	438.53
	.836	478.79
	.480	545.95
Methane	6.016	410.83
	4.188	438.53
	2.604	478.79
	1.894	515.77
	1.362	545.94
	1.030	579.85
	.916	607.19
Ethylene	28.177	438.52
	14.808	478.78
	9.098	515.76
	4.658	579.84
	3.618	607.19
	2.593	649.78
	1.857	699.15
Ethane	12.280	515.75
	8.644	545.91
	5.933	579.84
	4.368	607.19
	3.021	649.76
	2.002	699.12
Propylene	32.337	545.90
	20.417	579.84
	9.124	649.76
	6.197	699.11
Propane	37.535	545.90
	23.382	579.83
	16.436	607.16
	10.112	649.75
	6.398	699.10

Table 19. EGC data on SK charcoal, dependence of V^o_{ex} on temperature

Gas	V^o_{ex} (cm^3/g)	T(°K)
Argon	7.398	304.10
	3.380	351.35
	2.309	377.67
	1.673	408.76
	1.297	434.70
	1.065	462.52
	.820	490.52
	.576	553.02
Nitrogen	8.490	304.07
	3.756	351.33
	2.575	377.71
	1.761	408.76
	1.397	434.74
	1.085	462.09
Oxygen	7.549	304.10
	3.478	351.34
	2.324	377.69
	1.621	408.76
	1.190	434.72
Methane	15.375	351.35
	9.674	377.71
	6.098	408.76
	4.386	434.72
	2.254	490.51
	1.392	553.05
	1.105	590.75
Ethylene	20.088	462.64
	13.433	490.50
	6.190	553.04
	3.301	616.66
Ethane	28.432	462.07
	18.233	490.50
	8.366	553.04
	5.731	590.78
	4.312	616.67
	3.369	640.64

Table 19. (Continued)

Gas	V^o_{ex} (cm^3/g)	T(°K)
Propylene	33.047	553.04
	19.780	590.78
	14.232	616.62
	10.874	640.56
	8.417	664.99
Propane	37.720	553.05
	21.968	590.78
	15.692	616.64
	11.967	640.58
	9.077	665.00
Carbon dioxide	9.080	434.72
	6.278	462.07
	4.382	490.51
	3.459	506.25

Table 20. Gravimetric adsorption isotherms on Silica Gel

Gas	Temperature (°K)	Amount adsorbed (mg/g)	Pressure (mm)
Nitrogen	273.39	0.0411	14.834
		.1936	69.840
		.3656	131.652
		.4764	171.585
		.5937	214.045
		.7019	252.870
		.8193	295.683
	298.74	.0263	16.187
		.0850	51.774
		.1229	75.058
		.1685	102.949
		.2377	144.341
		.3016	183.109
		.3708	225.192
		.4661	285.846
	322.80	.0386	35.330
		.0569	53.344
		.0804	75.404

Table 20. (Continued)

Gas	Temperature (°K)	Amount adsorbed (mg/g)	Pressure (mm)
		0.1117	103.566
		.2004	184.086
		.3074	286.318
	346.69	.0128	17.572
		.0389	51.156
		.0637	83.531
		.0963	126.862
		.2151	286.240
Argon	273.49	.0507	14.675
		.1080	30.410
		.1810	51.693
		.2475	70.490
		.3165	90.529
		.4508	128.145
		.6006	171.691
	301.37	.0216	10.302
		.0425	18.969
		.0725	32.534
		.1182	53.433
		.1586	72.835
	324.80	.0899	62.385
		.1329	90.951
		.3104	213.382
		.3665	252.891
	349.04	.370	34.935
		.0670	63.340
		.0957	89.903
		.1388	131.015
		.1831	171.663
		.2236	211.506
Carbon monoxide	298.92	.1024	34.435
		.1663	55.738
		.2512	84.820
		.4788	162.987
		.5957	204.893
		.7314	252.663
	322.13	.0315	16.362
		.0680	35.419
		.1045	54.876

Table 20. (Continued)

Gas	Temperature (°K)	Amount adsorbed (mg/g)	Pressure (mm)
		0.1502	78.488
		.2076	109.639
		.2729	143.619
		.3446	183.748
		.4230	225.871
	345.41	.0747	56.344
		.1048	80.656
		.1426	108.944
		.1870	144.223
		.2418	185.560
		.2927	227.923
		.3579	279.807
Methane	299.38	.0584	15.869
		.1928	53.421
		.2646	74.164
		.3376	96.050
		.5790	171.980
	322.21	.0333	15.005
		.0737	34.548
		.1181	54.714
		.2081	98.545
		.2982	143.578
		.5017	253.741
	346.53	.0222	16.166
		.0770	56.482
		.1110	81.577
		.2206	163.757
		.3772	284.736

Table 21. Gravimetric adsorption isotherms on Columbia-L charcoal

Gas	Temperature (°K)	Amount adsorbed (mg/g)	Pressure (mm)
Argon	273.36	0.4938	15.017
		1.8208	55.970
		2.7356	84.933
		3.9339	123.853
		5.1321	163.862
		6.5751	213.496
	301.90	0.2675	15.490
		0.5561	32.416
		0.9323	54.462
		1.4425	84.779
		2.0919	123.447
		4.6119	279.474
		5.4236	331.545
	327.26	0.1649	15.351
		0.5772	53.966
		0.8864	83.279
		1.7367	164.624
		2.5613	245.323
		3.1024	299.578
		3.5765	346.999
	350.52	0.2293	31.411
		0.4071	55.938
		0.6081	83.869
		0.8967	124.068
		1.4738	205.564
		2.1979	309.634
		2.6102	370.137
Nitrogen	273.28	0.4520	15.510
		0.8775	30.349
		1.6602	58.422
		2.3977	85.921
		3.3738	123.825
	299.56	0.2285	14.557
		0.4966	31.720
		0.8937	57.771
		1.8787	124.174
		2.4511	164.710
		3.1885	218.473

Table 21. (Continued)

Gas	Temperature (°K)	Amount adsorbed (mg/g)	Pressure (mm)
	326.64	0.3218	35.497
		1.5851	180.220
		2.3018	266.633
	350.33	0.1932	32.408
		0.3531	59.223
		0.5180	87.595
		0.7423	126.098
		0.9872	168.103
		1.2424	212.483
		1.9771	343.912
Carbon monoxide	273.26	0.7010	14.659
		1.4612	31.289
		2.5951	56.649
		3.7290	83.560
		5.2623	122.874
	300.99	1.2601	55.157
		2.7159	122.635
		3.5662	164.254
		4.3650	205.023
	326.74	0.1779	13.420
		1.5847	122.858
		3.0689	245.632
		3.5481	286.753
		4.0325	329.755
	349.98	0.1174	13.771
		0.2566	30.129
		0.4575	53.978
		0.7049	83.572
		1.3696	164.653
Methane	273.36	0.8706	5.866
		1.3217	9.193
		2.2939	17.091
		2.8616	22.146

Table 21. (Continued)

Gas	Temperature (°K)	Amount adsorbed (mg/g)	Pressure (mm)
	297.65	0.4959	6.841
		1.0559	15.372
		1.3943	21.009
		1.7405	26.946
		2.1566	34.410
	350.33	0.1177	5.002
		0.2304	9.931
		0.3490	15.351
		0.4851	21.698
		0.6523	30.153
		0.8369	39.663
		1.0275	50.355

Table 22. Gravimetric adsorption isotherms on SK charcoal

Gas	Temperature (°K)	Amount adsorbed (mg/g)	Pressure (mm)
Argon	273.36	0.4581	13.212
		1.0487	30.406
		2.1043	61.922
		3.3743	100.942
	298.33	0.2721	14.178
		0.6326	33.214
		1.2490	66.198
		3.4744	190.626
		4.2736	237.954
	323.57	0.2629	23.074
		0.4797	42.278
		0.8480	75.412
		1.3207	118.777
	348.69	0.0714	9.756
		0.5088	69.604
		0.8587	117.900
		1.2426	170.363
		1.2922	177.989

Table 22. (Continued)

Gas	Temperature (°K)	Amount adsorbed (mg/g)	Pressure (mm)
Nitrogen	273.31	0.5576	20.390
		1.9156	71.917
		2.4840	94.502
		3.2051	123.821
	298.53	1.0441	71.819
		1.4231	98.951
		1.8915	132.508
		2.4441	173.308
		2.9809	214.098
	325.12	0.4363	50.953
		0.6639	78.078
		1.7113	205.422
		2.0534	248.179
		2.4218	295.304
	346.10	0.1954	33.063
		0.2993	50.936
		0.9295	160.176
		1.1887	205.939
		1.4807	257.817
		1.7017	298.423
Carbon monoxide	273.28	0.7545	16.346
		2.1515	48.253
		2.9303	66.877
		5.2534	128.335
	300.48	0.6809	30.446
		1.1229	50.709
		1.5438	70.380
		2.1357	98.793
		2.8460	134.006
	327.33	0.1005	8.056
		0.2005	16.093
		0.3649	29.380
		1.1607	95.112
		1.5842	131.392
		2.7127	231.516
	350.69	0.1322	16.822
		0.2361	29.901
		0.3808	48.558

Table 22. (Continued)

Gas	Temperature (°K)	Amount adsorbed (mg/g)	Pressure (mm)
		0.5281	67.409
		1.3816	179.963
		2.1995	291.539
		2.5257	337.571
Methane	273.23	0.6522	4.953
		1.3385	10.571
		2.0591	17.462
		3.2740	31.069
		4.5626	47.944
		6.0089	69.238
		7.6236	96.842
		9.0594	122.732
		11.0843	165.777
		12.8278	206.582
		14.5108	249.880
		16.3395	301.326
	302.93	0.9073	17.201
		1.4148	28.533
		2.1538	46.435
		3.0689	71.234
		4.0051	98.772
		4.9781	128.863
		6.1194	167.973
		6.9610	198.419
	326.99	0.4431	14.985
		0.7245	25.452
		1.7291	67.296
		2.4259	100.141
		3.1360	135.309
		3.9407	178.669
		4.8006	225.005
	350.28	0.7100	42.941
		1.0965	69.003
		1.5331	101.372
		2.0774	141.931
		2.6033	183.052
		3.3869	245.897
Ethylene	299.56	6.1057	4.671
		9.1809	8.374
		12.2430	12.947

Table 22. (Continued)

Gas	Temperature (°K)	Amount adsorbed (mg/g)	Pressure (mm)
		15.1080	18.105
		19.3922	27.748
		22.4148	35.899
		25.2141	44.885
		28.7230	57.092
		31.6273	68.934
		34.1374	80.699
		37.0287	94.957
		40.3667	114.070
		45.9520	151.105
	323.69	3.5820	6.209
		5.8484	11.476
		7.5496	16.227
		9.3881	21.889
		11.7074	30.210
		13.4984	37.409
		15.9234	48.582
		18.8026	63.503
		22.6276	86.754
		25.7182	108.900
		28.6504	132.411
		31.6221	159.046
		34.6071	189.959
	343.97	1.4369	4.467
		2.7100	9.055
		4.0042	14.512
		4.7950	22.903
		7.7918	33.816
		9.8943	46.785
		12.1499	62.674
		14.1784	78.448
		16.7933	97.358
		18.6765	119.979
		21.5159	150.692
		24.5005	187.134
		27.9870	237.152
	362.15	0.9164	4.916
		1.6612	9.299
		2.6120	15.376
		3.9748	25.094
		6.0163	41.570

Table 22. (Continued)

Gas	Temperature (°K)	Amount adsorbed (mg/g)	Pressure (mm)
		7.7699	57.824
		9.1644	71.701
		11.1504	93.495
		13.0784	117.222
		15.0750	144.556
		17.5760	185.507
		21.4452	252.716
Ethane	292.06	10.7746	3.957
		16.8881	8.264
		21.6019	12.825
		26.6723	19.063
		31.3994	26.437
		36.5226	36.225
		42.8869	51.538
		48.8288	68.982
		53.1201	84.299
		56.4872	97.513
		60.6201	116.129
		65.4396	141.290
		71.8172	180.663
	314.04	5.5583	3.941
		9.5058	8.480
		13.4930	14.406
		16.4240	19.625
		20.7148	29.221
		24.2663	38.678
		27.9498	50.091
		32.0030	65.206
		35.6997	80.979
		39.0003	96.846
		43.9777	125.392
		48.6778	156.322
		53.6551	195.460
	355.47	3.2320	4.582
		5.6929	9.291
		8.0324	14.793
		10.3983	21.185
		12.6163	28.106
		14.9400	36.343
		16.9520	44.308

Table 22. (Continued)

Gas	Temperature (°K)	Amount adsorbed (mg/g)	Pressure (mm)
		20.6065	61.032
		24.1447	80.126
		27.2341	99.386
		30.8516	124.868
		34.8652	158.284
	356.44	1.7479	4.598
		3.7017	11.040
		5.9407	19.714
		7.8206	28.293
		9.8008	38.377
		11.7230	49.534
		13.3177	59.316
		15.3930	73.819
		16.8663	84.763
		18.8607	101.417
		19.9607	110.553
		22.9126	138.476
		25.5476	166.633
		28.7292	204.506
Carbon dioxide	273.36	5.4603	4.806
		9.1409	9.055
		12.7820	13.958
		17.7902	21.747
		23.1401	31.313
		29.5942	44.885
		36.7581	62.145
		42.0161	76.306
		48.3913	95.104
		54.5694	115.577
		63.9942	150.801
		73.0641	188.941
		82.1341	231.316
		90.7571	276.029
	299.51	2.2029	5.299
		3.8748	9.903
		6.0620	16.476
		8.3437	24.088
		11.3721	34.937
		14.3164	46.687
		18.0887	63.385

Table 22. (Continued)

Gas	Temperature (°K)	Amount adsorbed (mg/g)	Pressure (mm)
		20.9277	76.944
		24.5291	95.104
		28.2752	115.581
		32.8887	143.221
		38.0543	176.727
		43.2067	213.398
		48.5431	254.246
		53.5509	296.341
	325.37	0.9989	5.748
		4.7314	30.328
		6.4405	42.705
		8.1965	56.348
		10.0261	71.258
		12.3920	91.768
		14.5003	110.975
		16.8924	134.225
		20.3046	169.362
		23.5906	205.902
		27.1263	247.369
		30.6094	290.469
		33.9217	334.442
	348.83	1.1224	12.960
		1.8164	21.352
		3.6985	45.235
		5.1075	64.084
		6.4901	83.255
		8.3933	111.747
		10.5698	145.375
		12.7779	181.831
		15.1331	222.612
		16.7839	252.252
		18.8396	290.685

APPENDIX C: COMPUTER PROGRAMS

```
C
C
C
C       PROGRAM 1         PROGRAM 1            PROGRAM 1              PROGRAM 1
C
C         PROGRAM FOR PROCESSING OF GAS CHROMATOGRAPHIC DATA TO OBTAIN
C
C                  BAS ( ZERO EXCESS VOLUME ) VS.  TEMP.
C
C
      DIMENSION T5(20),VR(20)
      WRITE (3,16)
      READ (1,2) SW
C                                SW = SAMPLE WT.
      READ (1,1) N
C                                N  = NO. OF TEMPS.
      DO 13 I=1,N
      READ (1,1) N1,NX,BP,ADP,VP
C
C         THE FIRST DATA CARD OR CARDS FOR A GIVEN SET OF GASES/TEMP. MUST
C              BE THE DATA FOR A NONADSORBED GAS SUCH AS NEON.
C
C         N1 = NO. PTS./GAS/TEMP., NX = NO. GASES/TEMP., BP = BARROMETRIC P  MM
C         ADP = PRESSURE DROP (MM), VP = VAPOR P SOAP SOL. (MM)
C
      PI=BP+ADP
      PO=BP-VP
      PM=(PI+PO)/2.0
      DP=PI-PO
      XX=PO*(1.0-0.0833*((DP/PM)**2))/PM
      DO 12 J=1,NX
      DO 7 K=1,N1
      READ (1,4) R,F1,T1,D,IDI
C
C         R = RESISTANCE OF PT RESIS. THERMOMETER, F1 = FLOW TIME (SEC),
C         T1 = TEMP FLOWMETER (DEG C), D = RETENTION DISTANCE (CM),
C         IDI = GAS IDENTIFICATION NO.
C
      F2=(48.712*60.0)/F1
C                                48.712 IS CALIBRATED VOL. OF FLOWMETER (CC
      T2=T1+273.16
      TR=D/2.54
C
C         DETERMINE TEMPERATURE OF PT RESIS. THERMOMETER
C
      T3=(R-25.5542)/(0.0039261*25.5542)
      T4=T3
    5 T5(K)=T3+1.4916*(T4/100.0-1.0)*(T4/100.0)
      IF(ABS(T5(K)-T4)-1.0E-3)15,6,6
    6 T4=T5(K)
      GO TO 5
   15 T5(K)=T5(K)+273.16
    7 VR(K)=F2*TR*T5(K)*XX/T2
      AV=0.0
      AT=0.0
      DO 8 K=1,N1
      AV=VR(K)+AV
    8 AT=T5(K)+AT
      A=N1
```

```
    9 AV=AV/A
      AT=AT/A
      IF(J-1)10,10,11
   10 VZ=AV/SW
      WRITE (3,17) VZ,AT
C
C          VZ = APPARENT VOLUME OF NONADSORBED GAS
C
      GO TO 12
   11 VG=AV/SW-VZ
      VF=ALOG(VG)
      T6=SQRT(AT)
      V1=VG*(1.0/T6)
      V2=ALOG(V1)
      T7=1000.0/AT
      WRITE (3,3) VG,VF,V2,AT,T7,IDI
C
C          VG = BAS OR  ZERO  EXCESS VOLUME
C          ALL OUTPUT QUANTITIES ARE PER GRAM ADSORBENT
C
   12 CONTINUE
   13 CONTINUE
    1 FORMAT(2I10,3F10.0)
    2 FORMAT(F10.0)
    3 FORMAT(5X5F20.4,I10)
    4 FORMAT(1E15.6,3E12.4,I10)
   16 FORMAT(@1@,5X@              BAS              LN(BAS)        LN(BAS(
     1T)-1/2)             T (DEG K)            1000/T           IDI@//)
   17 FORMAT(//5XF20.4,40XF20.4)
      STOP
      END
```

```
C
C
C
C     PROGRAM 2        PROGRAM 2        PROGRAM 2        PROGRAM 2
C
C
C          PROGRAM FOR PROCESSING MICROBALANCE DATA TO OBTAIN
C
C               GAS-SURFACE VIRIAL COEFFICIENTS AND
C
C                    HENRY@S LAW PARAMETERS
C
C
      DIMENSION D(20),P(20),AM(20),R(20),GAGE(20),GLAB(5),W(20),WA(20),
     1RNA(20),VA(20),TS(20),TT(20),       BAS(5),CAAS(4),VA1(20),BSA(5),
     2SAB(5),SUBA(20),SUBB(20),T1(11),P1(11),T(20),P2(3,9),NP(3),RW(20),
     3VX(20),VCA(20),DATLAB(5)
      COMMON PRESS(20),LX(20),CO(4,5),KPTS(4,5),LPTS(4),IT,MX
      COMMON Z(20),M1,M2,NX,ALPHA(20),M6,SM(9)
      REAL*8 Q(2)
    1 FORMAT(4I5)
    2 FORMAT(20A4)
    4 FORMAT(I10,3F10.0)
    5 FORMAT(I10,F10.0,5A4)
    7 FORMAT(F10.3,2F10.0,2F10.3)
    8 FORMAT(@1@,40X10A4////)
    9 FORMAT(45X@SAMPLE WT. =@,F10.4,@MG.@//)
   10 FORMAT(///12X18HWT. ADSORBED (MG.),2X18HVOL. ADSORBED (CC),5X16HR•
     1NA (CC•MM/DEG),4X@PRESSURE (MM)@,4X@PT. =@//)
   11 FORMAT(5XF20.4,3F20.3,I10)
   12 FORMAT(4X2F20.3,2E20.4,F20.3,I12)
   15 FORMAT(////11X@BAS =@,F10.4,9X@CAAS/RT =@,E12.4,10X@CAAS =@,E12.4/
     1/)
   16 FORMAT(35X9HCAAS/RT =,E12.4,10X6HCAAS =,E12.4,10X7HDAAAS =,E12.4)
   17 FORMAT(@0@,10X7HRATIO =,F10.4,10X@B2/A =@,E15.4////////)
   31 FORMAT(8F10.0)
   33 FORMAT(I5,F10.0)
   40 FORMAT(//@                    VA EXP                VA CALC       (VA-BA
     1S)/P EXP       (VA-BAS)/P CALC           PRESSURE     PT. =@//)
   45 FORMAT(4E20.8)
   60 FORMAT(@TEMP. = @,F6.2,@ DEG K@)
  110 FORMAT(//40X@ POINTS ELIMINATED FROM ABOVE SET ARE NOS.@,5I5//)
  120 FORMAT(40X@  BEST FIT OF VA VS. P  GIVEN BY DEGREE =@,I5)
  130 FORMAT(//40X@ BEST FIT OF (VA-BAS)/P VS. P GIVEN BY DEGREE =@,I5)
  140 FORMAT(40X@  BEST FIT OF WA VS. P  GIVEN BY DEGREE =@,I5)
   30 FORMAT(20X8H-E(XO) =,F10.2,10X9HLN(AZO) =,F10.4,10X5HAZO =,E12.4,
     110X7HSTDEV =,F10.5//)
  169 FORMAT(//10X@                 BAS        LN(BAS(T)-1/2) EXP    LN(BAS(
     1T)-1/2) CALC          1000/T             T DEG K@//)
  170 FORMAT(10X3F20.4,2F20.3)
      DO 3 I=1,20
    3 W(I)=1.0
C
C          INPUT PRESSURE GAGE AND TC CALIBRATIONS
C          SEE TABLE 3 FOR THE POLYNOMINAL COEFFICIENTS
C
      READ(1,1) NTEMP,(NP(I),I=1,3)
      READ(1,31) (T1(I),I=1,NTEMP)
      DO 35 I=1,3
```

```
      N3=NP(I)
      READ(1,45) (P2(I,J),J=1,N3)
   35 CONTINUE
      READ(1,4) NSETS
      DO 1000 NS=1,NSETS
      READ(1,4) N1,S,E,B
      READ(1,1) L8,N5,M9
C
C         NSETS = NO. OF SEPARATE SETS TO BE PROCESSED AT ONE TIME
C         N1 = NO. OF GASES/SET WITH SAME SET UP PARAMETERS (S,E,B,)
C         L8 = MAX DEGREE OF POLYNOMIAL USED TO FIT WA VS. P DATA
C         M9 = 0  IF WA VS. P DATA IS NOT TO BE CORRECTED
C         M9 = 1  IF WA VS. P DATA IS TO BE CORRECTED
C         N5 = NO. OF DATA PTS. TO BE USED IF M9 = 0
C
      TU=0.0
      NDEG=1
      DO 99 J=1,N1
      M8=L8
      READ(1,5) N2,AMOL,(GLAB(I),I=1,5)
C
C         N2 = NO. TEMPS/GAS, AMOL = MOL. WT. (MG), GLAB = DATA LABLE
C
      DO 100 I=1,N2
      JX=0
      READ(1,33)N,TT(I)
C
C         N = NO. PTS./TEMP/GAS, TT = TEMP. (EMF OF TC IN MV )
C
      READ(1,7) (D(K),AM(K),R(K),GAGE(K),P(K),K=1,N)
C
C         SEE RESULTS SECTION FOR NOTATIONS ( GAGE = PRESSURE GAGE READINGS
C
      WO=(D(1)-B)*AM(1)+P(1)*R(1)
      TS(I)=T1(1)
      DO 47 K=2,NTEMP
   47 TS(I)=TS(I)+T1(K)*TT(I)**(K-1)
      TS(I)=TS(I)+273.16
      SW=S-E+WO
      RR=6.2358E4
      PRESS(1)=0.0
      WA(1)=0.0
      RW(1)=0.0
      RNA(1)=0.0
      LX(1)=1
      VA(1)=0.0
      DO 97 K=2,N
      IF(GAGE(K)-40.154)101,101,102
  101 NPRESS=NP(1)
      N4=1
      GO TO 105
  102 IF(GAGE(K)-131.807)103,103,104
  103 NPRESS=NP(2)
      N4=2
      GO TO 105
  104 NPRESS=NP(3)
      N4=3
  105 CONTINUE
      DO 106 L=1,NPRESS
  106 P1(L)=P2(N4,L)
      PRESS(K)=P1(1)
      DO 79 L=2,NPRESS
   79 PRESS(K)=PRESS(K)+P1(L)*GAGE(K)**(L-1)
```

```
      WA(K)=(((D(K)-B)*AM(K)+P(K)*R(K))-WO)/(SW/1000.0)
      RW(K)=RR*WA(K)
      RNA(K)=RW(K)/AMOL
      LX(K)=K
   97 VA(K)=RNA(K)*TS(I)/PRESS(K)
      WRITE(12,60) TS(I)
      BACKSPACE 12
      READ (12,2) (DATLAB(K),K=1,5)
      BACKSPACE 12
C
C         DISK OR TAPE STORAGE MUST BE PROVIDED AT RUN TIME
C
      WRITE(3,8)(GLAB(K),K=1,5),(DATLAB(K),K=1,5)
      WRITE (3,9) SW
      WRITE(3,10)
      WRITE (3,11) (WA(K),VA(K),RNA(K),PRESS(K),LX(K),K=1,N)
C
C         ALL OUTPUT QUANTITIES ARE PER GRAM ADSORBENT
C
      SFWA=PRESS(2)/WA(2)
      DO 200 K=2,N
  200 WA(K)=WA(K)*SFWA
      DO 287 K=1,N
  287 ALPHA(K)=0.001*SFWA
      DO 300 K=1,N
  300 Z(K)=1.0
      LL=0
      IF(M9) 155,156,155
  156 DWAO=0.0
      IF(N5)831,832,831
  831 N=N5
  832 M6=3
      MX=0
      LL=-1
      GO TO 134
  155 M1=M8-1
      IF(M1-1) 1002,1001,1001
 1002 M1=1
      GO TO 1003
 1001 M1=2
 1003 M2=M1
      M6=2
      M7=5
      MX=0
      NX=1
C
C         DETERMINE AN APPROXIMATE CORRECTION FOR WA VS. P DATA
C
      CALL CORR(M7,WA)
      DWAO=CO(IT,1)
      IF(ABS(DWAO)-1.0)142,143,143
  143 DWA=-0.1*DWAO
      GO TO 144
  142 DWA=-0.1
  144 CONTINUE
      IF(N-12)133,133,132
  133 M6=3
      GO TO 134
  132 M6=5
  134 CONTINUE
      M1=M8
      M2=M1
```

```
C
C          IF M2 IS  SET TO A VALUE LESS THAN M1 THEN THE PROGRAM WILL DETERMINE
C               WHICH DEGREE BEST FITS THE DATA.
C
      NX=0
      MN=0
      MX=1
C
C          IF MX = 0  M6-1 PTS. WILL BE ELIMINATED IF ERROR LIMITS SET UP ARE
C          NOT MET.
C          IF MX = 1  0 PTS WILL BE ELIMINATED.
C
C          DETERMINE BEST CORRECTION  FOR WA VS. P DATA
C
      Z(1)=1.0E6
      WA(1)=1.0
      PRESS(1)=1.0
      DO 900 K=2,N
  900 WA(K)=(WA(K)-DWAO)/SFWA
      SFWA=PRESS(2)/WA(2)
      DO 901 K=2,N
      PRESS(K)=PRESS(K)+1.0
  901 WA(K)=WA(K)*SFWA+1.0
      DO 700 K=2,N
  700 Z(K)=(PRESS(N)*WA(N))/(PRESS(K)*WA(K))
  701 CONTINUE
  602 CONTINUE
      CALL CORR(N,WA)
      GO TO 601
  605 IF(CO(IT,4))600,600,601
  600 N=N-1
      GO TO 602
  601 IF(LL) 807,807,704
  807 N7=LPTS(IT)
      WRITE(3,110) (KPTS(IT,K),K=1,N7)
      WRITE (3,140) IT
      WRITE(3,10)
      DO 111 L=1,N7
      K1=KPTS(IT,L)
      IF(K1)115,111,115
  115 CONTINUE
      DO 112 K=1,N
      IF(LX(K)-K1)112,112,113
  113 LX(K-1)=LX(K)
      WA(K-1)=WA(K)
      PRESS(K-1)=PRESS(K)
  112 CONTINUE
      N=N-1
  111 CONTINUE
      IF(LL) 707,703,704
  703 LL=1
      MX=3
      M1=IT
      M2=M1
  705 SM1=SM(IT)
      DO 902 K=2,N
  902 WA(K)=WA(K)+DWA
      MN=MN+1
      IF(MN-30)701,709,709
```

```
  704 IF(SM(IT)-SM1)705,706,706
  706 IF(ABS(DWA)-0.01)707,708,708
  708 DWA=-DWA/2.0
      GO TO 705
  709 WRITE(3,710)
  710 FORMAT(//@      WO  UNDETERMINED   @//)
  707 CONTINUE
      PRESS(1)=0.0
      DO 150 K=2,N
      PRESS(K)=PRESS(K)-1.0
  150 WA(K)=(WA(K)-1.0)/SFWA
      DO 114 K=2,N
      RNA(K)=RR*WA(K)/AMOL
      VA(K)=RNA(K)*TS(I)/PRESS(K)
  114 CONTINUE
      N8=IT+1
      WA(1)=CO(IT,1)-1.0
      DO 590 K=2,N8
  590 WA(1)=WA(1)+CO(IT,K)
      WA(1)=WA(1)/SFWA
      WRITE (3,11) (WA(K),VA(K),RNA(K),PRESS(K),LX(K),K=1,N)
      DO 51 K=2,N
      VA(K-1)=VA(K)
      PRESS(K-1)=PRESS(K)
   51 LX(K-1)=LX(K)
      N=N-1
      SHIFT1=0.0
      SFVA=1.0
      DO 201 K=1,N
  201 VA(K)=(VA(K)-SHIFT1)*SFVA
      RS=RR*TS(I)
      DO 400 K=1,N
      ALPHA(K)=0.001*RS/(PRESS(K)*AMOL)
  400 Z1(K)=PRESS(K)/PRESS(1)
      M1=M1-1
      IF(M1) 1005,1005,1006
 1005 M1=1
 1006 M2=M1
      M6=4
      MX=3
      NX=0
C
C          DETERMINATION OF BAS AND CAAS
C
      CALL CORR(N,VA)
      CAAS(I)=CO(IT,2)/SFVA
      BAS(I)=CO(IT,1)/SFVA+SHIFT1
      N7=LPTS(IT)
      WRITE(3,110) (KPTS(IT,K),K=1,N7)
      WRITE (3,120) IT
      DO 121 L=1,N7
      K1=KPTS(IT,L)
      IF(K1)125,121,125
  125 CONTINUE
      DO 122 K=1,N
      IF(LX(K)-K1)122,122,123
  123 LX(K-1)=LX(K)
      VA(K-1)=VA(K)
      PRESS(K-1)=PRESS(K)
```

```
      Z(K-1)=Z(K)
  122 CONTINUE
      N=N-1
  121 CONTINUE
      N8=IT+1
      DO 196 K=1,N
      VX(K)=CO(IT,1)
      DO 197 L=2,N8
  197 VX(K)=VX(K)+CO(IT,L)*PRESS(K)**(L-1)
  196 VX(K)=VX(K)/SFVA+SHIFT1
      DO 95 K=1,N
      VA(K)=VA(K)/SFVA+SHIFT1
   95 VA1(K)=(VA(K)-BAS(I))/PRESS(K)
      SHIFT2=0.0
      SFVA1=1.0E3
      DO 202 K=1,N
  202 VA1(K)=(VA1(K)-SHIFT2)*SFVA1
      DO 800 K=1,N
  800 Z(K)=(PRESS(N)*PRESS(K))/(PRESS(1)*PRESS(1))
      MX=3
      M1=1
      M2=M2-1
      IF(M2)81,81,82
   81 M2=1
   82 CONTINUE
C
C          DETERMINATION OF CAAS AND DAAAS, ETC.
C
      CALL CORR(N,VA1)
      WRITE(3,130) IT
      WRITE (3,40)
      CAAS(3)=CAAS(1)*RR*TS(I)
      CAAS(2)=CO(IT,1)/SFVA1+SHIFT2
      CAAS(4)=CAAS(2)*RS
      DAAAS=CO(IT,2)*RS*RS/SFVA1
      RATIO=CAAS(3)/CAAS(4)
      B2=CAAS(4)/(2.0*BAS(I)*BAS(I))
      B2=-B2
      N8=IT+1
      DO 27 K=1,N
      VA1(K)=VA1(K)/SFVA1+SHIFT2
      VCA(K)=CO(IT,1)
      DO 157 L=2,N8
  157 VCA(K)=VCA(K)+CO(IT,L)*PRESS(K)**(L-1)
      VCA(K)=VCA(K)/SFVA1+SHIFT2
      WRITE(3,12) VA(K),VX(K),VA1(K),VCA(K),PRESS(K),LX(K)
   27 CONTINUE
      IF(JX)13,14,13
   14 JX=1
   13 CONTINUE
      WRITE(3,15) BAS(I),CAAS(1),CAAS(3)
      WRITE(3,16) CAAS(2),CAAS(4),DAAAS
      WRITE(3,17) RATIO,B2
   18 T(I)=1.0/TS(I)
      BSA(I)=ALOG(BAS(I)*SQRT(T(I)))
      SAB(I)=BSA(I)
  100 CONTINUE
C
C          DETERMINE HENRY'S LAW PARAMETERS
```

```
C
      DO 89 I=1,3
      CALL OPLSPA(NDEG,N2,T,SAB,W,Q,TU)
      EXO=Q(2)
      DO 88 K=1,N2
      SUBA(K)=(175.0*(1.0/T(K))/(216.0*EXO))
      SUBB(K)=((109480.0/93312.0)*(((1.0/T(K))/EXO)**2.0))
   88 SAB(K)=BSA(K)-SUBA(K)-SUBB(K)
   89 CONTINUE
      AA=Q(1)
      SUM=0.0
      DO 77 K=1,N2
      BB=T(K)*EXO+AA
      BB=SAB(K)-BB
      SAB(K)=T(K)*EXO+AA
      T(K)=1000.0*T(K)
   77 SUM=SUM+BB*BB
      C=N2
      STDEV=SQRT(SUM/(C-1.0))
      XAZO=AA-0.5*ALOG(6.28316/(27.0*EXO))
      AZO=EXP(XAZO)
      WRITE(3,30)EXO,XAZO,AZO,STDEV
      WRITE(3,169)
      WRITE(3,170) (BAS(K),BSA(K),SAB(K),T(K),TS(K),K=1,N2)
   99 CONTINUE
 1000 CONTINUE
      STOP
      END
```

```
C
C
      SUBROUTINE CORR(NA,AY)
C
C          SUBROUTINE THROUGH WHICH CURVE FITTINGS ARE PREFORMED, PTS. ARE
C              ELIMINATED AND DEGREE OF BEST FIT ( IF NECESSARY ) IS DETERMINED.
C
      DIMENSION AY(1),ST(9),BX(20),BY(20),W(20),DIF(20),LP(20),BA(20)
      COMMON PRESS(20),LX(20),CO(4,5),KPTS(4,5),LPTS(4),IT,MX
      COMMON Z(20),M1,M2,NX,ALPHA(20),M6,SM(9)
      REAL*8 QQ(10)
      TU=0.0
      DO 1 NDEG=M1,M2
      IF(NX)56,56,35
   56 CONTINUE
      DO 13 I=1,NA
      LP(I)=LX(I)
      W(I)=Z(I)
      BA(I)=ALPHA(I)
      BX(I)=PRESS(I)
   13 BY(I)=AY(I)
      GO TO 37
   35 CONTINUE
      DO 38 I=2,NA
      LP(I-1)=LX(I)
      W(I-1)=Z(I)
      BX(I-1)=PRESS(I)
      BA(I-1)=ALPHA(I)
   38 BY(I-1)=AY(I)
   37 CONTINUE
      MM=0
      M=1
      DO 21 I=1,4
   21 KPTS(I,1)=0
      NB=NA-NX
    4 M=M+1
   24 CONTINUE
      S=0.0
      DO 39 I=1,NB
   39 S=S+BA(I)*BA(I)
      C=NB-1
      BETA=SQRT(S/C)
      CALL OPLSPA(NDEG,NB,BX,BY,W,QQ,TU)
      L=NDEG+1
      SUM=0.0
      DO 2 J=1,NB
      A=QQ(1)
      DO 3 K=2,L
    3 A=A+QQ(K)*BX(J)**(K-1)
      DIF(J)=BY(J)-A
    2 SUM=SUM+DIF(J)*DIF(J)
      SM(NDEG)=SUM
      ST(NDEG)=SQRT(SUM/C)
      NC=NDEG+I
      DO 16 J=1,NC
   16 CO(NDEG,J)=QQ(J)
      IF(ST(NDEG)-1.2*BETA)58,58,36
   58 LPTS(NDEG)=NA-NB+1
      WRITE(3,100) NDEG,ST(NDEG),BETA
```

```
100 FORMAT(@      EXIT  1   @,10XI10,2E20.4)
    M2=NDEG
    GO TO 59
 36 IF(MM)9,25,9
 25 IF(MX)9,5,9
  5 RMAX=0.0
    DO 6 I=1,NB
    IF(RMAX-ABS(DIF(I))) 7,7,6
  7 RMAX=ABS(DIF(I))
    MT=I
  6 CONTINUE
    IF(BX(MT)-1.0)29,61,29
 61 WRITE(3,62) NDEG
 62 FORMAT(/@  EXIT  2   LARGEST  DEV.  AT (0,0)   DEG. =@,I10/)
    GO TO 9
 29 IF(1.5*ST(NDEG)-RMAX)8,63,63
 63 WRITE(3,64) NB,MT,NDEG,ST(NDEG),RMAX
 64 FORMAT(@      EXIT   3    @,3I5,2E20.4)
    GO TO 9
  8 CONTINUE
    DO 10 I=1,NB
    IF(I-MT)10,17,12
 12 BX(I-1)=BX(I)
    BY(I-1)=BY(I)
    LP(I-1)=LP(I)
    BA(I-1)=BA(I)
    W(I-1)=W(I)
    GO TO 10
 17 KPTS(NDEG,M)=LP(MT)
 10 CONTINUE
    NB=NB-1
    IF(M-M6)4,11,11
 11 MM=1
    GO TO 24
  9 LPTS(NDEG)=NA-NB+1
  1 CONTINUE
 59 IT=M1
    STMIN=ST(M1)
    IF(M1-M2)47,48,47
 47 M3=M1+1
    DO 14 I=M3,M2
    IF(ST(I)-STMIN)15,15,14
 15 STMIN=ST(I)
    IT=I
 14 CONTINUE
 48 RETURN
    END
```

```
C
C
      SUBROUTINE OPLSPA(NDEG,NPTS,X,Y,W,Q,TUWYLO)
C
C          SUBROUTINE TO PREFORM ACTUAL CURVE FITTING
C          TITLE- ORTHOGONAL POLYNOMIAL METHOD OF LEAST SQUARES POLYNOMIAL APPROX
C           AMES LAB DISTRIBUTION NO. 360400266110003
C
      DIMENSION X(1),Y(1),W(1)
      REAL*8 Q(1),PN(11),PN1(10),SUM(4),B,C,PNX,TMP
      IF (TUWYLO) 2,1,2
    1 N=0
      C=0.0
      PN(1)=1.0
      GO TO 6
    2 C=-SUM(3)/SUM(4)
    3 B=-SUM(1)/SUM(3)
      SUM(4)=SUM(3)
      N=N+1
      PN1(N)=0.0
      PN(N+1)=0.0
      DO 4 J=1,N
      TMP=PN(J)
      PN(J)=B*PN(J)+C*PN1(J)
    4 PN1(J)=TMP
      DO 5 J=1,N
    5 PN(J+1)=PN(J+1)+PN1(J)
    6 DO 7 K=1,3
    7 SUM(K)=0.0
      DO 11 I=1,NPTS
      PNX=1.0
      J=N
    8 IF (J) 10,10,9
    9 PNX=PN(J)+PNX*X(I)
      J=J-1
      GO TO 8
   10 SUM(1)=SUM(1)+W(I)*X(I)*PNX*PNX
      SUM(2)=SUM(2)+W(I)*Y(I)*PNX
   11 SUM(3)=SUM(3)+W(I)*PNX*PNX
      Q(N+1)=SUM(2)/SUM(3)
      IF (N) 3,3,12
   12 DO 13 J=1,N
   13 Q(J)=Q(J)+Q(N+1)*PN(J)
      IF (N-NDEG) 2,14,14
   14 RETURN
      END
```

```
C
C
C        PROGRAM 3        PROGRAM 3        PROGRAM 3        PROGRAM 3
C
C
C         PROGRAM FO PROCESSING  LOW TEMP. NITROGEN MICROBALANCE DATA BY
C
C               EITHER THE USUAL @∞-LAYER@ BET EQ. OR THE @N-LAYER@ BET EQ.
C
C                   WITH N = 1 AND N VARIABLE
C
C
      DIMENSION NP(3),P2(3,9),AM(50),R(50),D(50),P(50),GAGE(50),WA(50),
     1RNA(50),LX(50),VA(50),PR(50),PW(50),PV(50),PRESS(50),DIF(50),
     2PR1(50),PW1(50),LX1(50),P1(9),DA(10),TC(50),PO(50),WA1(50)
      REAL*8 CO(5)
  101 FORMAT(4I5)
  102 FORMAT(4E20.8)
  103 FORMAT(I5,3F5.0,10A4)
  104 FORMAT(F10.3,2F10.0,3F10.3)
C
C         INPUT PRESSURE GAGE CALIBRATIONS
C         SEE TABLE 3 FOR THE POLYNOMINAL COEFFICIENTS
C
      READ(1,101) (NP(I),I=1,3)
      DO 2 I=1,3
      N3=NP(I)
      READ(1,102) (P2(I,J),J=1,N3)
    2 CONTINUE
      READ(1,101) N1,NBET
C
C         N1 = NO. OF DATA SETS
C         NBET = 0   @N-LAYER@ BET EQ. USED
C         NBET = 1 @∞ -LAYER@ BET EQ. USED
C
      DO 100 I=1,N1
      READ(1,103) N,S,E,B,(DA(K),K=1,10)
C
C         N  = NO. OF PTS./SET, ( S,E,B ) ARE THE SET UP PARAMETERS, DA IS THE
C         DATA LABLE
C
      READ(1,104) (D(K),AM(K),R(K),GAGE(K),P(K),TC(K),K=1,N)
C
C
C         SEE RESULTS SECTION FOR NOTATIONS
C                   EXCEPTION-  TC = EMF OF TC AT EACH DATA PT. (MV)
C
      WO=(D(1)-B)*AM(1)+P(1)*R(1)
      WRITE(3,105)
      SW=S-E+WO
      RR=6.2358E4
      AMOL=28014.0
      WRITE(3,106) (DA(K),K=1,10)
      POO=0.0
      TS=0.0
      DO 3 K=2,N
      IF(GAGE(K)-40.154)11,12,12
   11 NPRESS=NP(1)
      N4=1
```

```
      GO TO 15
   12 IF(GAGE(K)-131.807)13,13,14
   13 NPRESS=NP(2)
      N4=2
      GO TO 15
   14 NPRESS=NP(3)
      N4=3
   15 CONTINUE
      DO 16 L=1,NPRESS
   16 P1(L)=P2(N4,L)
      PRESS(K-1)=P1(1)
      DO 17 L=2,NPRESS
   17 PRESS(K-1)=PRESS(K-1)+P1(L)*GAGE(K)**(L-1)
      TC(K-1)=87.25-64.0*(TC(K)-5.040)
      PO(K-1)=EXP(2.30258*(-339.80/TC(K-1)-0.00563*TC(K-1)+7.7106))
      WA(K-1)=(((D(K)-B)*AM(K)+P(K)*R(K))-WO)/(SW/1000.0)
      RNA(K-1)=WA(K-1)*RR/AMOL
      LX(K-1)=K-1
      VA(K-1)=RNA(K-1)*0.35941
      PR(K-1)=PRESS(K-1)/PO(K-1)
      PW(K-1)=PRESS(K-1)/(WA(K-1)*(PO(K-1)-PRESS(K-1)))
      TS=TS+TC(K-1)
      POO=POO+PO(K-1)
    3 PV(K-1)=PW(K-1)*AMOL*PRESS(K-1)/(RR*TC(K-1))
      N=N-1
      C=N
      TS=TS/C
      POO=POO/C
      J=1
      DO 4 K=1,N
C
C          THE CURRENT RANGE OF RELATIVE PRESSURES SET FOR THE APPLICATION OF
C          THE BET EQS. IS 0-0.6, BUT SHOULD BE CHANGED AS MAY BE REQUIRED.
C
      IF(PR(K)-0.00)4,5,5
    6 PR1(J)=PR(K)
      PW1(J)=PW(K)
      LX1(J)=LX(K)
      WA1(J)=WA(K)
      J=J+1
      GO TO 4
    5 IF(PR(K)-0.60)6,6,50
    4 CONTINUE
   50 CONTINUE
      NPTS=J-1
      WRITE (3,114) SW,POO,TS
      WRITE(3,107)
C
C          ALL OUTPUT QUANTITIES ARE PER GRAM ADSORBENT
C
      WRITE(3,108) (WA(K),VA(K),PR(K),PRESS(K),LX(K),K=1,N)
      IF(NBET) 41,40,41
   40 CALL BETNINPTS,PR1,WA1,LX1)
      GO TO 100
   41 CONTINUE
      WRITE(3,117)
      WRITE(3,109)
      WRITE (3,110) (TC(K),PO(K),PW(K),PV(K),PR(K),LX(K),K=1,N)
      NDEG=1
C
C          MM = 1   ND PTS. ARE ELIMINATED
C          MM = 0 M6-1 PTS. ARE ELIMINATED
C
```

```
      MM=1
      M6=4
      M=1
    7 M=M+1
   24 CALL OPS(NDEG,NPTS,PR1,PW1,CO)
      WRITE(3,111)
      SUM=0.0
      SLOPE=CO(2)
      AINT=CO(1)
      DO 8 K=1,NPTS
      A=AINT+SLOPE*PR1(K)
      DIF(K)=PW1(K)-A
      SUM=SUM+DIF(K)*DIF(K)
      WRITE(3,112) PW1(K),A,DIF(K),PR1(K),LX1(K)
    8 CONTINUE
      C=NPTS-1
      ST=SQRT(SUM/C)
      WRITE(3,113) SLOPE,AINT,ST
      WM=1.0/(SLOPE+AINT)
      SA=WM*3.397
      CC=1.0/(AINT*WM)
      WRITE(3,115) WM,SA,CC
      IF(MM) 9,25,9
   25 RMAX=0.0
      DO 29 K=1,NPTS
      IF(RMAX-ABS(DIF(K))) 27,27,29
   27 RMAX=ABS(DIF(K))
      MT=K
   29 CONTINUE
      IF(ST-RMAX) 28,9,9
   28 CONTINUE
      LZ=LX1(MT)
      DO 30 K=1,NPTS
      IF(K-MT)30,30,32
   32 PW1(K-1)=PW1(K)
      PR1(K-1)=PR1(K)
      LX1(K-1)=LX1(K)
   30 CONTINUE
      NPTS=NPTS-1
      WRITE(3,116) LZ
      IF(M-M6) 7,31,31
   31 MM=1
      GO TO 24
    9 CONTINUE
  105 FORMAT(@1@,20X@MICROBALANCE DATA PROCESSED TO OBTAIN SURFACE AREA
     1USING B.E.T. EQUATION@//)
  106 FORMAT(45X10A4//)
  107 FORMAT(T21,@WT. ADS. (MG)  VOL. ADS. STP (CC)            P/PO
     1     PRESSURE (MM)      PT. =@//)
  108 FORMAT(10X4F20.4,I10)
  109 FORMAT(@+@,T37,@P/W*(PO-P)           P/V*(PO-P)       P/PO      PT. =
     1@//)
  110 FORMAT(7X2F10.2,2E20.4,F10.4,I10)
  111 FORMAT(////T27,@P/W*(PO-P)     CALC. P/W*(PO-P)          DIFFERENCE
     1      P/PO      PT. =@//)
  112 FORMAT(17X3E20.6,F10.4,I10)
  113 FORMAT(//T21,@SLOPE =@,E15.6,10X@INTERCEPT =@,E15.6,10X@ST. DEV. =
     1@,E12.4/)
  114 FORMAT(T11,@SAMPLE WT. =@,F10.4,@  MG.@,10X@AVG. PO = @,F10.3,@ MM
     1@,10X@AVG. TEMP. =@,F10.3,@ DEG K@////)
  115 FORMAT(T21,@WM =@,F10.4,@ MG.@,10X@SURFACE AREA =@,F10.3,@  M*M/G@
     110X@C =@,F10.4/////)
  116 FORMAT(T41,@POINT ELIMINATED FROM ABOVE SET IS =@,I5//)
  117 FORMAT(////10X@T DEG K     PO@)
  100 CONTINUE
      STOP
      END
```

```
C
C
C
      SUBROUTINE BETN(NPTS,X,Y,LL)
C
C         SUBROUTINE FOR THE APPLICATION OF THE @N-LAYER@ BET EQ.
C         FOLLOWING THE METHOD OF JOYNER ET AL. JACS 67C 2182 (1944)
C
      DIMENSION X(1),Y(1),PHI(50),THETA(50),LL(1)
      REAL*8 CO(2)
      NDEG=1
      A=1.0
      L=-1
    1 CONTINUE
      DO 2 K=1,NPTS
      PHI(K)=(X(K)*((1.0-X(K))**A-A*(1.0-X(K))*X(K)**A))/((1.0-X(K))**2)
      THETA(K)=(X(K)*(1.0-X(K)**A))/(1.0-X(K))
    2 PHI(K)=PHI(K)/Y(K)
      CALL OPS(NDEG,NPTS,THETA,PHI,CO)
      SL=CO(2)
      AI=CO(1)
      SUM=0.0
      DO 3 K=1,NPTS
      DIF=PHI(K)-(AI+SL*THETA(K))
    3 SUM=SUM+DIF*DIF
      IF(L)9,4,6
    4 L=1
    5 SUM1=SUM
      A=A+DA
      GO TO 1
    6 IF(SUM-SUM1)5,7,7
    7 IF(ABS(DA)-0.02)9,8,8
    8 DA=-DA/2.0
      GO TO 5
    9 CONTINUE
      C=NPTS-1
      WM=1.0/SL
      ST=SQRT(SUM/C)
      CC=1.0/(AI*WM)
      SA=WM*3.397
      WRITE(3,10)
      WRITE(3,11) (PHI(K),THETA(K),LL(K),K=1,NPTS)
      WRITE(3,12) SL,AI,ST
      WRITE(3,13) WM,SA,CC
      WRITE(3,14) A
   10 FORMAT(///47X@PHI(N,X)            THETA(N,X)        PT. =@//)
   11 FORMAT(35X2E20.4,I10)
   12 FORMAT(//T21,@SLOPE =@,E15.6,10X@INTERCEPT =@,E15.6,10X@ST. DEV. =
     1@,E12.4/)
   13 FORMAT(T21,@WM =@,F10.4,@ MG.@,10X@SURFACE AREA =@,F10.3,@  M*M/G@
     110X@C =@,F10.4//)
   14 FORMAT(50X@N =@,F7.2)
      IF(L)15,16,16
   15 L=0
      A=2.0
      DA=-0.1
      GO TO 1
   16 RETURN
      END
```

```
C
C
C
      SUBROUTINE OPS(NDEG,NPTS,X,Y,Q)
C
C          SUBROUTINE OPS IS THE SAME AS SUBROUTINE OPLSPA WITHOUT WEIGHTS AND
C          IS USED TO CURVE FIT THE DATA
C
      DIMENSION X(1),Y(1)
      REAL*8 Q(1),PN(11),PN1(10),SUM(4),B,C,PNX,TMP
      N=0
      C=0.0
      PN(1)=1.0
      GO TO 6
    2 C=-SUM(3)/SUM(4)
    3 B=-SUM(1)/SUM(3)
      SUM(4)=SUM(3)
      N=N+1
      PN1(N)=0.0
      PN(N+1)=0.0
      DO 4 J=1,N
      TMP=PN(J)
      PN(J)=B*PN(J)+C*PN1(J)
    4 PN1(J)=TMP
      DO 5 J=1,N
    5 PN(J+1)=PN(J+1)+PN1(J)
    6 DO 7 K=1,3
    7 SUM(K)=0.0
      DO 11 I=1,NPTS
      PNX=1.0
      J=N
    8 IF(J) 10,10,9
    9 PNX=PN(J)+PNX*X(I)
      J=J-1
      GO TO 8
   10 SUM(1)=SUM(1)+X(I)*PNX*PNX
      SUM(2)=SUM(2)+Y(I)*PNX
   11 SUM(3)=SUM(3)+PNX*PNX
      Q(N+1)=SUM(2)/SUM(3)
      IF(N) 3,3,12
   12 DO 13 J=1,N
   13 Q(J)=Q(J)+Q(N+1)*PN(J)
      IF(N-NDEG) 2,14,14
   14 RETURN
      END
```

```
C
C
C          PROGRAM 4          PROGRAM 4          PROGRAM 4          PROGRAM 4
C
C
C          PROGRAM TO EVALUATE SURFACE AREAS AND GAS - SOLID  INTERACTION
C
C                POTENTIALS FROM HENRY@S LAW DATA
C
C
C          SUBROUTINE OPLSPA ( SEE PROGRAM 2 ) MUST BE SUPPLIED AT RUN TIME
C
      DIMENSION W(20),BAS(20),SAB(20),DATL(10),BSA(20),T(20),TS(20),
     1SUBB(20),SUBA(20)
      REAL*8 Q(5)
   30 FORMAT(20X8H-E(XO) =,F10.2,10X9HLN(AZO) =,F10.4,10X5HAZO =,F12.4,
     110X7HSTDEV =,F10.5//)
  101 FORMAT(I10,10A4)
  102 FORMAT(8F10.0)
  103 FORMAT(@1@,20X@ EVALUATION OF SURFACE AREAS AND GAS-SOLID INTERACT
     1ION POTENTIALS FROM HENRYS LAW DATA@)
  104 FORMAT(///10X10A4//)
  169 FORMAT(//10X@                BAS        LN(BAS(T)-1/2) EXP   LN(BASI
     1T)-1/2) CALC          1000/T             T DEG K@//)
  170 FORMAT(10X3F20.4,2F20.3)
      DO 1 I=1,20
    1 W(I)=1.0
      TU=0.0
      NDEG=1
      WRITE(3,103)
    4 READ(1,101) NPTS,(DATL(K),K=1,10)
C
C          NPTS = NO. OF DATA PTS./GAS, DATL = DATA LABLE
C          NPTS = 0  INDICATES NO MORE DATA TO BE PROCESSED
C
      IF(NPTS)2,100,2
    2 READ(1,102) (BAS(K),K=1,NPTS)
      READ(1,102) (TS(K),K=1,NPTS)
C
C          BAS = ZERO EXCESS VOLUME, TS = TEMP. (DEG K)
C
      DO 3 K=1,NPTS
      T(K)=1.0/TS(K)
      BSA(K)=ALOG(BAS(K)*SQRT(T(K)))
    3 SAB(K)=BAS(K)
      WRITE(3,104) (DATL(K),K=1,10)
      DO 89 I=1,3
      CALL OPLSPA(NDEG,NPTS,T,SAB,W,Q,TU)
      EXO=Q(2)
      DO 88 K=1,NPTS
      SUBB(K)=((109480.0/93312.0)*(((1.0/T(K))/EXO)**2.0))
      SUBA(K)=(175.0*(1.0/T(K))/(216.0*EXO))
   88 SAB(K)=BSA(K)-SUBA(K)-SUBB(K)
   89 CONTINUE
      AA=Q(1)
      SUM=0.0
      DO 77 K=1,NPTS
      BB=T(K)*EXO+AA
      BB=SAB(K)-BB
      SAB(K)=T(K)*EXO+AA
      T(K)=1000.0*T(K)
   77 SUM=SUM+BB*BB
      C=NPTS
      STDEV=SQRT(SUM/(C-1.0))
      XAZO=AA-0.5*ALOG(6.28316/(27.0*EXO))
      AZO=EXP(XAZO)
      WRITE(3,30) EXO,XAZO,AZO,STDEV
      WRITE(3,169)
      WRITE(3,170) (BAS(K),BSA(K),SAB(K),T(K),TS(K),K=1,NPTS)
      GO TO 4
  100 STOP
      END
```

```
C
C
C          PROGRAM 5          PROGRAM 5          PROGRAM 5          PROGRAM 5
C
C     PROGRAM TO EVALUATE SURFACE AREAS FROM EXPERIMENTAL VALUES OF B2/A VS. T
C
C                                BY METHODS OF
C
C                          BARKER + EVERETT  AND/OR  JOHNSON + KLEIN
C
C
      COMMON NPTS,E3,SIGMA3,GLAB(12),B2E(10),T(10),GAMMA(25),GAMMA1(25,
     125),S,A,EO,ZETA,JA
  101 FORMAT(3I2,I4,2F10.0,12A4)
  102 FORMAT(2F10.0)
      CALL GA
      CALL GA1
      READ(1,101) NGAS
C         NGAS = NO. OF GASES
      DO 4 KK=1,NGAS
      READ(1,101) JA,JB,JK,NPTS,E3,SIGMA3,(GLAB(K),K=1,12)
C
C         JA = 0  GAS-GAS INTERACTION POTENTIAL INCREMENTED OVER RANGE  OF
C                          VALUES ( SEE SUBROUTINE BARKER)
C         JA = 1  BEST FIT PARAMETERS OBTAINEED
C         JB = 0  BEST FIT PARAMETERS DETERMINED FOR BARKER-EVERETT MONOLAYER
C         JB = 1  BARKER-EVERETT MONOLAYER POTENTIAL NOT USED
C         JC = 0  BEST FIT PARAMETERS DETERMINED FOR SINANOGLU-PITZER MONOLAYER
C         JC = 1  SINANOGLU-PITZER MONOLAYER POTENTIAL NOT USED
C         NPTS = NO. PTS./GAS, E3 + SIGMA3 ARE BULK GAS INTERACTION PARAMETERS,
C         GLAB = DATA LABLE
C
      READ(1,102) (B2E(K),T(K),K=1,NPTS)
C
C         B2E = EXP. VALUE OF B2/A, T = TEMP. ( DEG K )
C
      IF(JB)2,1,2
    1 CALL BARKER
    2 IF(JK)4,3,4
    3 CALL KLEIN
    4 CONTINUE
      STOP
      END
```

```
C
C
      SUBROUTINE BARKER
C
C          SUBROUTINE FOR APPLICATION OF BARKER-EVERETT MONOLAYER POTENTIAL
C
      DIMENSION X(10),Y(10),BB(10),B2T(10),B2EX(10),B2TX(10),TT(10),
     1DIF(10),AR(10)
      COMMON NPTS,E3,SIGMA3,GLAB(12),B2E(10),T(10),GAMMA(25),GAMMA1(25,
     125),S,A,EO,ZETA,JA
      WRITE(3,99)
      WRITE(3,100) (GLAB(K),K=1,12)
      LL=0
      E2=0.9*E3
      DELTE=-10.0
      C=NPTS
      IF(JA)21,20,21
C
C          SETS UP INCREMENTS FOR GAS-GAS POTENTIAL IF JA = 0
C          IF THIS SECTION IS CHANGED, THEN STATEMENT BELOW MUST ALSO BE CHANGED.
C
   20 LL=-1
      E2=0.5*E3
      DE=E2/20.0
      M=1
   21 CONTINUE
      DO 1 K=1,NPTS
      Y(K)=B2E(K)
    1 X(K)=1.0/T(K)
    2 AA=0.0
      DO 3 J=1,NPTS
      EO=4.0*E2*X(J)
      CALL PSI1
      BB(J)=Y(J)/S
    3 AA=AA+BB(J)
      AA=AA/C
      XI=SQRT(E2/E3)
      SIGMA2=SIGMA3*((1.0/XI)**(1.0/6.0))
      ALPHA=SIGMA2*SIGMA2*18921.
      AREA=ALPHA/AA
      SUM=0.0
      DO 4 J=1,NPTS
      AR(J)=ALPHA/BB(J)
      DIF(J)=ABS(BB(J)-AA)
    4 SUM=SUM+DIF(J)*DIF(J)
      IF(JA)24,22,24
   22 WRITE(3,399)
      WRITE(3,400) E2,AA,SUM,XI,SIGMA2,AREA
      WRITE(3,401) (B2E(K),BB(K),DIF(K),AR(K),T(K),K=1,NPTS)
C
      IF(M-20)23,23,24
C
C          TO BE CHANGED IF NO. OF INCREMENTS ABOVE ARE CHANGED
C
   23 M=M+1
      E2=E2+DE
      GO TO 2
   24 CONTINUE
      IF(LL)75,5,7
    5 LL=1
    6 SUM1=SUM
      E2=E2+DELTE
      IF(E2-1.1*E2) 301,301,10
```

```
301 IF((E2/E3)-0.5)10,2,2
  7 IF(SUM-SUM1)6,8,8
  8 IF (ABS(DELTE)-0.1)10,9,9
  9 DELTE=-DELTE/2.0
    GO TO 6
 10 CONTINUE
    STDEV=SQRT(SUM/(C-1))
    SUM=0.0
    DO 11 K=1,NPTS
    B2EX(K)=B2E(K)/AA
    B2T(K)=AA*Y(K)/BB(K)
    B2TX(K)=B2T(K)/AA
    DAF=ALPHA*(1.0/BB(K)-1.0/AA)
    SUM=SUM+DAF*DAF
 11 TT(K)=E2/T(K)
    DEV=SQRT(SUM/C)
    WRITE(3,101)
    WRITE(3,102) (B2E(K),B2T(K),B2EX(K),B2TX(K),TT(K),T(K),K=1,NPTS)
    WRITE(3,103) AREA,DEV,STDEV
    WRITE(3,104) E3,SIGMA3
    WRITE(3,105) E2,SIGMA2,XI
 99 FORMAT(@1@,10X@ EVALUATION OF SURFACE AREA FROM EXPERIMENTAL VALUE
   1S OF B2/A VS. TEMP. BY THE METHOD OF EVERETT+ BARKER@//)
100 FORMAT(40X12A4///)
101 FORMAT(@           B2/A  EXP            B2/A  THEO            B2  EXP
   1              B2  THEO               E2/KT             T  DEG K @//)
102 FORMAT(4E20.6,2F20.4)
103 FORMAT(////20X@SURFACE AREA =@,F10.2,@  M*M/G  +/-@,F7.2,10X@STDEV
   1 =@,E10.4//)
104 FORMAT(20X@E3 =@,F10.3,10X@SIGMA3 =@,F10.3//)
105 FORMAT(20X@E2 =@,F10.3,10X@SIGMA2 =@,F10.3,10X@XI =@,F10.3)
399 FORMAT(20X@     B2/A  EXP        ALPHA/A        DIFFERENCE
   1AREA          T DEG K@)
401 FORMAT(20X,E15.4,4F15.2)
400 FORMAT(//5X@E2 =@,F8.2,5X@AVG. ALPHA/A =@,F10.2,5X@SUM =@,E10.4,
   15X@XI =@,F6.2,5X@SIGMA2 =@,F6.2,5X@AVG. A =@,F8.2/)
 75 RETURN
    END
```

```
C
C
      SUBROUTINE KLEIN
C
C          SUBROUTINE FOR APPLICATION OF SINANOGLU-PITZER MONOLAYER POTENTIAL
C
      DIMENSION X(10),Y(10),BB(10),CC(10),B2EX(10),B2T(10),B2TX(10),
     1TT(10)
      COMMON NPTS,E3,SIGMA3,GLAB(12),B2E(10),T(10),GAMMA(25),GAMMA1(25,
     125),S,A,EO,ZETA,JA
      WRITE(3,99)
      WRITE(3,100) (GLAB(K),K=1,12)
      DO 1 K=1,NPTS
      X(K)=1.0/T(K)
      Y(K)=B2E(K)
      EO=4.0*E3*X(K)
      CALL PSI1
    1 BB(K)=S
      LL=0
      DZETA=-0.01
      ZETA=-0.03
      C=NPTS
    2 AA=0.0
      DO 3 K=1,NPTS
      CALL PSI2
      CC(K)=Y(K)/(BB(K)+S)
    3 AA=AA+CC(K)
      AA=AA/C
      SUM=0.0
      DO 4 K=1,NPTS
      DIF=AA-CC(K)
    4 SUM=SUM+DIF*DIF
      ALPHA=SIGMA3*SIGMA3*18921.
      AREA=ALPHA/AA
      ETA=-ZETA
      IF(LL)5,5,7
    5 LL=1
    6 SUM1=SUM
      ZETA=ZETA+DZETA
      IF(ABS(ZETA)-0.2) 2,10,10
    7 IF(SUM-SUM1)6,8,8
    8 IF(ABS(DZETA)-0.001)10,9,9
    9 DZETA=-DZETA/2.0
      GO TO 6
   10 CONTINUE
      STDEV=SQRT(SUM/(C-1))
      SIGMA2=SIGMA3
      RO=SIGMA3*(2.0**(1.0/6.0))
      ROO=RO
      DO 11 K=1,1000
      SIGMA2=SIGMA2+0.001
      AB=SIGMA3/SIGMA2
      ETA1=(AB**3.0)-(AB**9.0)
      IF(ETA-ETA1)12,12,11
   11 CONTINUE
   12 CONTINUE
      DO 13 K=1,1000
      ROO=ROO+0.001
      AB=SIGMA3/ROO
      ETA1=20
      ETA1=2.0*(AB**3.0)-4.0*(AB**9.0)
      IF(ETA-ETA1)14,14,13
   13 CONTINUE
```

```
 14 CONTINUE
    E2=-(4.0*E3*(AB**12.0-AB**6.0+ETA*AB**3.0))
    SUM=0.0
    DO 15 K=1,NPTS
    B2EX(K)=B2E(K)/AA
    B2T(K)=AA*Y(K)/CC(K)
    B2TX(K)=B2T(K)/AA
    DIF=ALPHA*(1.0/CC(K)-1.0/AA)
    SUM=SUM+DIF*DIF
 15 TT(K)=E2/T(K)
    DEV=SQRT(SUM/C)
    WRITE(3,101)
    WRITE(3,102) (B2E(K),B2T(K),B2EX(K),B2TX(K),TT(K),T(K),K=1,NPTS)
    WRITE(3,103) AREA,DEV,STDEV
    WRITE(3,104) E3,SIGMA3,RO
    WRITE(3,105) E2,SIGMA2,ROO,ETA
 99 FORMAT(@1@,@ EVALUATION OF SURFACE AREA FROM EXPERIMENTAL VALUES
   1OF B2/A VS. TEMP. BY THE METHOD OF JOHNSON + KLEIN@//)
100 FORMAT(40X12A4///)
101 FORMAT(@           B2/A  EXP            B2/A  THEO            B2  EXP
   1                B2  THEO               E2/KT             T  DEG K @//)
102 FORMAT(4E20.6,2F20.4)
103 FORMAT(////20X@SURFACE AREA =@,F10.2,@  M*M/G  +/-@,F7.2,10X@STDEV
   1 =@,E10.4//)
104 FORMAT(20X@E3 =@,F10.3,10X@SIGMA3 =@,F10.3,10X@RO =@,F10.3//)
105 FORMAT(20X@E2 =@,F10.3,10X@SIGMA2 =@,F10.3,10X@RO =@,F10.3,10X@
   1ETA =@,F10.4)
    RETURN
    END
```

```
C
C
      SUBROUTINE GA
C
C          SUBROUTINE TO EVALUATE GAMMA FUNCTIONS FOR B-E MONOLAYER POTENTIAL
C
      COMMON NPTS,E3,SIGMA3,GLAB(12),B2E(10),T(10),GAMMA(25),GAMMA1(25,
     125),S,A,EO,ZETA,JA
      GAMMA(1)=-6.77274
      GAMMA(2)=2.67888
      DO 1 J=3,25
      B=J
    1 GAMMA(J)=((3.0*(B-3.0)-1.0)/6.0)*GAMMA(J-2)/((B-1.0)*(B-2.0))
      RETURN
      END


C
C
      SUBROUTINE GA1
C
C          SUBROUTINE TO EVALUATE GAMMA FUNCTIONS FOR S-P MONOLAYER POTENTIAL
C
      COMMON NPTS,E3,SIGMA3,GLAB(12),B2E(10),T(10),GAMMA(25),GAMMA1(25,
     125),S,A,EO,ZETA,JA
      GAMMA1(1,1)=11.4984
      GAMMA1(2,1)=1.33944
      GAMMA1(3,1)=0.25364
      GAMMA1(4,1)=0.06271
      GAMMA1(1,2)=1.52187
      GAMMA1(2,2)=0.564395
      GAMMA1(3,2)=0.15970
      GAMMA1(4,2)=0.04961
      DO 2 K=1,2
      B=K
      DO 1 J=5,25
      C=J
    1 GAMMA1(J,K)=[(3.0*(C-5.0)+6.0*(B-1.0)+1.0)/12.0)*GAMMA1(J-4,K)/(C*
     1(C-1.0)*(C-2.0)*(C-3.0))
    2 CONTINUE
      DO 4 J=1,25
      C=J
      DO 3 K=3,25
      B=K
    3 GAMMA1(J,K)=((3.0*(C-1.0)+6.0*(B-3.0)+1.0)/12.0)*GAMMA1(J,K-2)/(C*
     1(B-1.0)*(B-2.0))
    4 CONTINUE
      RETURN
      END
```

```
C
C
      SUBROUTINE PSI1
C
C         SUBROUTINE TO EVALUATE THE REDUCED SECOND GAS-GAS VIRIAL COEFFICIENT
C         FOR THE B-E MONOLAYER POTENTIAL
C
      COMMON NPTS,E3,SIGMA3,GLAB(12),B2E(10),T(10),GAMMA(25),GAMMA1(25,
     125),S,A,EO,ZETA,JA
      A=(EO**(1.0/6.0))*(1.0/12.0)
      S=GAMMA(1)
      JX=1
      P=EO**0.5
      TERM=1.0
    1 TERM=TERM*P
      B=TERM*GAMMA(JX+1)
      S=S+B
      IF(B-1.0E-6)2,3,3
    3 JX=JX+1
      IF(JX-25)4,5,5
    4 GO TO 1
    5 WRITE(3,6)
    6 FORMAT(20X,@GAMMA TABLE HAS BEEN OVERRUN@)
    2 S=-A*S
      RETURN
      END
```

```
C
C
      SUBROUTINE PSI2
C
C         SUBROUTINE USED IN ADDITION TO PSI1 TO EVALUATE THE REDUCED SECOND
C         GAS-GAS VIRIAL COEFFICIENT FOR S-P MONOLAYER POTENTIAL
C
      COMMON NPTS,E3,SIGMA3,GLAB(12),B2E(10),T(10),GAMMA(25),GAMMA1(25,
     125),S,A,EO,ZETA,JA
      S=0.0
      D=1.0
      DO 3 M=1,25
      D=D*ZETA
      Y=M-1
      DO 2 N=1,25
      X=N-1
      P=EO**((2.0*X+3.0*Y+3.0)/4.0)
      Q=P*GAMMA1(M,N)*D
      S=S+Q
      IF(ABS(Q)-1.0E-6)1,2,2
    1 IF(N-1)4,4,3
    2 CONTINUE
    3 CONTINUE
    4 S=-A*S
      RETURN
      END
```